An Investigation into the Complex Formation and Potential Solvent Extraction of Os(IV/III) with *N*, *N* - dialkyl - *N*′- acyl(aroyl)thioureas

by

Reynhardt Klopper

Thesis submitted in fulfillment
of the requirements for the degree of

Magister Scientiae

In the Faculty of Science
at the University of Stellenbosch
April 2006

I, the undersigned, hereby declare that the work contained in this thesis is my own original work and that it has not been presented partially or in full at any university for a degree.

_____ _____

Reynhardt Klopper Date

Abstract

This study involved the preliminary investigation into the potential liquid-liquid extraction of Os(IV/III) from hydrochloric acid solutions with ligands of type *N,N*-dialkyl-*N′*-acyl(aroyl)thioureas (HL), and ultimate selective pre-concentration and separation of Os(IV/III) from the other platinum group metals. Investigations have also been focused towards understanding the speciation of Os(IV) in hydrochloric acid medium.

A series of osmium complexes with ligands of type HL have been synthesised and characterised. This has been done with a view towards understanding the interaction of Os(IV/III) with the HL ligands, and what the resultant stereochemical influences would be on the solvent extraction capabilities of the ligands.

The structures of two novel osmium-containing compounds have been verified by means of X-ray crytallography. Firstly, the ion pair $OsCl_6[(C_4H_9)_4N]_2$ was obtained as a result of liquid-liquid extraction experiments. Secondly, the only known example (in our knowledge) of an Os(III) - *N,N*-dialkyl-*N′*- aroylthiourea complex, in this case tris(*N,N*-diethyl-*N'*-benzoylthioureato)osmium(III), was successfully synthesised and characterised.

Lastly, preliminary studies into the substitution reactions of ruthenium-polypyridine complexes with *N,N*-dialkyl-*N′*-acyl(aroyl)thioureas were conducted. A series of *cis*-bis(2,2′-bipyridine)(*N,N*-dialkyl-*N′*-acyl(aroyl)thioureato)ruthenium(II) complexes have been successfully synthesised and characterised. The electronic absorption behaviour of the formed complexes have been investigated in detail via UV-Vis spectrophotometry.

Abstrak

Dié studie behels die voorlopige ondersoek aangaande die potensiële vloeistof-vloiestof ekstraksie van Os(IV/III) vanuit soutsuur media met ligande van die tipe *N,N*-dialkiel-*N′*-asiel(aroïel)tioureas (HL), en die uiteindelike selektiewe pre-konsentrasie en skeiding van Os(IV/III) van die ander platinum groep metale.'n Gefokusde ondersoek was ook onderneem om te bepaal wat die spesifieke spesiasie van Os(IV) in soutsuur media behels.

'n Reeks van osmium komplekse met ligande van die tipe HL was gesintetiseer and gekaraktiriseer. Dit was onderneem om lig te skep op die interaksie van Os(IV/III) met die HL ligande, asook watter impak die resulterende stereochemiese invloede sal hê op die ekstraksie potensiaal van die ligande.

Die strukture van twee unieke osmium bevattende spesies was geverifieer deur middel van X-straal kristallografie. Eerstens, die ioon-paar $OsCl_6[(C_4H_9)_4N]_2$ was verkry as gevolg van vloeistof-vloiestof ekstraksie eksperimente. Tweedens, die enigste gepubliseerde voorbeeld (volgens ons kennis) van 'n Os(III) - *N,N*-dialkiel-*N′*-aroïeltiourea kompleks, naamlik tris(*N,N*-di-etiel-*N′*-bensoïelthioureato)osmium(III), was suksesvol gesintetiseer en gekaraktiriseer.

Laastens, voorlopige ondersoeke was onderneem om die interaksies van ruthenium-polipiridien komplekse met *N,N*-dialkiel-*N′*-asiel(aroïel)tioureas te verken. 'n Reeks van *cis*-bis(2,2′-bipiridien)(*N,N*-dialkiel-*N′*-asiel(aroïel)tioureato)ruthenium(II) komplekse was suksesvol gesintetiseer en gekaraktiriseer. Die elektroniese absorpsie gedrag van die gevormde komplekse was in detail ondersoek deur middel van UV-Vis spektrofotometrie.

Table of Contents

Acknowledgements

I would like to express my thanks to Prof KR Koch for his continued support and constructive criticism during the course of this project. Dr. Dave Robinson is also thanked for his positive contributions.

I am grateful to the following institutions for financial support:

- Anglo American Platinum Corporation Ltd.
- National Research Foundation
- University of Stellenbosch

I would also like to thank all previous and present members of the Platinum Group Metals Research Group at the University of Stellenbosch for interesting discussions and providing a stimulating working environment.

Abbreviations

Chemicals

HL	*N,N*-dialkyl-*N′*-acyl(aroyl)thiourea
HCl	Hydrochloric Acid
EtOH	Ethanol
TBATFB	Tetrabutylammonium tetrafluoroborate
bpy/bipy	2,2′-Bipyridine
Ph	Phenyl
py	Pyridine
phen	1,10-Phenanthroline
DMF	*N,N*-dimethylformamide
DBBT	*N,N*-dibutyl-*N′*-benzoylthiourea
DEBT	*N,N*-diethyl-*N′*-benzoylthiourea
DEPT	*N,N*-diethyl-*N′*-pivaloylthiourea

General

PGMs	Platinum Group Metals
HPTLC	High Performance Thin Layer Chromatography
HPLC	High Performance Liquid Chromatography
FT-IR	Fourier Transform Infrared
mmol	millimole
K	Kelvin
C	Celcius
PTC	Phase Transfer Catalyst
M	mol/dm^3
UV-Vis	Ultraviolet-Visible
nm	nanometre
λ_{max}	Wavelength of maximum absorbance
Å	Angström
ν_{max}	Maximum frequency
v/v	volume per volume
LMCT	Ligand to metal charge transfer
MLCT	Metal to ligand charge transfer
HOMO	Highest occupied molecular orbital
LUMO	Lowest unoccupied molecular orbital
O_h	Octahedral
HSAB	Hard-soft Acid-base
ESMS	Electrospray Mass Spectrometry

Chapter 1

General Introduction

The Platinum Group Metals (PGMs: Pt, Pd, Ir, Rh, Os and Ru) have over the last few decades found increased application in industry for a variety of purposes, such as their incorporation into electrical and electronic devices, as catalysts for automobile exhaust emission control, dental application and jewelry[1;2]. Therefore, their inherent importance to the above mentioned industries, linked to the fact that all the PGMs are only scarcely found in nature, has caused their prices on the world market to be very high. Hence, much work has been published on the efficient recycling and recovery of precious metals[3]. Moreover, a thorough understanding into the fundamental chemistries of each of the PGMs will lead to more efficient processing capabilities.

For years osmium has been a troublesome impurity encountered in the South African platinum mining industry. Due to its limited application in industry, and the fact that it occurs as an impurity during the refining process of the other more valuable PGMs, research into its fundamental chemistry with a view towards future applications has up to date been rather limited. Some applications of the metal are its use in the manufacturing of high-pressure ball bearings, electrical contacts and fountain pen nibs. As early as 1906 it was used in the filaments for incandescent lighting and is from where the company Osram derives it name. Osmium, in its tetroxide form of OsO_4, is also used for the detection of fingerprints and as a stain for DNA samples during forensic investigations.

The historical discovery of osmium is rather interesting. Having discovered platinum and palladium, William Hyde Wollaston handed over the remaining residues of ore to his commercial partner Smithson Tennant, a fellow Cambridge graduate with whom he had forged a partnership in 1800. In 1804, Tennant isolated osmium from the residues by treating it with aqua regia, and due to the distinctive chlorine-like odour of its oxide, named it after the Greek for smell, "osme".

Osmium is a bluish-white metal in its ground state, with a high specific gravity of 22.61, which is exceeded only by that of iridium (22.65). Oxidation of the metal by air, in its finely powdered state, occurs easily at room temperature, affording the volatile and highly poisonous tetroxide OsO_4. At temperatures below 400 °C the metal is not attacked by air. In its solid metal form, osmium's

brittleness and hardness make it extremely difficult to work with, and industrially it is usually produced as a finely divided powder[4].

Osmium resembles ruthenium in its chemistry, especially with regard to the number of oxidation states, from VIII to 0 inclusive. And like the latter, it forms a number of polynuclear complexes with oxygen or nitrogen bridging ligands. In its higher oxidation states, osmium tends to resemble rhenium more than ruthenium. Although several complexes of osmium in all of its oxidation states have been reported, its most common states are VIII, VI, IV, III and II.

The octavalent state of osmium is more stable than that of ruthenium, and occurs most commonly as the tetroxide, OsO_4. It is stabilised by ligands that are strong π-donors, such as F^- and OH^-, affording species such as the perosmate $[OsO_4(OH)_2]^{2-}$ and the difluoroperosmate $[OsO_4F_2]^{2-}$. Octavalent species are all easily reduced to the hexavalent or lower states.

Osmium(VI) occurs not only in the hexafluoride OsF_6, but also in a large number of species involving the linear osmyl (O = Os = O) grouping, e.g. potassium osmate $K_2[OsO_2(OH)_4]$ which has an octahedral structure with the two oxo groups *trans* in relation to each other.

The tetravalent state of Os(IV) is the most common, and many Group VII and Group VI ligands that are π-acceptors and σ-donors form complexes with it. Examples are the hexahalogeno-osmates(IV) $[OsX_6]^{2-}$ (X = F, Cl, Br, I) and the oxide OsO_2.

Complexes of Os(III) are less numerous than those of Ru(III). Most complexes are octahedral and may easily be oxidised to the tetravalent state, but if the ligands have strong π-acceptor properties reduction to the divalent state may occur. Complexes of nitrogen ligands are numerous, e.g. $[Os(NH_3)_6]^{3+}$ and $[Os(bipy)_3]^{3+}$.

Os(II) complexes are octahedral and diamagnetic with the stable $(t_{2g})^6$ configuration, and are usually kinetically inert. A wide range of complexes with Group V and Group IV π-acceptor ligands exist, e.g. $[Os(CN)_6]^{4-}$ and $Os(CO)_4Cl_2$.

Limited use of osmium in industrial applications, coupled with the fact that its only significant economic value is the cost of separating it from platinum during the refining process, has lead to limited academic research into its fundamental and applied chemistry. Therefore the need arises to grasp a better understanding into the fundamental characteristics of the metal in all of its oxidation

states, in a variety of reaction milieus. This holds especially true for the separation and refinement of PGMs, where highly efficient processes currently exist[5], but there are emerging trends to develop newer, more cost-effictive processes. This is mainly driven by increased environmental awareness and stricter legislation for the control of industrial effluents.

In this context, recent research by the group of Koch, *et al.*[6] have been focused on the coordination of PGMs with ligands of the type *N*,*N*-alkyl-*N*′-acyl(aroyl)thioureas (HL, ***Fig. 1.1***), and their associated analytical and process chemistry applications. Unfortunately, the main focus of the research was on the chemistry of the above mentioned ligands with Pt(II), Pd(II) and Rh(III), with hardly any exploration into the complex formation of Os(IV/III), and subsequent analytical and process chemistry potential.

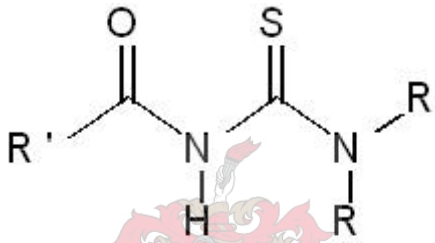

Figure 1.1. ***N*,*N*-alkyl-*N*′-acyl(aroyl)thiourea motif (R′ = aryl/alkyl; R = alkyl)**

Therefore the need arose for a more thorough understanding into the chemical interaction of osmium with the *N*,*N*-alkyl-*N*′-acyl(aroyl)thiourea ligands. Especially interesting was the possibility of utilising ligands of the type HL in the extraction of Os(IV/III) from hydrochloric acid medium at a rate different from Pt(IV), thereby achieving possible separation. Moreover, an understanding of the nature of these complexes in terms of their structure and properties could lead to interesting pre-concentration applications.

Preliminary studies have also been focused towards the incorporation of *N*,*N*-alkyl-*N*′-acyl(aroyl)thiourea ligands into the bis(bipyridyl)ruthenium complex system. Substitution products of bis(bipyridyl)ruthenium complexes have for years been incorporated intensively in intramolecular electron transfer processes due to their interesting spectroscopic and electrochemical properties. These properties make the complexes excellent chromophores to observe and investigate metal-ligand interactions[7].

Since the ligands incorporated into the polypyridyl ruthenium complexes have a substantial influence on the phototochemical behaviour of the complexes[8], research was directed towards gaining a better understanding of what role the *N*,*N*-alkyl-*N'*-acyl(aroyl)thiourea ligands could play in these complexes.

References

[1] M.S. Alam and K. Inoue, *Hydrometallurgy*, 46 (1997) 373.

[2] C.H. Kim, S.I. Woo and S.H. Jeon, *Ind Eng Chem Res*, 39 (2000) 1185.

[3] M.S. Alam, K. Inoue and K. Yoshizuka, *Hydrometallurgy*, 49 (1998) 213.

[4] W.P. Griffith, C.J. Raub and K. Swars, *Gmelin Handbuch der Anorganischen Chemie*, Springer-Verlag, Berlin (1980).

[5] R.I. Edwards, A.J. Bird and G.J. Berfeld, *Gmelin Handbook of Inorganic Chemistry*, Springer, Berlin (1986).

[6] K.R. Koch, *Coord Chem Rev*, 216-217 (2001) 473.

[7] B. Durham, J.V. Caspar, J.K. Nagle and T.J. Meyer, *J Am Chem Soc*, 104 (1982) 4803.

[8] A. Juris and V. Balzani, *Coord Chem Rev*, 84 (1988) 85.

Chapter 2

Potential Solvent Extraction of Os(IV/III) with *N*,*N*-dialkyl-*N*′-acyl(aroyl)thioureas

2.1 Introduction

For the last three decades pioneering work on the coordination chemistry of transition metals with the ligands of type *N*,*N*-alkyl-*N*′-acyl(aroyl)thioureas have been undertaken by the group of Beyer and Hoyer. Their initial research was focused on the coordination of ligands of type *N*′-acylthiourea with some first and second row transition metal ions such as Pd(II), Ag(I), Cd(II), Co(III), Zn(II) and Ni(II) [1]. Of particular interest was initial research done on the possible application of *N*-alkyl-*N*′-acyl(aroyl)thioureas for the liquid-liquid extraction and separation of transition metals such as Au(III), Pd(II) and Cu(II) [2]. Studies into the application of *N*,*N*-alkyl-*N*′-acyl(aroyl)thioureas for liquid-liquid extraction of PGMs from hydrochloric acid solutions followed, further exemplifying the versatility of these ligands [3-5].

Also of interest was the study of Schüster, *et al.* [6], in which liquid-liquid extraction of several PGMs with a variety of *N*,*N*-alkyl-*N*′-acyl(aroyl)thioureas were investigated. Moreover, the separation of the complexes formed was investigated via high performance thin layer chromatography (HPTLC), as a means to achieve adequate separation of the PGMs. In this study osmium, as Os(III), was successfully extracted with a variety of *N*,*N*-alkyl-*N*′-acyl(aroyl)thiourea ligands, but no attempt was made to characterise the complexes formed.

In this chapter an investigation was undertaken to assess the possibility of selectively extracting Os(IV) from hydrochloric acid media into chloroform. Moreover, preliminary research was focused into understanding the speciation of Os(IV) in hydrochloric acid medium, and in what manner this influences the rate and manner of extraction.

2.2 Experimental Section

2.2.1 Analysis of standard $OsCl_6^{2-}$ solutions

A range of standard $[OsCl_6]^{2-}$ solutions were made up in hydrochloric acid matrices of varying concentration strengths, i.e. 1.0, 2.0 and 5.0 mol/dm^3. Initial osmium stock solutions of 100.0 µg/l concentration were prepared in the following manner :

> An undefined amount of osmium salt was heated *in vacuo* at 70 ºC for a duration of 60 min, affording anhydrous $Na_2[OsCl_6]$. 23.599 mg (0.052567 mmol) of this dark brown salt was weighed off (in a fume hood) and added to a 100 cm^3 volumetric flask. The flask was made up to the mark with hydrochloric acid of particular concentration.

A range of standard solutions was prepared from diluted aliquots of the original 100 µg/ml osmium stock solutions, affording the concentration series :

50.0, 40.0, 30.0, 20.0, 10.0 and 5.00 µg/ml

Such a series was made up for each hydrochloric acid matrix solution.

All the standards were measured at ambient temperature (298 K) against hydrochloric acid background solutions in 1 cm quartz cuvettes. After each measurement the cuvette was rinsed three times with distilled water and with the standard to be measured. Measurements were performed in an ascending order from the lowest concentration, so as to limit experimental errors incurred.
Absorption spectra were recorded on an HP Agilent Spectrophotometer, with detection by a Diode-Array detector.

2.2.2 Speciation changes of $OsCl_6^{2-}$ in HCl matrices

$[OsCl_6]^{2-}$ solutions of concentration 50.0 µg/ml were prepared in hydrochloric acid matrices of varying concentration strengths. An initial stock hydrochloric acid solution of concentration 10 mol/dm^3 was prepared, from which aliquots were used in preparation of successive solutions. For each osmium solution, 5.899 mg (0.01314 mmol) of $Na_2[OsCl_6]$ was weighed off and added to a 50 cm^3 volumetric flask. A particular volume of the stock HCl solution was added and the flask was filled up to the mark with distilled water. Final solutions were of the following HCl concentration strengths : 9.0, 8.0, 7.0, 6.0, 5.0, 2.0, 1.0, 0.5, 0.1 and 0.05 mol.dm^{-3}.

Absorption spectra of all the osmium solutions were recorded using the HP Agilent UV-Vis Diode-Array Spectrophotometer. Measurements were performed at ambient temperature against hydrochloric acid background using a 1 cm quartz cuvette. As previously, solutions were measured in ascending concentration strength.

2.2.3 Solvent Extraction with N,N-dibutyl-N'-benzoylthiourea (DBBT) performed at room temperature

Solvent extractions were performed with either 1.0 or 2.0 mol/dm^3 hydrochloric acid matrices containing osmium, as $[OsCl_6]^{2-}$, of concentration 50.0 μg/ml (refer to section *2.3.3*). To a 100 cm^3 round-bottomed flask containing 20 cm^3 chloroform was added 4.612 mg (0.01577 mmol) and *N*,*N*-dibutyl-*N*′-benzoylthiourea (in 3:1 molar ratio w.r.t. osmium). Addition of 20 cm^3 aqueous osmium solution resulted in a bilayer. A reflux condenser was attached to the flask and agitation of the bilayer solution was ensured by means of magnetic stirring.

***N,N*-dibutyl-*N'*-benzoylthiourea:**

Ligand synthesised by Miller [7]. 95.8% yield; m.p. 88-89ºC; *Anal*. Found: C, 65.58; H, 8.59; N, 9.76; S, 10.89% Calculated for $C_{15}H_{22}N_2SO_4$: C, 65.70; H, 8.29; N, 9.58; S, 10.96%.

2.2.4 Varying DBBT : Os ratios and incorporation of a Phase Transfer catalyst

Experimental set-up was the same as for room temperature solvent extraction experiments. The amounts of ligand present in the organic phase varied as either 3:1, 12:1 or 24:1 w.r.t. initial osmium.

To a 100 cm^3 round-bottomed flask containing 20 cm^3 chloroform was added either 4.612 mg (0.01577 mmol, 3:1), 18.445 mg (0.06307 mmol, 12:1) or 36.895 mg (0.1262 mmol, 24:1) *N*,*N*-dibutyl-*N*′-benzoylthiourea. In the case where *N*,*N*-diethyl-*N*′-benzoylthiourea was used, 3.861 mg (0.01634 mmol, 3:1) of ligand was weighed off. To the clear chloroform layer was added 20 cm^3 of a 1.0 M HCl solution containing 50.0 μg/ml osmium. All solutions were agitated at 80 ºC by means of magnetic stirring. Refluxing was ensured by attachment of a reflux condenser to the reaction flask.

***N,N*-diethyl-*N*′-benzoylthiourea:**

Synthesis procedure is provided in section *3.2.2*. Yield of 85.4 %; m.p. 98-100 ºC; *Anal*. Found: C, 60.91; H, 6.92; N, 11.60 %. Calculated for $C_{12}H_{16}N_2SO$: C, 60.99; H, 6.82 ; N, 11.85 %.

In experiments utilising the phase transfer catalyst tetrabutylammonium tetrafluoroborate (TBATFB), its concentration was always 0.01 mol/dm^3 in 20 cm^3 aqueous phase, i.e. 0.06586 g (0.200 mmol).

2.2.5 Effect of phase transfer catalyst concentration

In order to ascertain the effect of phase transfer catalyst concentration on the outcome of solvent extraction, successive extractions were performed under the following parameters:

- 20.0 cm^3 2 M HCl containing osmium at a concentration of 50.0 μg/ml
- TBATFB added to aqueous phase in varying concentrations (with regard to the starting osmium concentration)
- One set of experiments had DBBT present in the organic phase (20 cm^3), in 3:1 ligand to metal ratio. The other set had zero ligand present in the organic phase.
- All experiments were agitated at 80 °C for 4½ h.

Mass (mg)	Concentration ($\times 10^{-3}$ mol.dm^{-3})		
TBATBF	**TBATBF**	**Os**	**TBATBF : Os**
1.73	0.263	0.263	1 : 1
5.19	0.789	0.263	3 : 1
10.4	1.58	0.263	6 : 1
15.6	2.37	0.263	9 : 1

Table 2.1. **Varying ratios of phase transfer catalyst versus metal**

After the period of agitation the absorption spectra of the aqueous and organic phases were recorded using a 1 cm quartz cuvette.

2.2.6 Reduction with $SnCl_2$

The reduction process of $[OsCl_6]^{2-}$ with $SnCl_2$ was investigated in a systematic process, consisting of a series of experiments labeled ***I*** through ***IX***. Reactions were monitored *via* absorption spectrophotometry, utilising an HP Agilent UV-Vis Diode-Array Spectrophotometer and 1 cm quartz cuvette.

For experiments ***I-IV*** a $SnCl_2$ stock solution was prepared as follows:

To a 200 cm^3 volumetric flask containing 20 cm^3 degassed conc HCl (32 % v/v) was added 2.256 g $SnCl_2 \cdot 2H_2O$ (10 mmol). This solution was then diluted up to the mark with degassed distilled water and covered with aluminium foil for insulation against UV light.

Thus, [HCl] = 1.018 mol/dm^3 and [$SnCl_2$] = 0.050 mol/dm^3.

For experiments ***V-IX*** a second $SnCl_2$ stock solution was prepared, since higher concentrations of the reducing agent were needed:

To a 100 cm^3 volumetric flask containing 10 cm^3 degassed conc HCl (32% v/v) was added 11.28 g $SnCl_2 \cdot 2H_2O$ (50.0 mmol). This solution was diluted to the mark with degassed distilled water and covered with aluminium foil.

Thus, [HCl] = 1.018 mol/dm^3 and [$SnCl_2$] = 0. 50 mol/dm^3

*Experiments **I** and **II*** :

44.9 mg (0.100 mmol) $Na_2[OsCl_6]$ was weighed off in a 50 cm^3 round bottom flask and dissolved in 10 cm^3 1M HCl. To this orange-yellow solution was added 2.00 cm^3 (***I***), or 6.00 cm^3 (***II***) of the 0.050 mol/dm^3 $SnCl_2$ stock solution. No initial discolouration was observed and the solution was heated under inert atmosphere at 100 ºC, while absorption spectra were recorded at 30 min intervals.

*Experiments **III**, **IV** and **V*** :

22.4 mg (0.050 mmol) $Na_2[OsCl_6]$ was weighed off in a 50 cm^3 round bottom flask and dissolved in 10 cm^3 1M HCl. To this orange-yellow solution was added 10.0 cm^3 (***III***), or 20.0 cm^3 (***IV***) of the 0.050 mol/dm^3 $SnCl_2$ stock solution. For experiment (***V***), 20 cm^3 of the 0.50 mol/dm^3 $SnCl_2$ stock solution was added to the osmium salt solution. No initial discolouration was observed and the solution was heated under inert atmosphere at 100 ºC, while absorption spectra were recorded at 30 min intervals.

*Experiments **VI**, **VII** and **VIII*** :

To a 50 cm^3 round bottom flask containing 20 cm^3 of a 50.0 µg/ml $[OsCl_6]^{2-}$ solution was added 5 cm^3 (***VI***), 15 cm^3 (***VII***) or 30 cm^3 (***VIII***) of the 0.50 M $SnCl_2$ stock solution. The yellow coloured solutions were heated at 100 ºC under inert atmosphere, while absorption spectra were recorded at 30 min intervals.

*Experiment **IX*** :

20 cm^3 of the 0.50 mol/dm^3 $SnCl_2$ stock solution was added to 10 cm^3 1 M HCl containing 7.079 mg (0.0158 mmol) $Na_2[OsCl_6]$, and heated at 100 ºC under inert atmosphere. Absorption spectra were recorded at 30 min intervals

2.2.7 Solvent Extraction with N,N-dialkyl-N′-benzoylthioureas and $SnCl_2$

General experimental procedures of previous solvent extractions were followed, with incorporation of the reducing agent $SnCl_2$ and a phase transfer catalyst in the form of the commercially available Aliquat® 336. All extractions were performed using 100 cm^3 round-bottom flasks fitted with reflux condensers. Agitation was facilitated by means of magnetic stirring.

*Experiments **X** and **XI**:*

Varying volumes of $SnCl_2$ solution was added to 20 cm^3 of a 1.0 mol/dm^3 HCl solution containing osmium of concentration 50.0 μg/ml. For experiment ***X,*** 1.05 cm^3 of a 0.05 M $SnCl_2$ solution was added to the aqueous phase to effect a 10:1 tin to osmium ratio. Experiment ***XI*** required a 200:1 tin to osmium ratio, *viz.* adding 2.10 cm^3 of a 0.5 M $SnCl_2$ solution to the aqueous phase.

For both reactions the chloroform organic phase contained 4.6 mg (0.01577 mmol) *N*,*N*-dibutyl-*N′*-benzoylthiourea, affording a 3:1 ligand to metal ratio. The bilayer solutions were agitated for 3 h at 100 °C. Absorption spectra of both the aqueous and organic phases were recorded.

*Experiments **XII** and **XIII**:*

Same experimental procedure as mentioned above was followed, with 200:1 tin to osmium ratio for both reactions. To both organic phases was added 19.12 mg (0.04731 mmol) Aliquat® 336, its concentration in solution was equal to nine times that of osmium. For reaction ***XII*** the organic phase contained 9.2 mg (0.03154 mmol) *N*,*N*-dibutyl-*N′*-benzoylthiourea, while that of reaction ***XIII*** contained zero ligand. The bilayer solutions were agitated for 3 h at 100 °C. Absorption spectra of both the aqueous and organic phases were recorded.

*Experiments **XIV** and **XV**:*

To 10 cm^3 of a 1.0 mol/dm^3 HCl solution containing 7.1 mg (0.01577 mmol) $Na_2[OsCl_6]$ was added 20 cm^3 of a 0.5 mol/dm^3 $SnCl_2$ solution, affording an osmium concentration of 50.0 μg/ml and $SnCl_2$ concentration of 0.333 mol/dm^3. To 30 cm^3 of chloroform was added 13.8 mg (0.04731 mmol) *N*,*N*-dibutyl-*N*′-benzoylthiourea, resulting in a 3:1 ligand to metal ratio. For reaction ***XV*** the organic phase also contained 57.4 mg (0.1419 mmol) Aliquat® 336, its concentration was nine times that of the initial osmium concentration. The bilayer solutions were agitated for 3 h at 100 °C. Absorption spectra of both the aqueous and organic phases were recorded.

*Experiment **XVI:***

Same experimental conditions followed as for reaction ***XV***, with the organic phase containing 41.5 mg (0.1419 mmol) *N*,*N*-dibutyl-*N*′-benzoylthiourea, affording a 9:1 ligand to metal ratio. As before agitation occurred at 100 °C for 3 h, with absorption spectra recorded upon completion.

2.2.8 Crystal structure determination of $[OsCl_6]^{2-}$ - PTC ion-pair

A suitable crystal was mounted on a thin glass fibre and coated in silicone-based oil to prevent decomposition. Data were collected on a Nonius Kappa CCD diffractometer using graphite monochromated Mo Kα radiation (λ = 0.7107 Å) with a detector to crystal distance of 45 mm. A total of either 453 oscillation frames were recorded, each of width 1º in ϕ, followed by 551 frames of 1° width in ω (with κ ≠ 0). Crystals were indexed from the first ten frames using the DENZO package [8] and positional data were refined along with diffractometer constants to give the final cell parameters. Integration and scaling (DENZO, Scalepack [8]) resulted in unique data sets corrected for Lorentz-polarisation effects and for the effects of crystal decay and absorption by a combination of averaging of equivalent reflections and an overall volume and scaling correction. Crystallographic data are contained in ***Table 2.9***. The structures were solved using SHELXS-97 [9] and developed *via* alternating least squares cycles and Fourier difference synthesis (SHELXL-97 [9]) with the aid of the interface program X-SEED [10]. All non-hydrogen atoms were modelled anisotropically. Hydrogen atoms were assigned an isotropic thermal parameter 1.2 times that of the parent atom (1.5 times for terminal atoms) and allowed to ride on their parent atoms

2.3 Results and Discussion

2.3.1 Analysis of standard $[OsCl_6]^{2-}$ solutions

The behaviour of standardised $[OsCl_6]^{2-}$ solutions in hydrochloric acid matrix were recorded by means of UV-Vis spectrophotometry. Since solvent extraction investigations dictated the use of an analysis method for metal concentration determinations, the chosen method was UV-Vis absorption spectrophotometry. Therefore, calibration curves were constructed using standard solutions of varying concentrations.

All solutions were prepared freshly, using different mineral acid matrices. A 1cm quartz cuvette contained the standards, while all absorbances were recorded at a wavelength of 371 nm.

1 M HCl		2 M HCl		5 M HCl	
Conc (µg/ml)	**Absorbance**	**Conc (µg/ml)**	**Absorbance**	**Conc (µg/ml)**	**Absorbance**
5.00	0.170709	5.00	0.171713	5.00	0.172523
10.0	0.363926	10.0	0.339046	10.0	0.346942
20.0	0.739513	20.0	0.678709	20.0	0.708959
30.0	1.103452	30.0	1.010275	30.0	0.895814
40.0	1.452676	40.0	1.339648	40.0	1.190757
50.0	1.822961	50.0	1.677087	50.0	1.720965

Table 2.2. **Absorbance maxima of $[OsCl_6]^{2-}$ standard solutions (λ_{max} = 371 nm)**

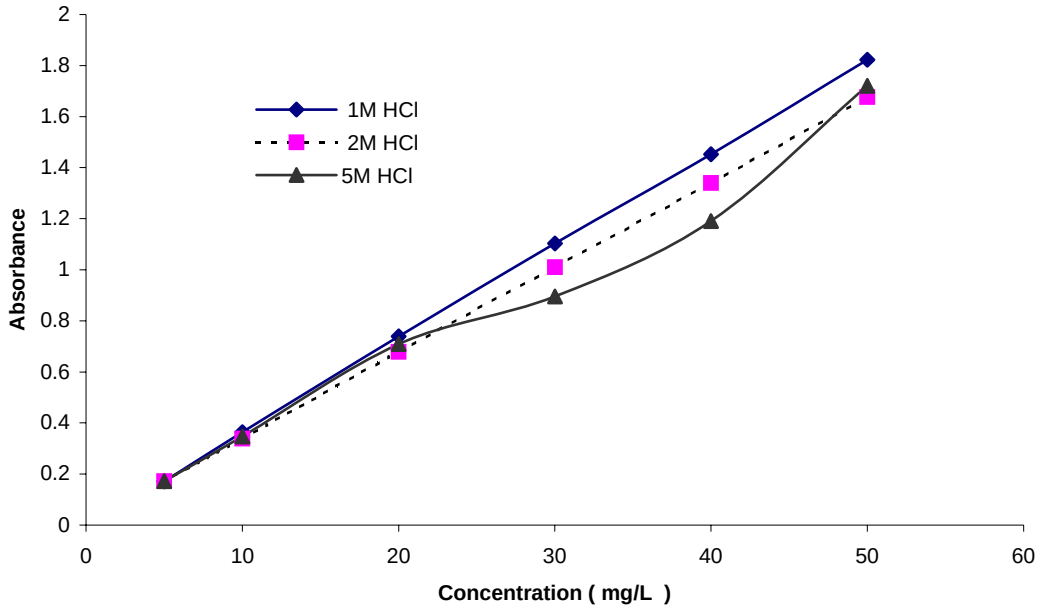

Fig. 2.1. **Calibration curves for 1M and 2M HCl matrices**

For the 5M HCl matrix no linear calibration curve could be constructed. The determination of absorbances in 5M HCl were determined three times with the same results. So far no explanation could be given for the deviation from linearity, but the most probable cause could be speciation changes that were brought about by the highly concentrated chloride milieu of the mineral acid matrix.

Nearly linear calibration curves for the other two matrices prompted their exclusive use in the solvent extraction studies :

- 1 M HCl : $y = 0.0366x - 0.0022$; $R^2 = 0.9998$
- 2 M HCl : $y = 0.0334x + 0.0063$; $R^2 = 0.9999$

2.3.2 Speciation changes of $[OsCl_6]^{2-}$ in HCl matrices

The stability of the $[OsCl_6]^{2-}$ species in different mineral acid matrices was investigated. Hydrochloric acid concentrations ranged from 0.05 M - 10 M HCl. Standard solutions of $[OsCl_6]^{2-}$ in matrices of varying concentration were monitored on a daily basis by means of UV-Vis absorption spectrophotometry.

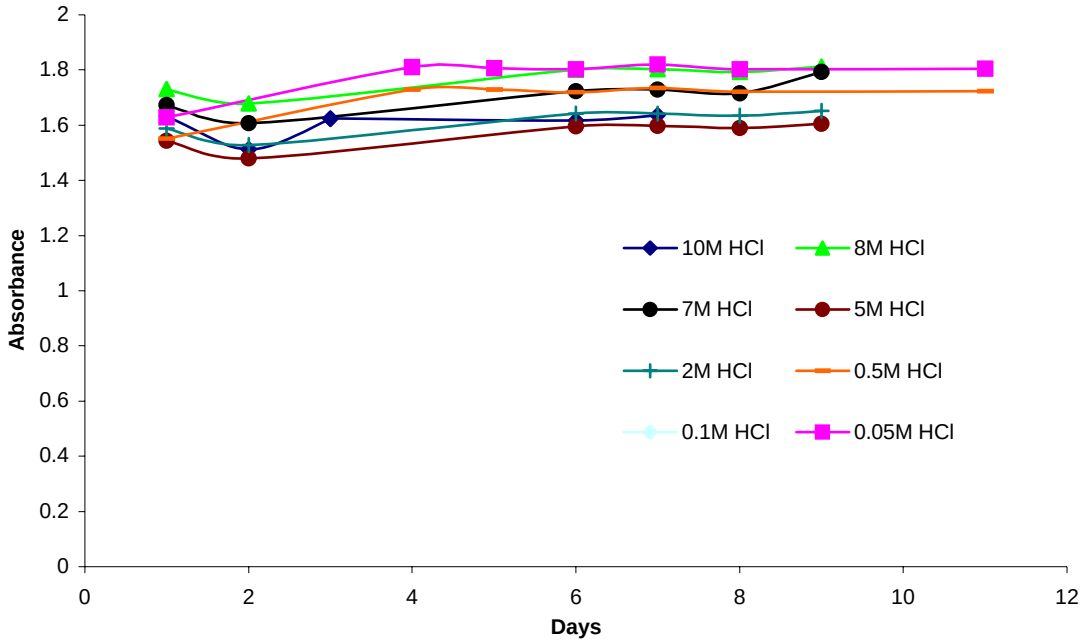

Fig. 2.2. **Variation of $[OsCl_6]^{2-}$ absorbance over time (HCl matrix). Absorption maxima recorded at λ_{max} = 371 nm**

All of the solutions seemed to be quite stable while being stored at room temperature devoid of any direct sunlight. Hydrochloric acid solutions below 0.1 mol/dm^3 were found to contain small amounts of fine black precipitates after three weeks of standing under the aforementioned environmental conditions. The precipitates are most probably metal hydroxides or metal oxides that form very gradually in a weakly acidic milieu. The apparent stability of the $[OsCl_6]^{2-}$ species in hydrochloric acid solution substantiates the findings made by Miano, *et al,* [11], who concluded that aquation to $[Os(H_2O)Cl_5]^-$ only occurs at elevated temperatures (80 ºC), with the rate of aquation being 3.5×10^{-6} s^{-1}.

The same experiment was repeated for LiCl matrices of the following concentrations: 1.0, 0.5 and 0.1 mol/dm^3. After standing for three days, under the same conditions as for the hydrochloric acid solutions, the LiCl solutions contained a large amount of flocculent black precipitate. An accompanying decrease in the characteristic absorption maxima of $[OsCl_6]^{2-}$ verified the suggestion that it is in fact osmium metal or insoluble metal oxides that have precipitated from the solution as a result of either aquation, hydrolysis or possible reduction.

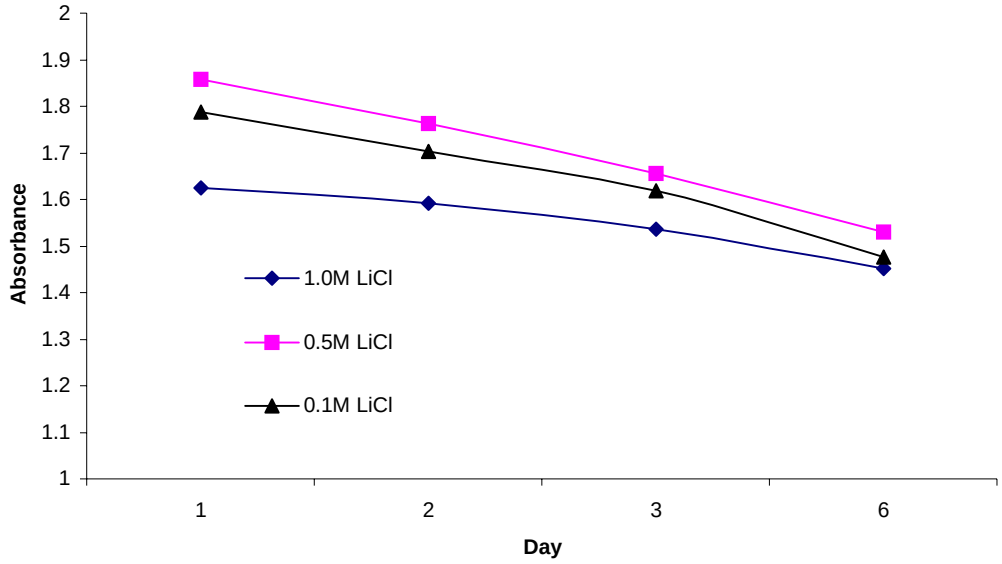

Fig. 2.3. **Variation of $[OsCl_6]^{2-}$ absorbance over time (LiCl matrix). Absorption maxima recorded at λ_{max} = 371 nm**

2.3.3 Solvent extraction with N,N-dibutyl-N'-benzoylthiourea (DBBT) at room temperature

An aqueous hydrochloric acid solution (1.0 and 2.0 mol/dm^3) containing $[OsCl_6]^{2-}$ was contacted with a chloroform solution containing the DBBT ligand (in 3 times excess w.r.t. osmium). The bilayer was stirred continuously for a period of 24 h at room temperature, whereby the absorption spectrum of the aqueous solution was recorded. It was noted that after the period of agitation the aqueous layer still possessed a bright yellow colour, while the organic phase was still clear and colourless. An initial presumption would be that no extraction occurred. Osmium content of the aqueous phase was determined against a previously constructed calibration curve.

Solution	Absorbance (λ = 371 nm)	Initial Os conc (µg/ml)	Resulting Os conc (µg/ml)
1M HCl	1.794043	50.0	49.1
2M HCl	1.620025	50.0	48.3

Table 2.3. **Results of extraction with 3 times excess of DBBT (room temperature).**

Results indicate that no significant extraction of osmium into the organic phase had occurred. Concentration values obtained from the absorption spectra are extremely close to the initial osmium concentration of 50.0 µg/ml. Since the absorption spectra of the aqueous phases still exhibited the

characteristic absorption profile of the $[OsCl_6]^{2-}$ species, one may conclude that the $[OsCl_6]^{2-}$ species underwent no speciation changes while being contacted with the ligand containing organic phase.

2.3.4 Varying N,N-dibutyl-N'-benzoylthiourea to osmium ratios and incorporation of a Phase Transfer Catalyst (PTC)

Unconvincing results from section *2.3.3* prompted the incorporation of elevated temperatures in future solvent extraction experiments. Comparative investigations done by König *et al* [12] were also performed at temperatures ranging from 60°-100°C for extractions of platinum group metals. Experimental conditions were as indicated in the experimental section, with the amount of ligand being varied from 3, 12 and 24 times excess with regard to osmium present in the aqueous phase.

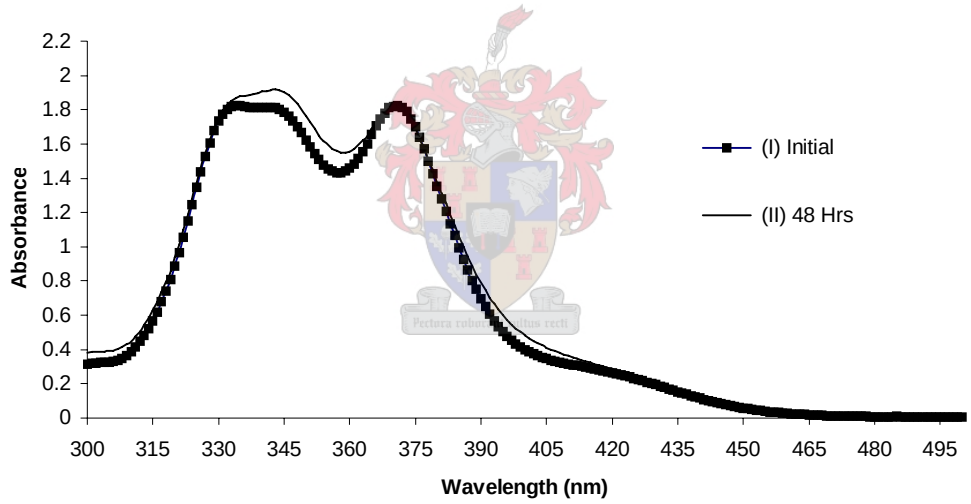

Fig. 2.4. **Solvent extraction with 3:1 DBBT to osmium ratio. Absorption spectra of aqueous phases: (I) initial solution before agitation (50 ppm $[OsCl_6]^{2-}$), (II) solution after 48 h agitation at 80 °C**

For the case of the 3:1 ligand to osmium ratio, it is evident from ***Fig. 2.4.*** that the absorption spectrum of the aqueous phase did not change significantly after the period of agitation. The concentration of osmium (as $[OsCl_6]^{2-}$) in the aqueous phase was calculated to be 49.43 µg/ml, compared to the initial concentration of 50.0 µg/ml. Allowing for experimental errors one could safely assume that no significant extraction to the organic phase had occurred. More interesting though is the increase in absorbance at a wavelength of 343 nm. This points towards an increase in the amount of $[Os(H_2O)Cl_5]^-$ in solution, due to aquation brought upon by continued heating at elevated temperatures, as discovered by Miano, *et al.* [11].

With reference to the work of König, *et al.* [3] it was decided to increase the amount of ligand with respect to osmium metal in solution. Solvent extractions were performed under the same experimental conditions as for the previous experiment, but ligand to metal ratios were increased to 12:1 and 24:1. Absorption spectra were recorded upon completion of agitation periods.

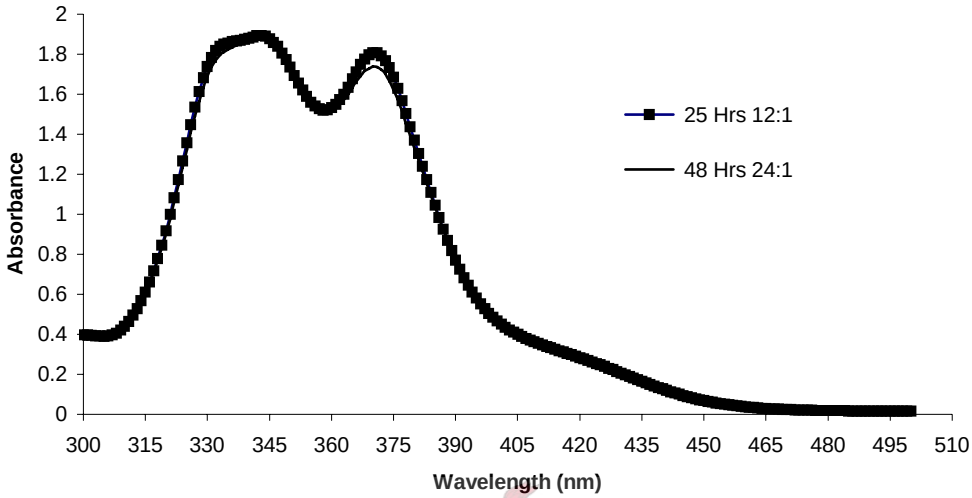

Fig. 2.5. **Solvent extraction with 12:1 and 24:1 DBBT to osmium ratios. Absorption spectra of aqueous phases recorded after indicated period of heating at 80 °C**

Results were much the same as for the 3:1 ligand to osmium ratio. Aqueous phase absorption spectra still exhibited the characteristic absorption profile of the $[OsCl_6]^{2-}$ species, with a very slight change in absorbance values compared to initial absorbance values.

Ratios	Absorbances				Conc (ppm)
	λ_{max} = 371 nm		λ_{max} = 343 nm		
	Before	After	Before	After	After
3:1	1.809	1.807	1.812	1.917	49.43
12:1	1.823	1.807	1.812	1.893	49.43
24:1	1.823	1.735	1.812	1.890	47.41

Table 2.3. **Absorbances of aqueous phases at characteristics wavelengths before and after agitation periods.**

Absorbances measured at 343 nm showed a slight increase after the heating and agitation periods. As previously mentioned, this is probably due to an aquation process occurring in the aqueous phase, giving rise to the $[Os(H_2O)Cl_5]^-$ species, which has its characteristic absorption maxima at 343 nm. This line of reasoning would explain the slight decrease in absorbance recorded at 371 nm, indicating "loss" of the $[OsCl_6]^{2-}$ species due to formation of $[Os(H_2O)Cl_5]^-$ and Cl^-.

As before, absorption spectra of the organic chloroform phases showed no presence of osmium precipitate in any form whatsoever.

Solvent extraction with DBBT while utilising a phase transfer catalyst

In order to facilitate the interaction of $[OsCl_6]^{2-}$ with the ligand in the organic chloroform phase, it was decided to incorporate a Phase Transfer Catalyst (PTC) into the solvent extraction mechanism. The PTC is usually a quartenary ammonium cation, containing long-chain aliphatic groups in order to render it highly lipophillic. In the aqueous phase, the bulky PTC will form a loose ion-pair with the anion to be transferred, and distribute between the aqueous and organic phases. Once in the organic phase, the metal chloro complex is now available for further chemical reactions. An excellent review of industrial applications of PTCs has recently been published [13]. Initial trial solvent extractions were performed with tetrabutylammonium tetrafluoroborate (TBATFB), in order to ascertain the viability of using these transfer catalysts. Later on a commercially available PTC, Aliquat® 336, was incorporated into solvent extraction studies.

In order to obtain information on the behaviour of TBATFB in the solvent extraction milieu, a preliminary experiment was performed as follows:

20 cm^3 of an aqueous 1M HCl solution containing $[OsCl_6]^{2-}$ (50.0 µg/ml) and 65.9 mg TBATFB (0.01 mol/dm^3) was contacted with 20 cm^3 of chloroform containing a three times excess of DBBT (w.r.t. osmium). The bilayer solution was shaken at room temperature for a period of 15 minutes.
Upon completion of the period of agitation it was noted that the initial intense bright yellow colour of the aqueous phase had changed to a dull light yellow colour, while the initial clear and colourless appearance of the organic phase changed to a murky yellow colour. Absorption spectra of the aqueous phase were recorded before shaking, and also after extraction.

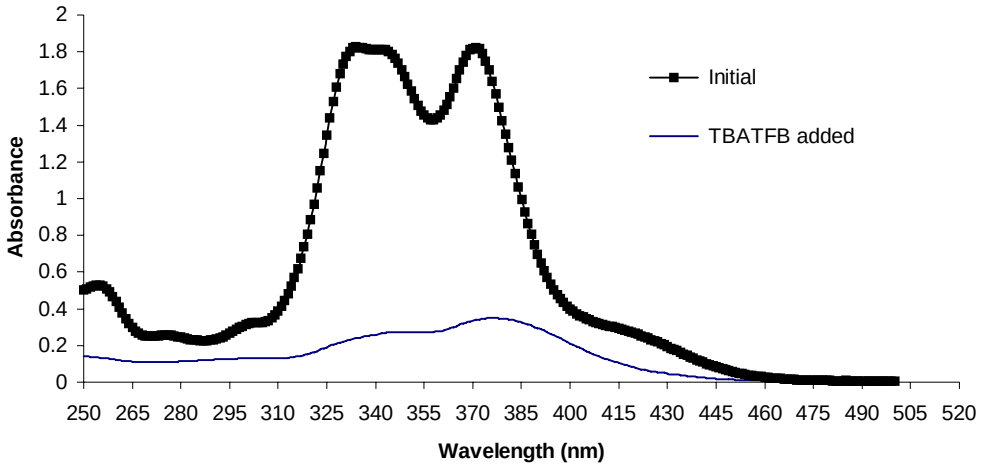

Fig. 2.6. **Solvent extraction with 3:1 DBBT to osmium ratio, 0.01 M TBATFB. Absorption spectra of aqueous phases before and after extraction.**

The spectrum of the initial aqueous phase exhibited the characteristic absorption profile of the $[OsCl_6]^{2-}$ species (λ_{max} = 334, 371 nm), but during the period of agitation the absorption spectrum underwent a remarkable change. Absorbance values were greatly reduced, indicating a decrease in metal concentration, while the absorbance maxima were now located at λ_{max} = 347, 375 nm, possibly indicating the existence of the osmium-TBATFB ion-pair. It was therefore plausible to continue the use of the PTC in future solvent extraction studies.

Encouraging results obtained from the use of a PTC prompted a repeat of the experiment just mentioned, but at elevated temperatures and for a period of 24 h. The result is displayed in ***Fig. 2.7***.

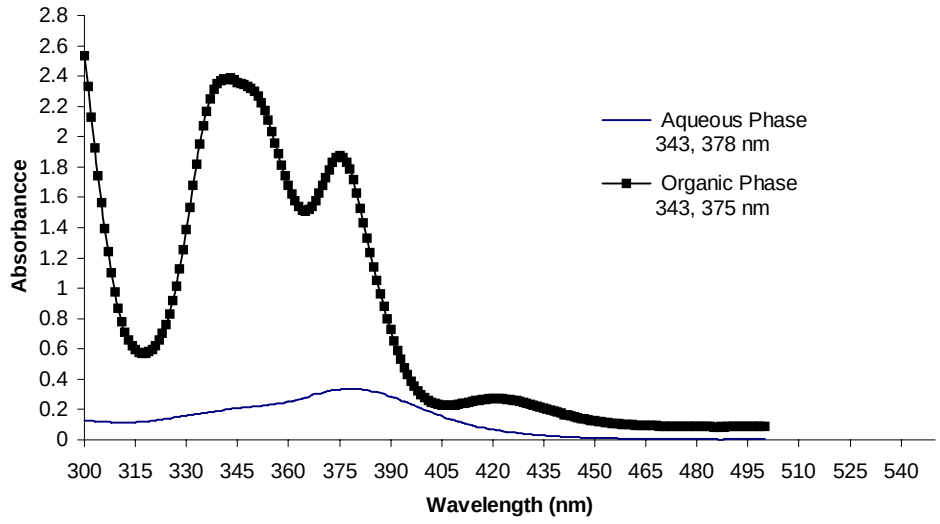

Fig. 2.7. **Solvent extraction with 3:1 DBBT to osmium ratio, 0.01 M TBATFB, heating at 80 °C for 24 h. Absorption spectra of aqueous and organic phases.**

Information obtained from the absorption spectra once again pointed towards a decrease of osmium in the aqueous phase, with a corresponding increase of osmium concentration in the organic phase. Absorption maxima were at the same wavelengths as before, possibly indicating the presence of the osmium-TBATFB ion-pair in the organic phase.

For the following experiments, the hydrochloric acid concentration was changed to 2.0 mol/dm^3, while it was decided to attempt solvent extraction with another ligand, in this case *N,N*-diethyl-*N'*-benzoylthiourea (DEBT). It was hoped that the change in ligand could lead to a change in the absorption profile of the organic phase after the period of heating, therefore possibly indicating interaction of osmium metal with the ligand.

Experimental conditions were the same as before, with a 3:1 ligand to metal ratio, and a TBATFB concentration of 0.01 mol/dm^3. The bilayer solution was agitated at 80 °C for a period of 24 h. The results of extraction with DEBT is compared to that of extraction with DBBT (3:1 ligand to metal ratios) (***Fig. 2.8***).

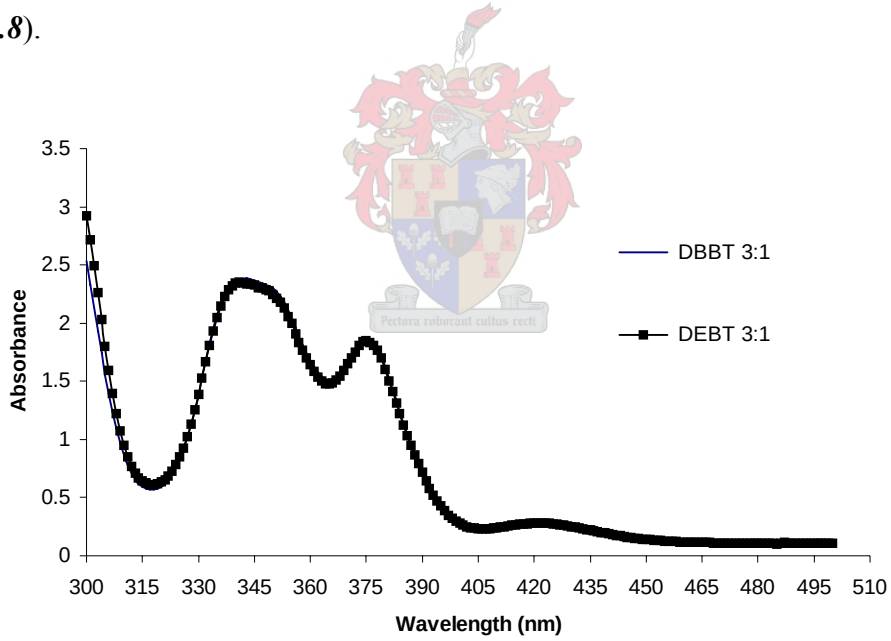

Fig. 2.8. **Comparative results of solvent extraction with DBBT and DEBT (3:1 ligand to metal). Absorption maxima of organic phases: DBBT (343, 375 nm); DEBT (341, 375 nm)**

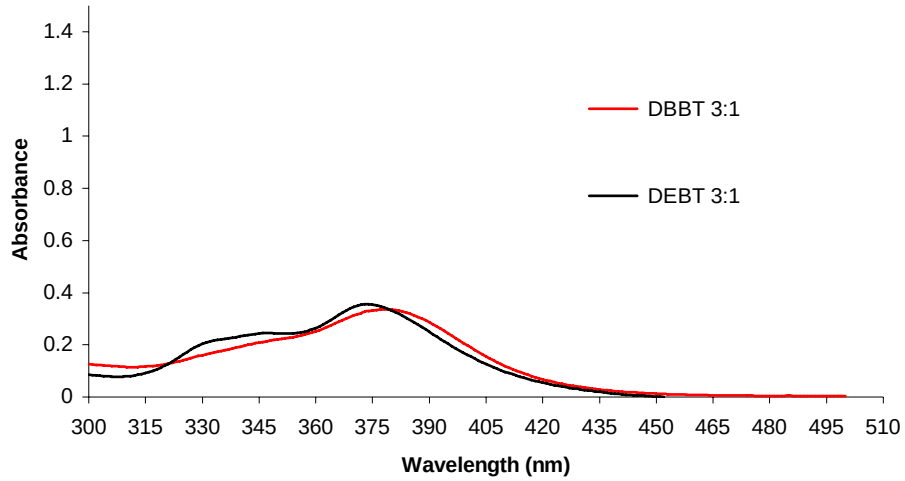

Fig. 2.9. **Comparative results of solvent extraction with DBBT and DEBT (3:1 ligand to metal). Absorption maxima of aqueous phases: DBBT (343, 378 nm); DEBT (347, 374 nm)**

From ***Fig. 2.8, 2.9*** it is clear that solvent extraction with either DBBT or DEBT leads to the same results. Absorption spectra of the organic phases do not deviate much from each ligand, and the absorbance values are comparable (*cf.* ***Fig. 2.10*** where no ligand was present in the reaction mixture). One concludes then that the type of ligand has no effect on the transfer of osmium to the organic phase. Moreover, it seems that there is no reaction between metal and ligand in the organic phase, since the absorption spectrum is the same as for the case where no ligand is present in solution.

Finally, the solvent extraction experiment was repeated as before, but with a 6:1 DBBT to osmium ratio. A phase transfer catalyst was added (0.01 mol/dm^3 TBATFB), and the solution was agitated at 80 °C for a period of 24 h. Upon completion the absorption spectra of aqueous and organic phases were recorded (***Fig. 2.10***). In an attempt to substantiate the conjectures made in the previous paragraphs, another extraction experiment was undertaken, but without any ligand present in the chloroform phase. As before, the bilayer solution was agitated for 24 h at 80 °C. ***Fig. 2.10*** clearly illustrates that comparative results were obtained whether any ligand was present in the chloroform layer or not. Results therefore indicate that under the mentioned experimental conditions, the ligand present in the chloroform phase did not contribute towards extraction of the metal into the organic phase.

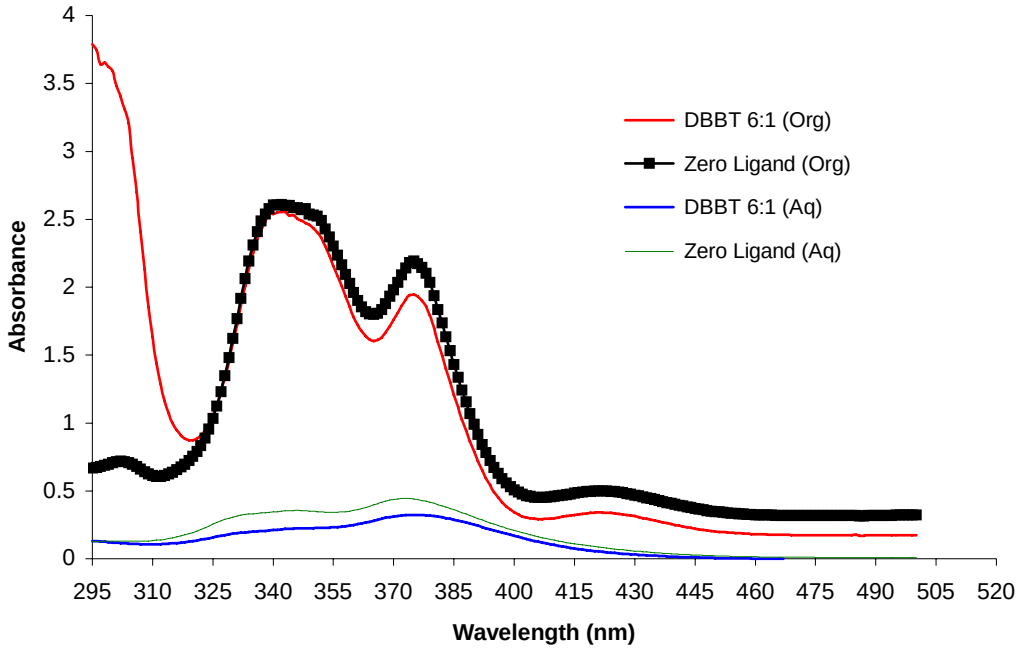

Fig. 2.10. **Comparative results of solvent extraction with and without the ligand (6:1 ligand to metal) present. Absorption spectra of aqueous and organic phases.**

2.3.5 Effect of phase transfer catalyst concentration

Experimental results are shown for the case where ligand (as DBBT) was present in the organic phase. The same results were obtained for the case where no ligand was present in solution (refer to ***Fig. 2.10***).

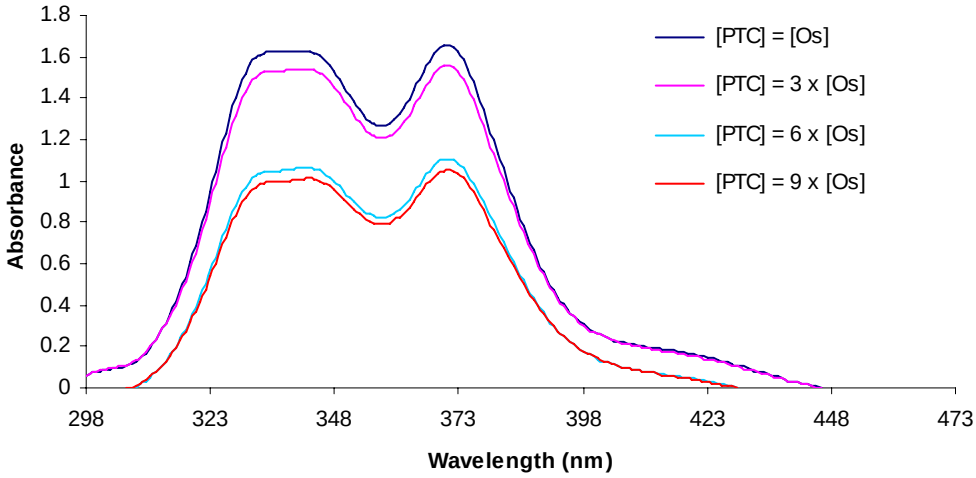

Fig. 2.11. **Variation of phase transfer catalyst concentration w.r.t. initial osmium concentration. Ligand present as three times excess. Absorption spectra of aqueous phases (λ_{max} = 343, 371 nm).**

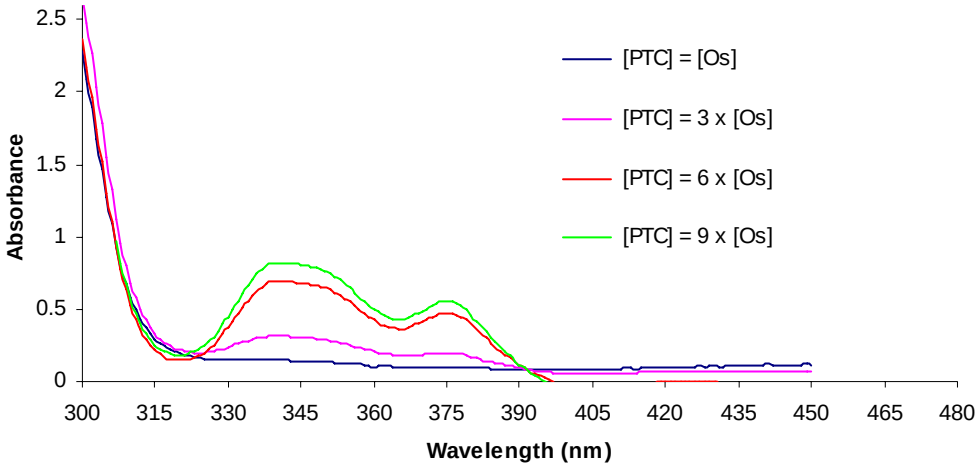

Fig. 2.12. **Variation of phase transfer catalyst concentration w.r.t. initial osmium concentration. Ligand present as three times excess. Absorption spectra of organic phases (λ_{max} = 341, 375 nm).**

From ***Fig. 2.11, 2.12*** it is quite evident that a reduction in the absorbance of the characteristic $[OsCl_6]^{2-}$ profile occurs with increasing PTC concentration, while the characteristic absorption profile of the Os-PTC ion-pair present in the organic phase increases in absorbance. ***Fig. 2.13*** contains the combined results of the aqueous and organic phases, with the ligand present or absent in the organic phase. Although there are slight differences in absorbances, one cannot concretely deduce that the ligand has any effect on the extraction process, since the absorption profiles are almost the same, and absorption maxima occur at the same wavelengths. Moreover, the absorbance values are quite high. At such high absorbance values the experimental error increases and deviates from Beer-Lambert absorbance. ***Fig. 2.14*** illustrates the distributions between aqueous and organic phases as a function of PTC concentration, and to what extent the presence of ligand in the organic phase influences the distributions. Therefore, it seems that the PTC quantitatively transports the $[OsCl_6]^{2-}$ species from the aqueous to the organic phase in the form of an ion-pair.

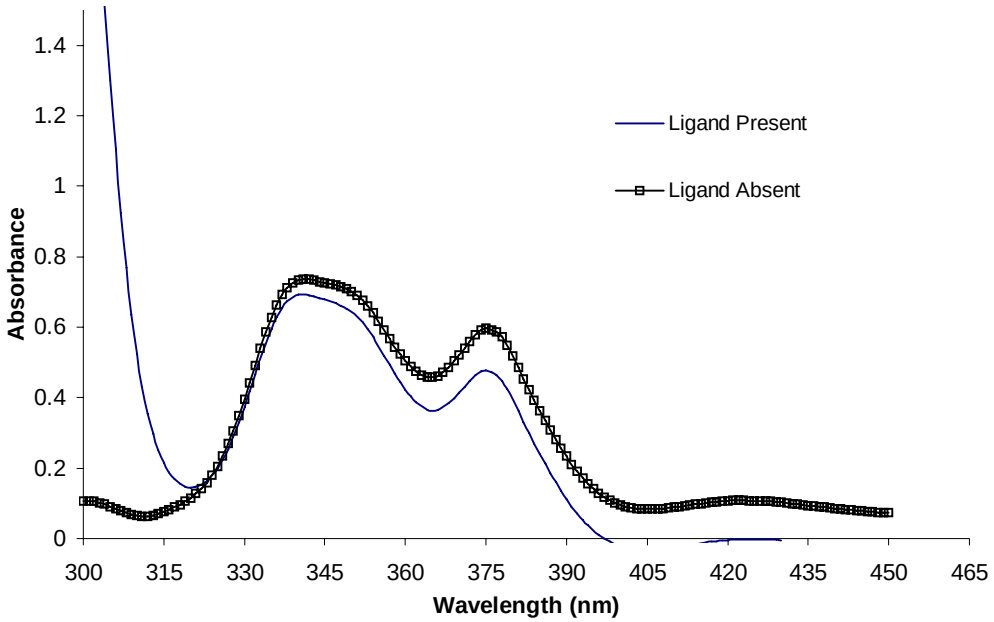

Fig. 2.13. **Effect of ligand presence on extraction with PTC. Comparative results for organic phases, where the PTC concentration is equal to six times the initial osmium concentration. Ligand present in 3:1 ration w.r.t. osmium. Absorption maxima at 341, 375 nm.**

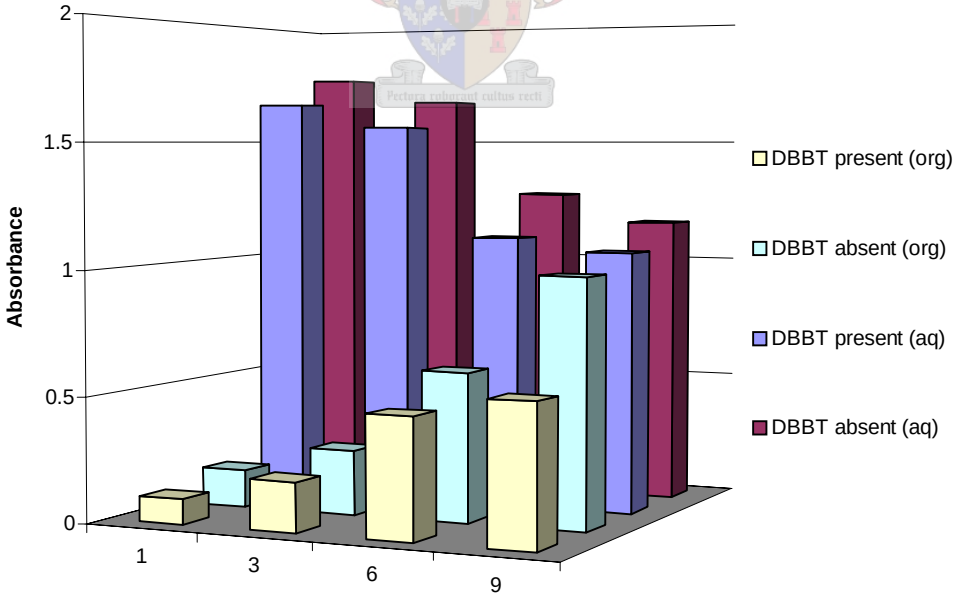

Fig. 2.14. **Effect of ligand presence on extraction with PTC. Combined results of aqueous and organic phases.**

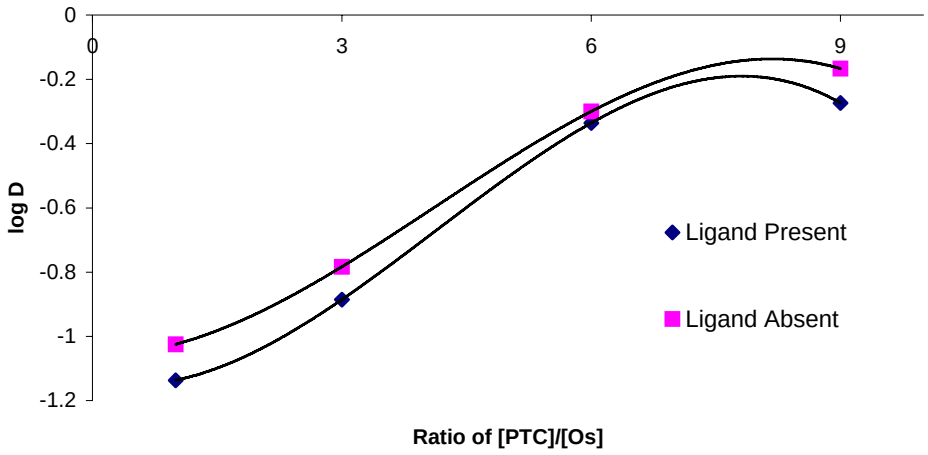

Fig. 2.15. **Distribution of osmium between organic and aqueous phases as function of PTC concentration. Effect of ligand presence in organic phase.**

Results from all the previous experiments pointed towards the fact that osmium, in its quadrivalent form of $[OsCl_6]^{2-}$ is too inert to react with the ligand once present in the organic phase under these conditions, and that extraction of osmium only takes place via PTC ion pairing.

2.3.6 Reduction of Os(IV) species with $SnCl_2$

It was decided to investigate the reduction of the tetravalent osmium to the possibly less inert trivalent or divalent state [14]. The chemistry of platinum group metals with $SnCl_2$ have been studied exhaustively [15], with the related study of osmium being rather dated and not very clear [16]. Therefore a systematic investigation into the reduction of osmium with $SnCl_2$ was embarked upon, with a view towards utilising the possible reduction product(s) in the solvent extraction process.

A set of experiments with particular parameters were drawn up and performed, afterwards being interpreted systematically in order to ascertain the prerequisites required for a controlled and reproducible reduction process. The following table summarises the list of different experiments as they were set out in the experimental section *2.2.6:*

Exp	$SnCl_2$ (mmol)	$[SnCl_2]$ (mol/dm^3)	Os (mmol)	[Os] (μg/ml)	Sn:Os
I	0.1	0.00830	0.1	1585	1:1
II	0.3	0.0188	0.1	1188	3:1
III	0.5	0.0250	0.05	475.7	10:1
IV	1.0	0.0333	0.05	317.0	20:1
V	10	0.333	0.05	317.0	200:1
VI	2.5	0.100	0.00526	40.00	476:1
VII	7.5	0.214	0.00526	28.57	1427:1
VIII	15	0.300	0.00526	20.00	2850:1
IX	10	0.333	0.0158	100.0	634:1

Table 2.4. **Summary of $SnCl_2$ reduction experiments. The amount of $SnCl_2$ w.r.t. osmium was varied in order to obtain a single reduced osmium species.**

Experiments ***I-IV*** all exhibited similar changes in their respective absorption spectra. The initial spectrum of two absorption bands (371, 334 nm) changed to an intermediate which had only one absorption band at 375 nm (see ***Fig. 2.16***, which illustrates the result for experiment ***III***). This intermediate species was usually observable after a particular duration of heating. As the Sn(II) to Os(IV) ratio increased, the heating time needed to observe the intermediate was reduced accordingly:

	Sn : Os	λ_{max} (nm)	Time (min)
I	1 : 1	374	90
II	3 : 1	375	50
III	10 : 1	375	30
IV	20 : 1	374	20

Table 2.5. **Reaction time required for appearance of intermediary species (max absorbance at 375 nm)**

Interestingly, this intermediate species was only present in solution for a few minutes, converting back into a species which once again afforded two absorption bands, with maxima at 370 and 344 nm. (***Fig. 2.16***). The blue-shift of the original 334 nm band to a 344 nm band may well be ascribed to the formation of the mono-aquo substituted species $[OsCl_5(H_2O)]^-$. Conditions under which the reaction was performed certainly suggests the formation of the pentachloro complex. In a kinetic study by Miano, *et al.* [11] it was reported that in HCl medium of pH ≤ 5 the rate of aquation was 3.5×10^{-6} sec^{-1} at 80 ºC. Therefore it seems that a tin-containing osmium complex intermediate exists

for a brief period, where after it reverts back to $[OsCl_6]^{2-}$ and $[OsCl_5(H_2O)]^-$, possibly due to subsequent reoxidation. The exact ratio of the two products is unknown at the present moment.

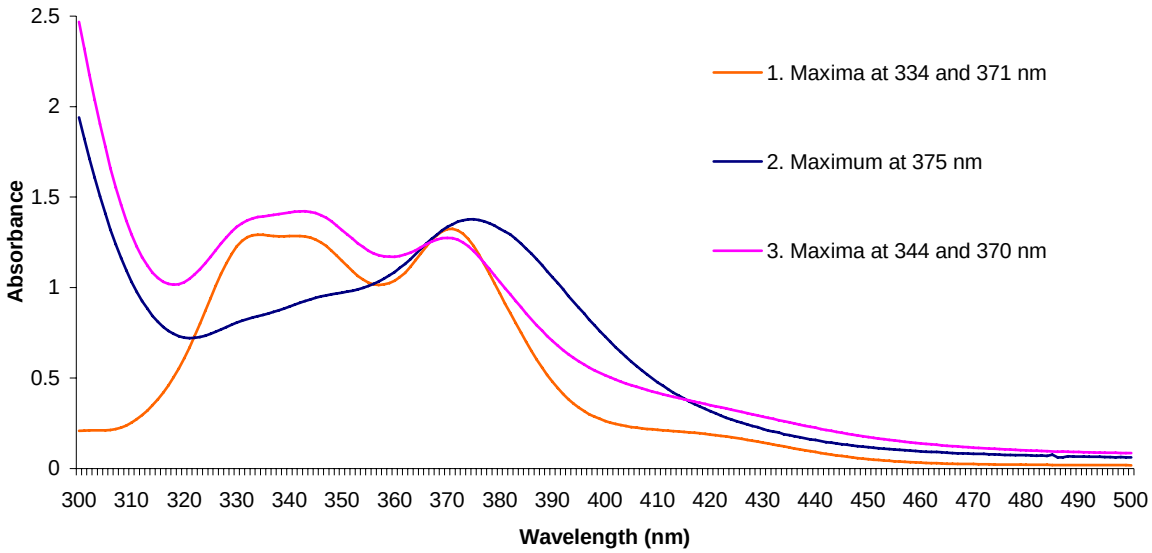

Fig. 2.16. **Reaction of $[OsCl_6]^{2-}$ with $SnCl_2$, with Sn(II) : Os(IV) ratio of 10 : 1. Absorption spectra recorded at following heating intervals : (1) 0 min, (2) 30 min and (3) 75 min**

The seemingly unsuccessful results obtained from experiments ***I-IV***, for which the Sn:Os ratio was relatively low, prompted the use of a large excess of $SnCl_2$ with regard to osmium in solution. Thus, for experiment ***V***, an arbitrary ratio of 200:1 was chosen, with the rest of the conditions being the same as for experiments ***III*** and ***IV***.

Even after 15 minutes of heating a single absorption band at 378 nm was observed. A further heating period of 15 min resulted in the formation of a species with a single absorption band at 383 nm. This particular absorbance was observed for consecutive heating periods, up to a total heating time of 90 min. The single absorbance at 383 nm is in accordance with previous reduction studies done by Antonov, *et al.* [16], and was observed to be stable in solution for up to two weeks.

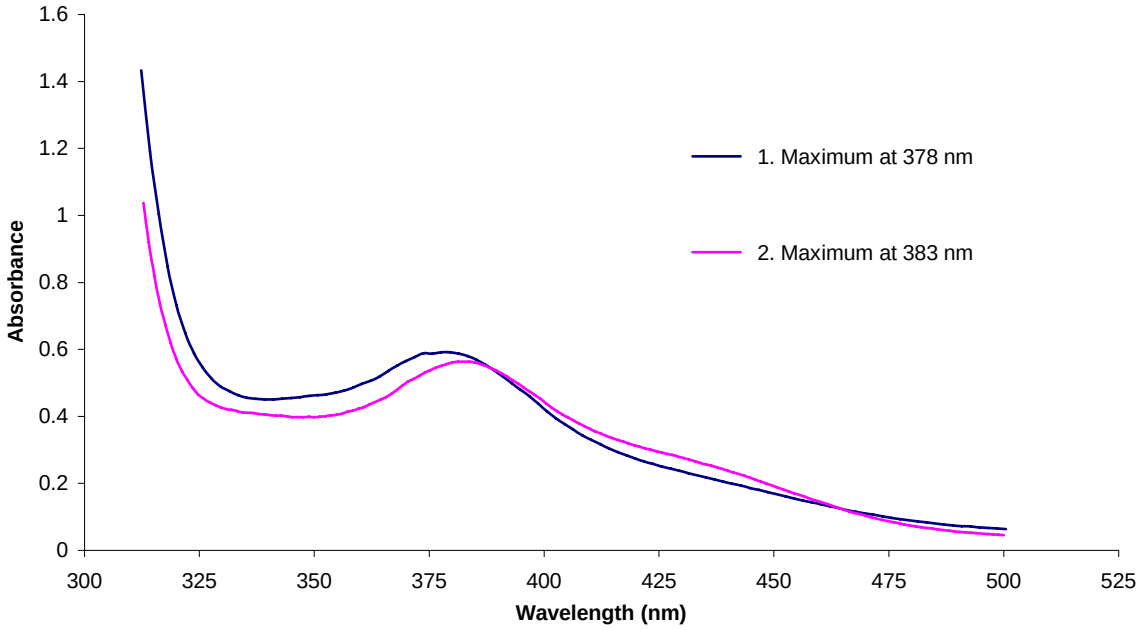

Fig. 2.17. **Reaction of $[OsCl_6]^{2-}$ with $SnCl_2$ in Sn(II) : Os(IV) ratio of 200 : 1. Absorption spectra recorded at following heating intervals : (1) 15 min, (2) 90 min**

Results from experiment ***V*** confirmed the observations made by Balcerzak [17], that a quantitative conversion of $[OsCl_6]^{2-}$ to $[Os(SnCl_3)_5Cl]^{4-}$ for $[SnCl_2] \geq 0.3$ M appears to occur. In the study of Balcerzak it was also noted that for $SnCl_2$ concentrations in the range 1×10^{-5} - 1×10^{-2} M a reduction of Os(IV) to Os(II) takes place (ie. a decrease in the characteristic absorption band of $[OsCl_6]^{2-}$); while for $SnCl_2$ concentrations above 5×10^{-2} M the gradual formation of $[Os(SnCl_3)_5Cl]^{4-}$ was observed.

Positive results from experiment ***V*** prompted further investigations into the effect of $SnCl_2$ concentration on the reduction and complex formation processes. Consequently experiments ***VI-VIII*** were performed:

	$SnCl_2$ conc (mol/dm^3)	Os conc (µg/ml)	Sn : Os	UV-Vis spectra (nm)
VI	0.100	40.0	476:1	371 (weak shoulder)
VII	0.214	28.6	1427:1	376 (weak shoulder)
VIII	0.300	20.0	2850:1	378 (shoulder)

Table 2.6. **Experimental experiments for *VI - VIII*, with Sn:Os ratios exceeding 200:1. Absorption spectra recorded after 60 min heating at 100 ºC.**

Results from experiments ***VI*** and ***VII*** indicate that a reduction process takes place, i.e. the original absorption band of $[OsCl_6]^{2-}$ disappeared almost completely, with only very weak shoulders

observable at 371 and 376 nm respectively (***Fig. 2.18***). Experiment ***VIII*** resulted in the formation of a species with a single well-defined absorption band at 378 nm (see ***Fig. 2.19***).

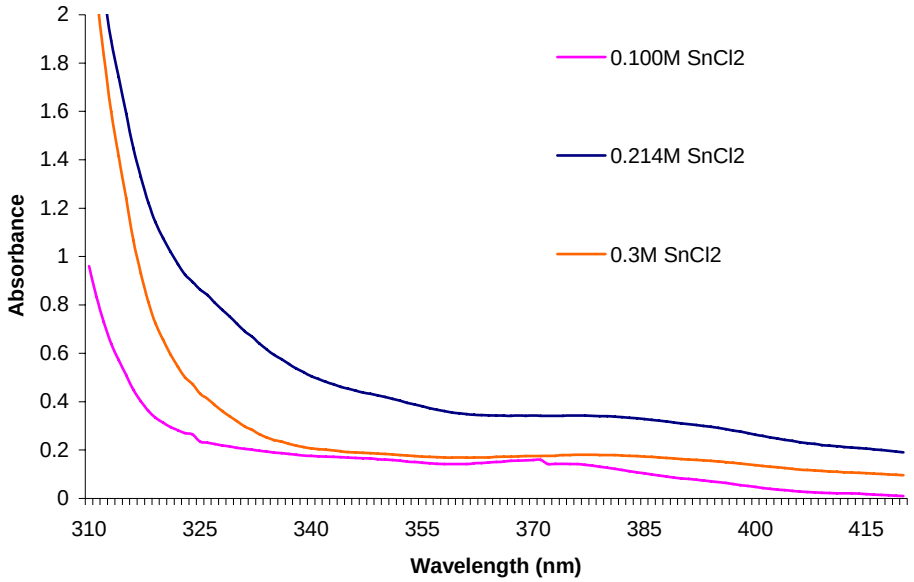

Fig. 2.18. **Reaction of $[OsCl_6]^{2-}$ with $SnCl_2$ concentrations of varying molarity. Absorption spectra recorded after 60 min heating at 100 °C**

The result obtained from experiment ***VIII*** was not quite expected, since experimental conditions were almost identical to that of experiment ***V*** (w.r.t. the $SnCl_2$ concentration). Therefore, a single absorbance peak at 383 nm was expected, rather only a weak shoulder at 378 nm resulted (see ***Fig. 2.19*** for a comparison of the absorption spectra of experiments ***V*** and ***VIII***).

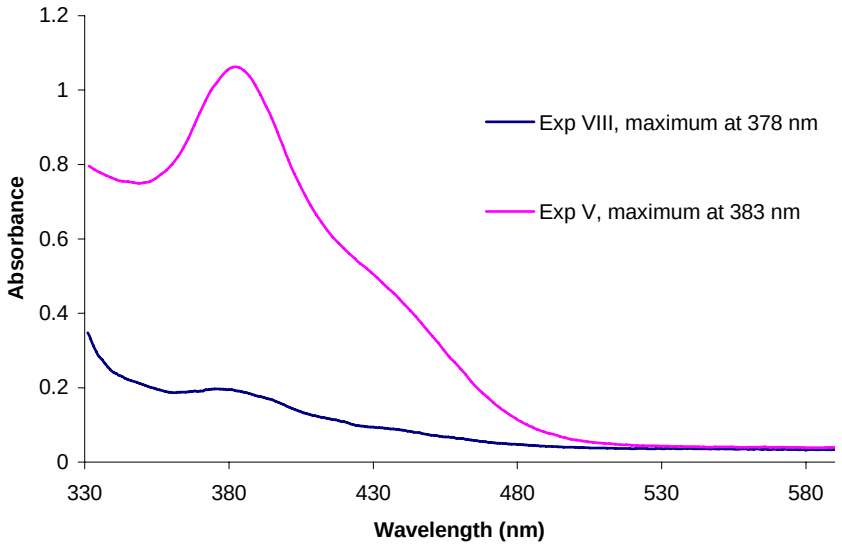

Fig. 2.19. **Comparative absorption spectra of experiments *V* and *VIII*.**

The disparity in results must have been emanating from the concentration of osmium in solution. The concentration of osmium in the total reaction volume for reaction ***VIII*** was calculated as 1.05×10^{-4} M , which corresponds with the limiting concentration determined by Antonov, *et al.* [16]. In the Russian study it was found that for low concentrations of osmium ($c_{osmium} \leq 10^{-4}$ M) apparently no complexation of a bimetallic compound, i.e. $[Os(SnCl_3)_5Cl]^{4-}$ took place, with the reduction process predominating.

To confirm this hypothesis, experiment ***IX*** was undertaken with the aforementioned in mind. The $SnCl_2$ concentration was kept greater or equal to 0.3 mol/dm^3, while the osmium concentration was equal to 5.26×10^{-4} mol/dm^3.

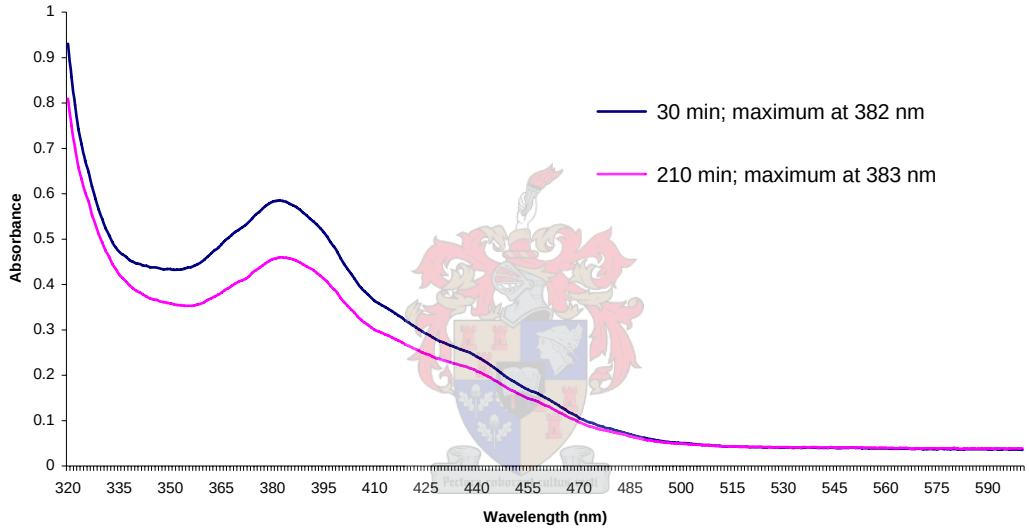

Fig. 2.20. **Absorption spectra of experiment *IX*. Reaction of $[OsCl_6]^{2-}$ with $SnCl_2$ concentration of 0.333 M, heating at 100 ºC. Recorded at 30 min (382 nm) and 210 min (383 nm)**

Repeat experiments performed under the same conditions as for experiment ***IX*** all yielded the same results, indicating that the found experimental conditions led to highly reproducible results.

Upon completion of the reduction process, it became evident that particular experimental parameters gave rise to a single species, $[Os(SnCl_3)_5Cl]^{4-}$. This may be postulated in the following manner. For low $SnCl_2$ concentrations (< 0.3 M) in dilute HCl the reduction of Os(IV) to Os(II) takes place rapidly:

$$[OsCl_6]^{2-} + [SnCl_3]^- \rightarrow [Os^{III}] \rightarrow [Os^{II}]$$

For higher $SnCl_2$ concentrations (≥ 0.3 M), the reduction process is followed by complex formation, presumably relatively slowly:

$$[Os^{II}Cl_n]^{2-n} + m SnCl_3^- \rightarrow [OsCl_{n-m}(SnCl_3)_m]^{2-(n+m)} + Cl^-$$

which then ultimately leads to the formation of $[Os(SnCl_3)_5Cl]^{4-}$.

Solvent extraction studies were resumed with a view towards incorporating the reducing agent, $SnCl_2$, into the process.

A systematic investigation was undertaken to examine the effect of $SnCl_2$ on the solvent extraction of $[OsCl_6]^{2-}$ by DBBT, with and without the use of a phase transfer catalyst (in this case the commercially available Aliquat 336). The experimental conditions are summarised in ***Table 2.7*** (***cf.*** section *2.2.7*).

Exp	Sn:Os	DBBT:Os	PTC
X	10 : 1	3 : 1	---
XI	200 : 1	3 : 1	---
XII	200 : 1	6 : 1	Aliquat 336
XIII	200 : 1	---	Aliquat 336

Table 2.7. **Summary of experiments incorporating $SnCl_2$, DBBT and PTC**

Results from experiments ***X*** and ***XI*** indicate that a reduction process occurs rapidly in the aqueous phase, since the characteristic absorbance profile of $[OsCl_6]^{2-}$ was barely visible after a particular period of heating. For the 10:1 Sn:Os ratio the absorbance maxima were recorded at 346 and 371 nm, while the 200:1 Sn:Os ratio had a weak and broad band at 374 nm (presumably due to a reduced $[OsCl_{n-m}(SnCl_3)_m]^{2-(n+m)}$ species. Analysis of the organic phases did not indicate the presence of osmium complexes, since only the absorbance of the ligand was observable (maximum absorbance below 290 nm). Combined aqueous and organic phase spectra of both reactions are illustrated in ***Figs. 2.21 & 2.22***.

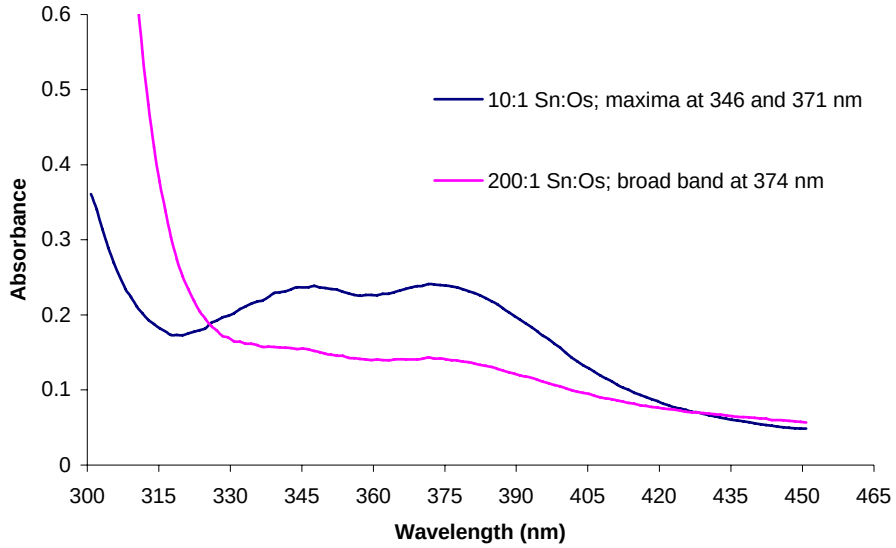

Fig. 2.21. **Combined aqueous phase absorption spectra of experiments *X, XI*. Recorded after 3 h heating at 100 ºC.**

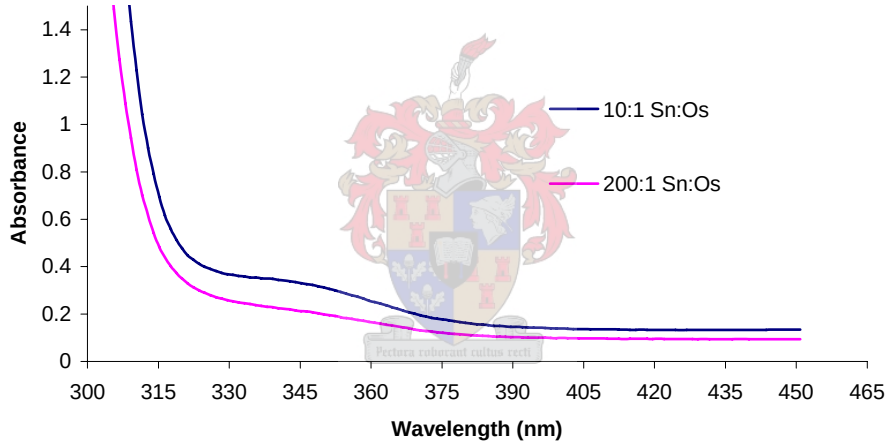

Fig. 2.22. **Combined organic phase absorption spectra of experiments *X, XI*. Recorded after 3 h heating at 100 ºC.**

It seems that although a reduction process is taking place in the aqueous phase, the resultant $[Os(SnCl_3)_5Cl]^{4-}$ species, like the $[Os^{IV}Cl_6]^{2-}$ is simply not kinetically labile enough to be extracted by the DBBT ligand in the organic phase, so that effectively no transfer of osmium complexes takes place into the organic phase. Thus, as with previous extraction experiments, it was decided to employ the use of a phase transfer catalyst, in the form of the commercially available Aliquat 336, which is a quartenary ammonium cation with the chemical formula $[CH_3N((CH_2)_7CH_3)]^+ Cl^-$. It is quite evident that the long alkyl chains contribute to the inherent lipophilicity of the PTC, therefore ensuring a high distribution of the PTC-anion ion-pair in the organic phase.

Experiments ***XII, XIII*** were performed under the same conditions as for the two preceding experiments. Aliquat 336 of concentration that is nine times that of the initial osmium was added to

the organic phase, while for experiment ***XIII*** the DBBT ligand was present in a 6:1 ratio with regard to initial osmium.

After two hours of agitation at 100 °C the aqueous phases were pale yellow in colour, while the organic phases changed to a bright yellow colour, indicating the presence of an osmium complex. As before the absorption spectra of the aqueous phases exhibited a reduction in the characteristic spectral profile of $[OsCl_6]^{2-}$, suggesting complete reduction and complex formation with $[SnCl_3]^-$, while the organic profile showed an intense and broad absorbance below 300 nm (***Fig. 2.23***).

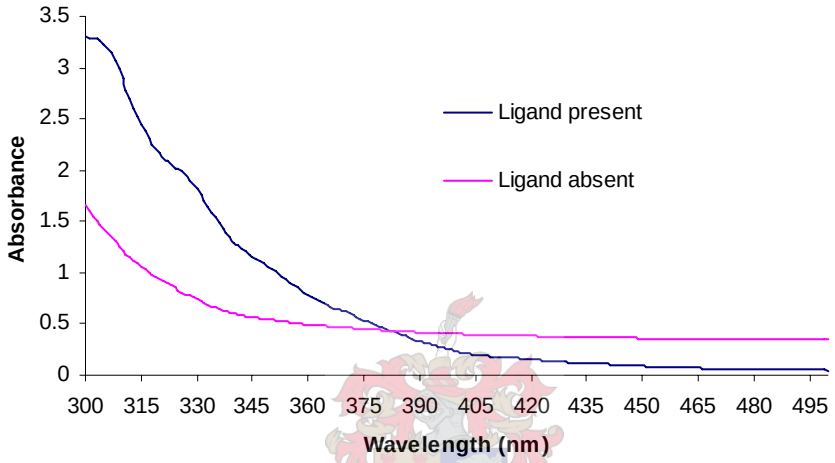

Fig. 2.23. **Combined organic phase absorption spectra of reactions *XII, XIII*. Recorded after 3 h heating at 100 °C.**

The presence of the DBBT ligand in the organic phase seems to have no effect on the extraction of osmium, only contributing to absorbance below 300 nm. One may thus deduce that either the reduced osmium species gets transported to the organic phase, as an ion pair with the PTC where it does not react with the DBBT ligand; or $[OsCl_6]^{2-}$ is transported to the organic phase before it is reduced by $[SnCl_3]^-$. The possibility also exists that the partially reduced species, $[OsCl_{n-m}(SnCl_3)_m]^{2-(n+m)}$, might be transferred to the organic phase by the PTC, therefore accounting for the yellow colour of the organic phase. Consequently a new set of experiments were carried out, incorporating the knowledge obtained from experiment ***IX***, where a $SnCl_2$ concentration of 0.333 mol/dm^3 (in 20 cm^3 volume) was needed.

Exp	[$SnCl_2$]	DBBT:Os	PTC
XIV	0.333	3 : 1	---
XV	0.333	3 : 1	Aliquat 336
XVI	0.333	9 : 1	Aliquat 336

Table 2.8. **Summary of experiments incorporating $SnCl_2$, DBBT and PTC**

Experiments ***XIV*** and ***XV*** were performed under the exact same conditions, where the osmium and $SnCl_2$ were present in the hydrochloric acid aqueous phase, while the phase transfer catalyst and ligand were contained in the chloroform organic phase. Both experiments were agitated at 100 °C and analysed via absorption spectrophotometry after three hours contact time. Aqueous phase absorption spectra of experiments ***XIV*** and ***XV*** are shown in ***Fig. 2.24***

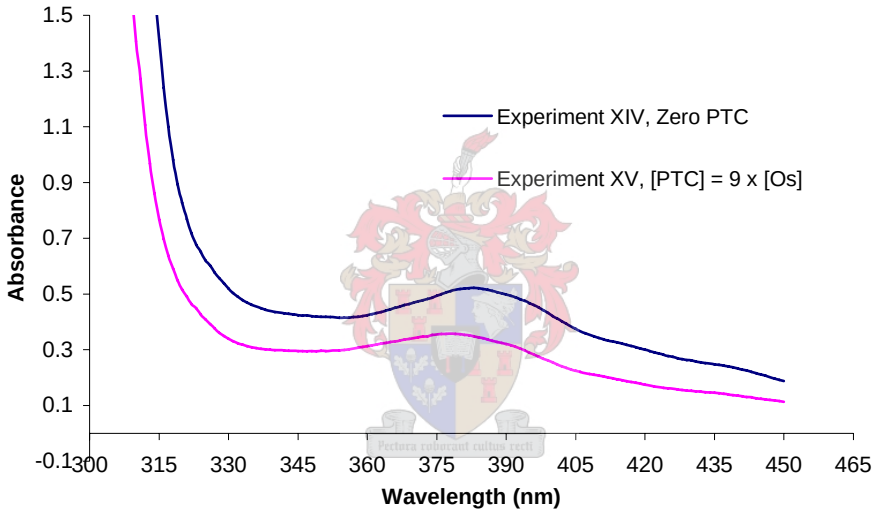

Fig. 2.24. **Combined aqueous phase absorption spectra of reactions *XIV* and *XV*. Absorbance maxima at 382 nm.**

From the aqueous phase spectra (***Fig. 2.24***) it is evident that $[OsCl_6]^{2-}$ has been reduced and complexed with $[SnCl_3]^-$ to presumably give rise to the $[Os(SnCl_3)_5Cl]^{4-}$ species, exhibiting the single absorption band at 382 nm, which is in agreement with findings from the preceding sections. It is also noticeable that the absorbance values of the two experiments differ only slightly. For the case of experiment ***XV***, the lower overall absorbance is probably due to the decreasing osmium concentration present in the aqueous phase, as a result of some osmium complex, in the form of $[OsCl_6]^{2-}$, being extracted to the organic phase by the PTC before being reduced to a lower oxidation state.

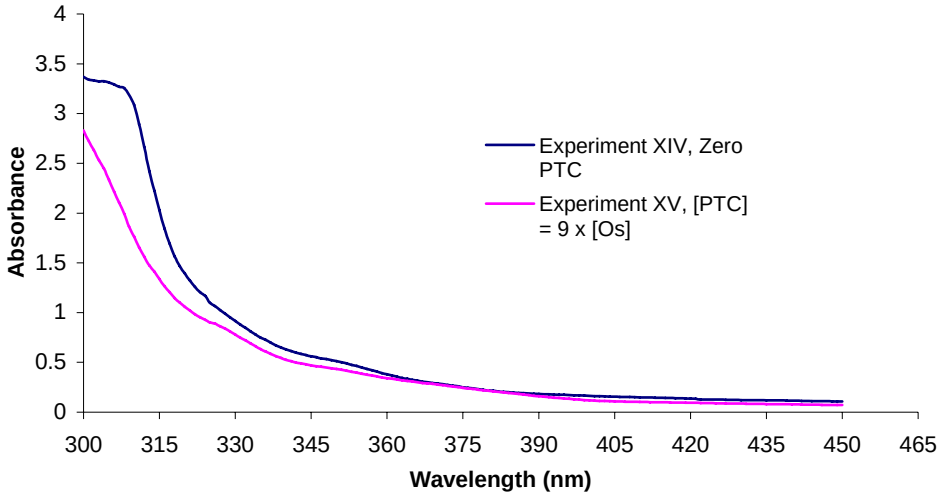

Fig. 2.25. **Combined organic phase absorption spectra of experiments *XIV* and *XV*.**

Exactly the same results were obtained for experiment ***XVI*** (***Fig. 2.26***), where the amount of ligand (as DBBT) was trebled. Absorption profiles and absorbances for both the aqueous and organic phases did not differ from those of experiment ***XV***.

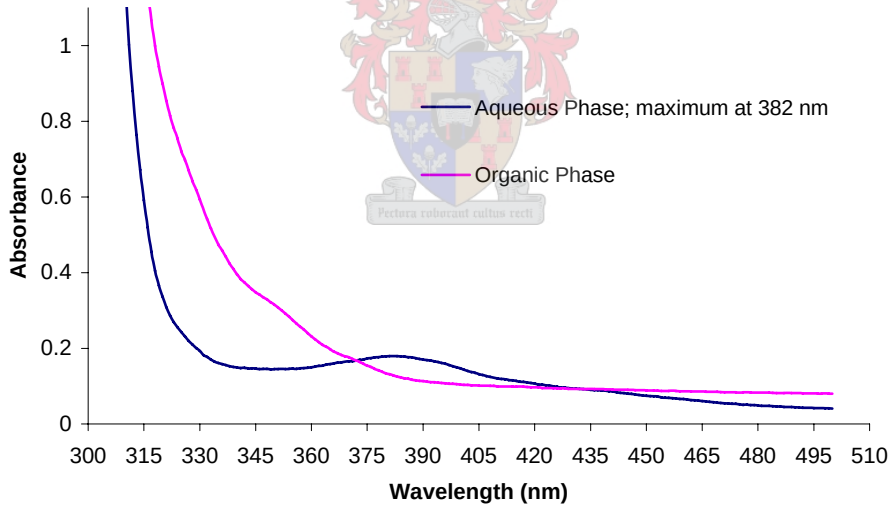

Fig. 2.26. **Absorption spectra of aqueous and organic phases of experiment *XVI* after 3 h agitation at 100 °C**

At this juncture it is possible to draw the following conclusions :

- Liquid-liquid extraction of $[OsCl_6]^{2-}$ with *N,N*-dibutyl-*N'*-benzoylthiourea at room temperature for a period of 24 hours resulted in no meaningful transfer of osmium into the organic phase. Moreover, increasing the reaction temperature and the ligand to osmium ratio (up to 24 times molar excess of ligand) gave no positive extraction results.
- The addition of a phase transfer catalyst, in the form of tetrabutylammonium tetrafluoroborate (TBATFB), resulted in quantitative transfer of the $[OsCl_6]^{2-}$ ion into the organic phase.

Experiments with two different ligands, *N,N*-dibutyl-*N'*-benzoylthiourea and *N,N*-diethyl-*N'*-benzoylthiourea, resulted in organic phase absorption spectra that were comparable to each other, therefore suggesting that the osmium-TBATFB ion pair present in the organic phase does not react with either of the ligands under these particular conditions. This was confirmed by evaluating the effect of TBATFB concentration on osmium present in the aqueous phase (section ***2.3.5***). The following reaction scheme is suggested, which illustrates the fashion in which transport of the $[OsCl_6]^{2-}$ occurs :

$$[OsCl_6]^{2-} + (C_4H_9)_4N^+BF_4^- \rightarrow [(C_4H_9)_4N]_2OsCl_6$$

- Under specific experimental conditions, it is possible to reduce the tetravalent $[OsCl_6]^{2-}$ species, by means of $SnCl_2$, to a divalent bimetallic species (section ***2.3.6***). The following reaction scheme is proposed:

$$[OsCl_n]^{2-n} + m SnCl_3^- \rightarrow [OsCl_{n-m}(SnCl_3)_m]^{2-(n+m)} \rightarrow [Os(SnCl_3)_5Cl]^{4-}$$

- In the presence of $SnCl_2$ (sufficient amount to afford quantitative reduction), phase transfer catalyst and ligand, it seems that although the reduced species (as $[Os(SnCl_3)_5Cl]^{4-}$) was transported to the organic phase via the PTC, but no observable reaction with the DBBT ligand occurred.

2.3.7 Crystal structure determination of $[OsCl_6]^{2-}$ - PTC ion-pair

Discussions emanating from content of the preceding sections were all based on the postulate that the use of a cationic phase transfer catalyst during solvent extraction experiments resulted in the formation of an $[OsCl_6]^{2-}$ - PTC ion-pair present in the organic phase. Fortunately it was possible to obtain solid crystals of the afore-mentioned ion-pair, emanating from one of the numerous extraction experiments that were performed.

Formation of the crystals occurred in a rather serendipitous manner. A bilayer solution of hydrochloric acid and chloroform containing $[OsCl_6]^{2-}$, DBBT and tetrabutylammonium tetrafluoroborate was agitated for 15 min at room temperature, where after it was left to stand for an indefinite period devoid of any ambient light. After two weeks light yellow crystals were beginning to form at the interface between the two phases. The relatively large yellow crystals were carefully

removed from solution and cut into smaller crystals suitable for X-ray diffraction crystallography. The X-ray diffraction analysis was performed by Prof. S. Bourne at the Department of Chemistry at UCT.

Empirical formula	$C_{69}\ H_{149}\ Cl_{27}\ N_4\ Os_2$
Formula weight	2372.65
Temperature	193(2) K
Wavelength	0.71073 Å
Crystal system, space group	Orthorhombic, $P2_12_12_1$
Unit cell dimensions	a = 16.501(3) Å α = 90º
	b = 20.640(4) Å β = 90º
	c = 32.134(6) Å γ = 90º
Volume	10944(4) $Å^3$
Z, Calculated density	4, 1.4400(5) mg/m^3
Absorption coefficient	3.01 mm^{-1}
F(000)	4808
Crystal size	0.10 × 0.10 × 0.10 mm
Theta range for data collection	1.17º to 27.49º
Limiting indices	$-21 \le h \le 21, -26 \le k \le 26, -41 \le l \le 41$
Reflections collected / unique	25055 / 25055 [R(int) = 0.0000]
Completeness to theta = 27.49	99.7 %
Max. and min. transmission	0.7576 and 0.7576
Refinement method	Full-matrix least-squares on F^2
Data / restraints / parameters	25055 / 0 / 976
Goodness-of-fit on F^2	0.877
Final R indices [I > 2σ(I)]	$R_1 = 0.0402$, $wR_2 = 0.1121$
R indices (all data)	$R_1 = 0.0643$, $wR_2 = 0.1494$
Absolute structure parameter	0.444(6)
Largest diff. peak and hole	0.937 and -0.846 e. $Å^{-3}$

***Table 2.9*. Crystallographic data for Os-PTC ion-pair**

The asymmetric unit consists of two independent $[OsCl_6]^{2-}$ ions, four $(C_4H_9)_4N^+$ ions and five $CHCl_3$ molecules. One butyl chain is disordered in that the terminal carbon was modelled over two positions with site occupancies of 51 and 49%. In addition, chloroform molecule E displayed

disorder of the chlorine atoms over two positions (site occupancies 67 and 33%). Each $[OsCl_6]^{2-}$ ion exhibits octahedral configuration with equal Os-Cl bond lengths. The tetrabutyl ammonium ions are in the staggered conformation. The spatial orientation of the tetrabutyl ammonium cations towards the single $[OsCl_6]^{2-}$ anion is illustrated in ***Fig. 2.27*** (for sake of clarity the chloroform solvent molecules and hydrogen atoms have been excluded).

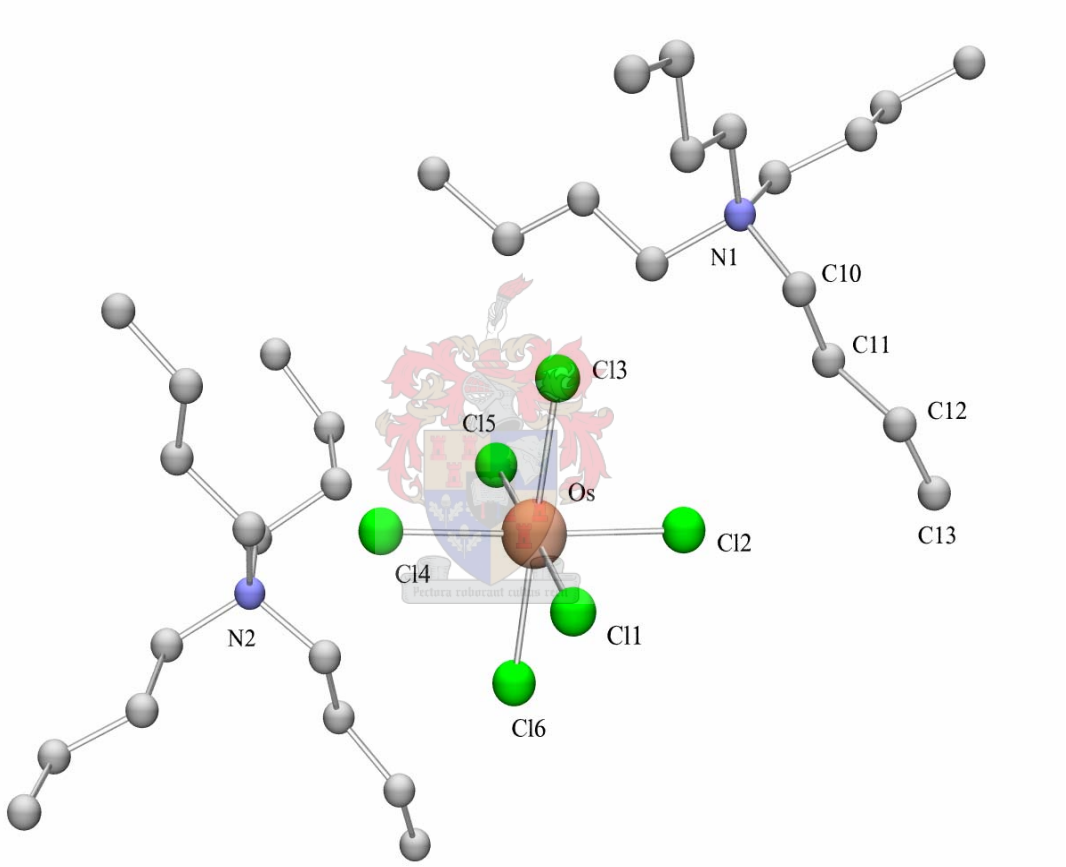

Fig. 2.27. **Partial asymmetric unit of $OsCl_6[(C_4H_9)_4N]_2$ without solvent molecules**

Selected bond lengths and angles for components contained in the asymmetric unit are shown in ***Table 2.10.***

Bond Lengths (Å)		Angles (º)	
Os - Cl (1)	2.338 (19)	Cl (1) - Os - Cl (2)	90.61 (9)
Os - Cl (2)	2.336 (2)	Cl (1) - Os - Cl (3)	89.00 (8)
Os - Cl (3)	2.326 (19)	Cl (1) - Os - Cl (4)	89.50 (9)
Os - Cl (4)	2.347 (19)	Cl (1) - Os - Cl (5)	178.80 (8)
Os - Cl (5)	2.340 (2)	Cl (1) - Os - Cl (6)	90.68 (7)
Os - Cl (6)	2.339 (19)	Cl (2) - Os - Cl (3)	89.75 (8)
N (1) - C (10)	1.520 (10)	Cl (2) - Os - Cl (4)	178.79 (8)
C (10) - C (11)	1.459 (12)	Cl (2) - Os - Cl (5)	89.27 (9)
C (11) - C (12)	1.557 (14)	Cl (2) - Os - Cl (6)	89.58 (8)
C (12) - C (13)	1.454 (15)	Cl (3) - Os - Cl (4)	89.80 (8)
		Cl (3) - Os - Cl (5)	91.45 (8)
		Cl (3) - Os - Cl (6)	179.25 (8)
		Cl (4) - Os - Cl (5)	90.65 (8)
		Cl (4) - Os - Cl (6)	90.51 (8)
		Cl (5) - Os - Cl (6)	89.22 (8)

Table 2.10 **. Selected bond lengths and angles contained in the asymmetric unit cell**

The structural components in the asymmetric unit are also linked by various weak hydrogen bond interactions such as C-H·····Cl. A selection of these interactions are reproduced in ***Fig. 2.28*** , with the thin red lines indicating the afore-mentioned hydrogen bonds.

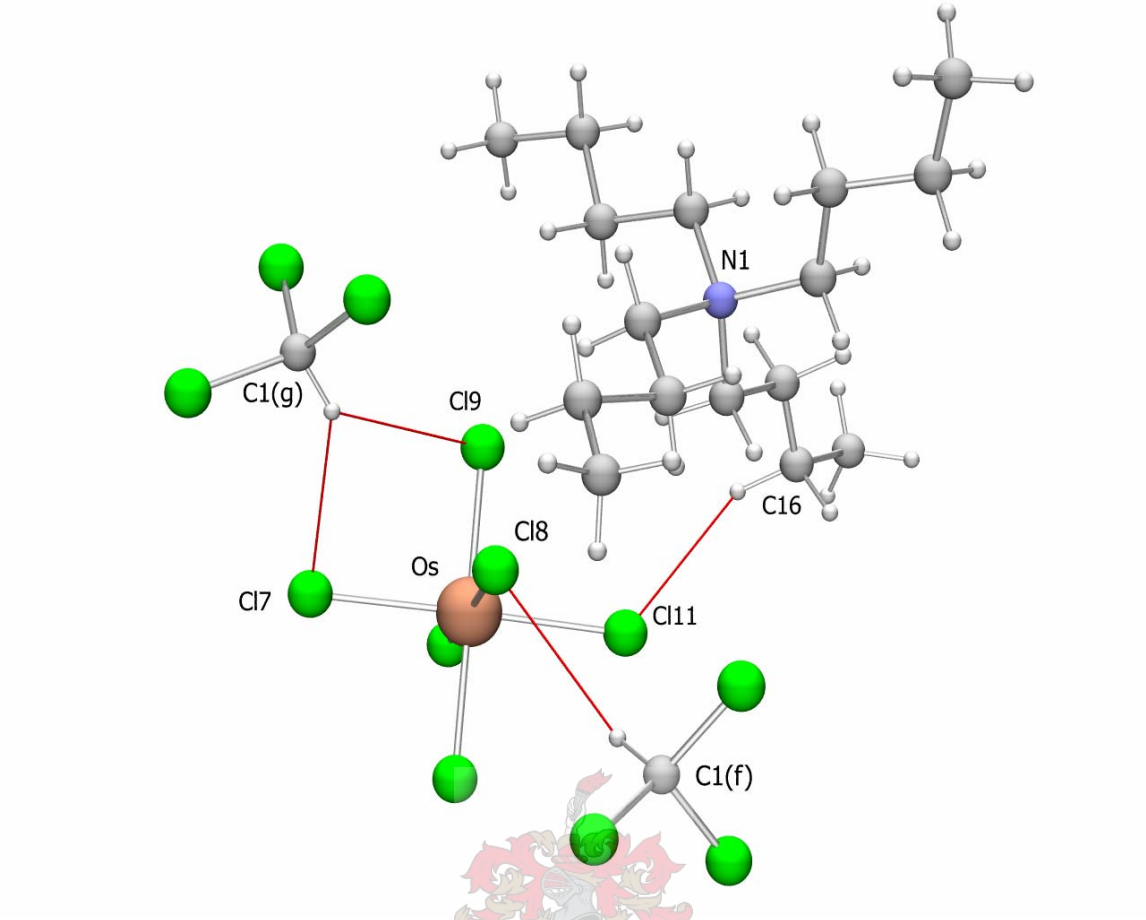

Fig. 2.28. **Asymmetric unit displaying weak hydrogen bond interactions (indicated by the red lines)**

The dimensions of the interactions are contained in ***Table 2.11.***

A - H ····· B	Bond Lengths (Å)			Angles (º)
	A - H	H·····B	A·····B	∠ (AHB)
C(1g) - H·····Cl(7)	0.9800	2.7085	3.5389	142.78
C(1g) - H·····Cl(9)	0.9800	2.7907	3.5992	140.26
C(1f) - H·····Cl(8)	0.9800	2.7973	3.5652	135.72
C(16) - H·····Cl(11)	0.9701	2.6571	3.5245	149.05

Table 2.11 **. Summary of weak hydrogen bond interactions contained in the asymmetric unit cell**

The packing order of this compound is quite unusual, giving rise to the space group $P2_12_12_1$, containing no chiral components. However, the putative 2-fold symmetry is broken by the coordination of tetrabutyl ammonium ions in different orientations and by the inclusion of an uneven number of solvent molecules. The chloroform molecules are included in channels running through the structure parallel to [0 1 0] and centred at $x = z = 0, x = 0;\ z = 0.5, x = 0.5,\ z = 0$ and $x = 0.5;\ z = 0.5$. Packing of the different components within the unit cell is illustrated by means of ***Fig. 2.29***, with the solvent molecules left out for sake of clarity. Another perspective may be obtained from ***Fig. 2.30***, which illustrates the packing configuration of multiple unit cells.

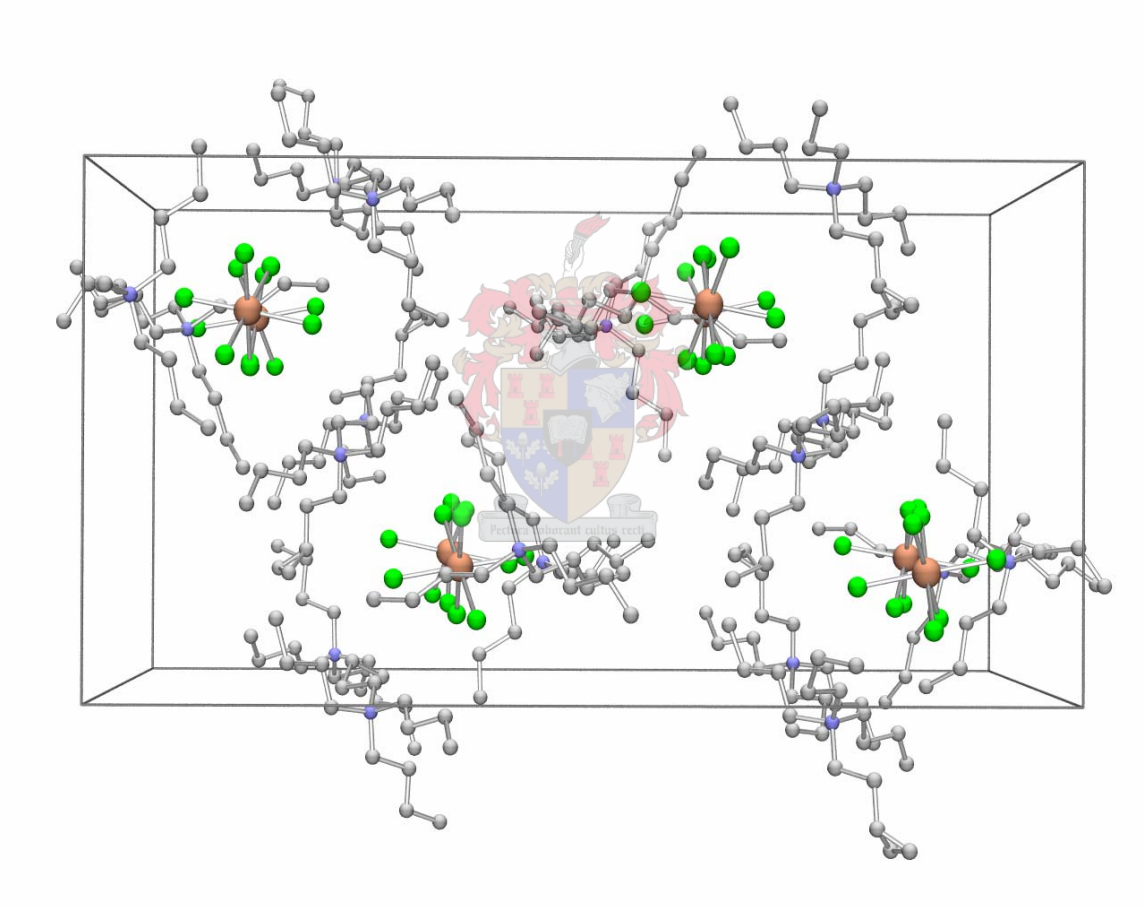

Fig. 2.29. **Unit cell configuration without solvent molecules**

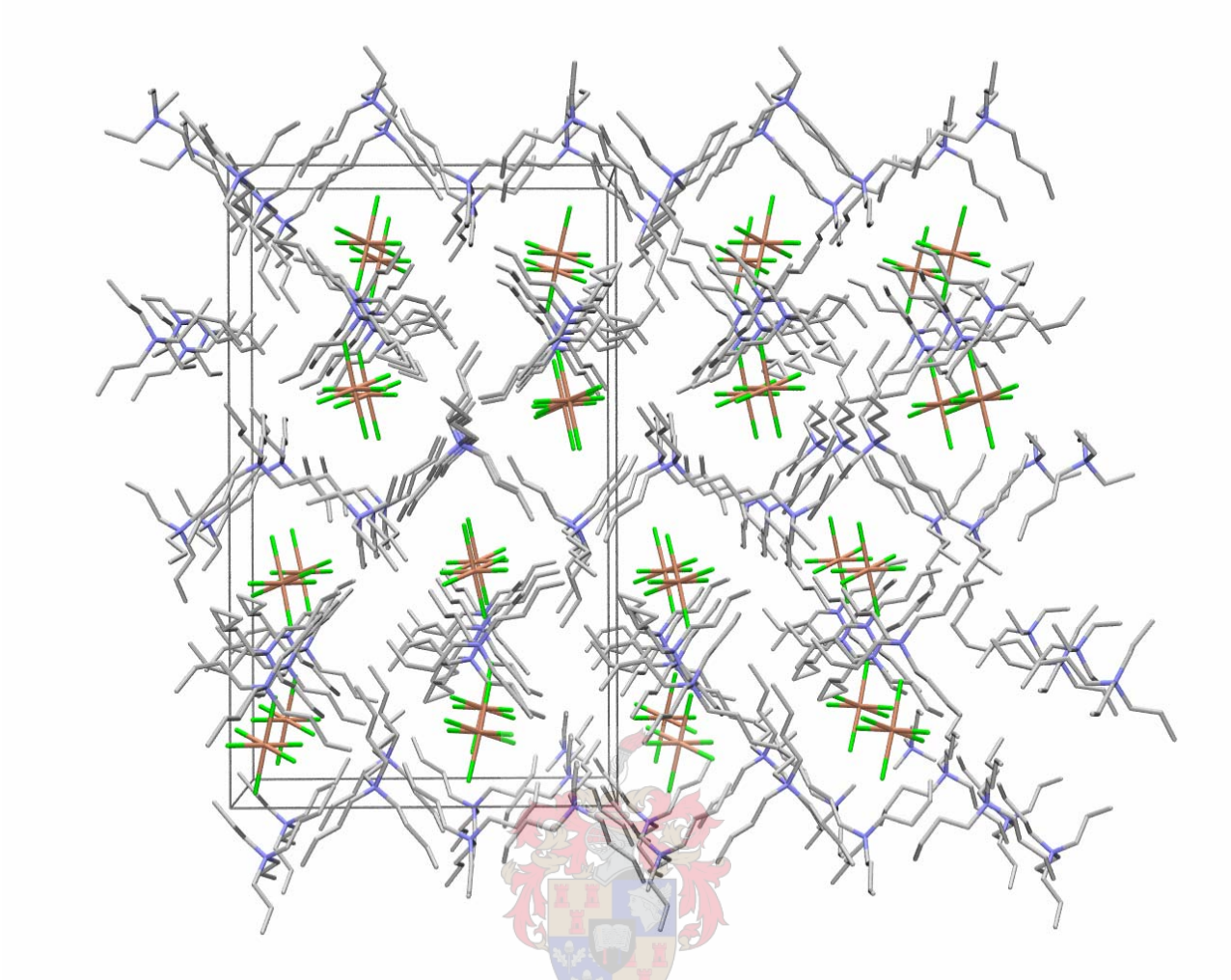

Fig. 2.30. **Packing configuration of multiple unit cells**

2.4 Summary and conclusions

Attempts at liquid-liquid extraction of osmium, in the form of the tetravalent $[OsCl_6]^{2-}$, with ligands of the type *N*,*N*-dialkyl-*N'*-benzoylthiourea, have proved unsuccessful. It has been shown that the tetravalent ion can be successfully transported to the organic phase by means of a phase transfer catalyst, where after no observable interaction with the ligand occurs. The tetravalent ion can be reduced to the divalent bimetallic species $[Os(SnCl_3)_5Cl]^{4-}$ by an excess of $SnCl_2$, but remains kinetically inert towards interaction with an excess of ligand.

Unconvincing results prompted a change in research direction towards obtaining a more thorough understanding of the interaction between osmium and ligands of type *N*,*N*-dialkyl-*N'*-(acyl)aroylthiourea. Therefore a systematic investigation into complex formation of osmium with the aforementioned ligands follows in chapter 3.

References

[1] L. Beyer, E. Hoyer, H. Hartman and J. Liebscher, *Z Chem*, 21 (1981) 81.

[2] P. Mühl, K. Gloe, F. Dietze, E. Hoyer and L. Beyer, *Z Chem*, 26 (1986) 81.

[3] K.H. Konig, *Fres Z Anal Chem*, 321 (1985) 457.

[4] P. Vest, M. Schuster and H. Konig, *Fresenius Z Anal Chem*, 335 (1989) 759.

[5] P. Vest, M. Schuster and K.H. Konig, *Fresenius J Anal Chem*, 341 (1991) 566.

[6] M. Schuster, H. Konig and B. Kugler, *Fres J Anal Chem*, 338 (1990) 717.

[7] Miller, J. D. Ph.D. Thesis (2000), University of Cape Town.

[8] Z. Otwinowski and W. Minor, *Methods Enzymol*, 276 (1996) 307.

[9] Sheldrick, G. M., SHELX-97 (1997), University of Göttingen.

[10] Barbour, L. J., X-SEED (1999), University of Missouri-Columbia.

[11] R.R. Miano and C.S. Gartner, *Inorg Chem*, 4 (1965) 337.

[12] K.H. Konig, H.J. Pletsch and M. Schuster, *Fresenius Z Anal Chem*, 325 (1986) 621.

[13] Halpern, M., *Proceedings of the International Solvent Extraction Conference, Johannesburg South Africa* (2002) 24.

[14] W.P. Griffith, C.J. Raub and K. Swars, *Gmelin Handbuch der Anorganischen Chemie*, Springer-Verlag, Berlin (1980).

[15] P. Vest, M. Schuster and H. Konig, *Fres J Anal Chem*, 339 (1991) 142.

[16] P.G. Antonov, Y.N. Kukushkin and V.I. Konnov, *Koord Khim*, 3 (1977) 757.

[17] M. Balcerzak, *Analyst*, 113 (1988) 129.

Chapter 3

Complexes of Os(III) with *N*, *N*-dialkyl-*N'*-acyl(aroyl)thioureas

3.1 Introduction

N,*N*-dialkyl-*N'*-acyl(aroyl)thiourea (HL) ligands have been shown to be selective towards PGMs (platinum group metals), coordinating predominately in a bidentate fashion through the sulphur and oxygen donor atoms [1]. Although seemingly simple, it is their affinity for the PGMs, and therefore selectivity over other transition metals that make them invaluable in a variety of applications, such as solvent extraction [2], pre-concentration [3] and quantitative separation via reversed-phase HPLC [4].

Although much work has been focused on the coordination of these ligands with Pd [5], Pt [6], Ni [7] and Cu [8], resulting in formation of bis-chelating complexes, tris-chelating complexes have taken much of a back seat. Previous publications involved HL complexes of ruthenium[9] and rhodium [10], and were published quite some time ago. Interest in these ligands arose from possibilities of application towards the solvent extraction of osmium from hydrochloric acid solutions.

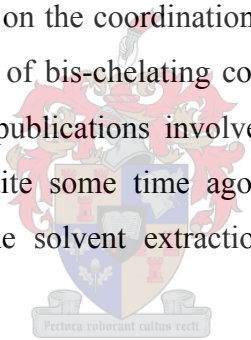

As was discovered during experimental investigations contained in Chapter 2, the metal in its tetravalent state in $[OsCl_6]^{2-}$, proved to be quite inert towards solvent extraction with these particular HL ligands, contrary to previous findings involving other PGMs [11]. In an attempt to elucidate the coordination of osmium with these ligands, a series of complexes were prepared and characterised. Their physiochemical properties were also investigated with a view towards future incorporation into other technical and analytical applications.

3.2 Experimental

3.2.1 Analytical Methods

Solutions of the individual complexes were contained in 2 mm quartz cuvettes and their UV-Vis absorption spectra were measured with an HP Agilent Diode Array Spectrophotometer. Infrared

spectra were recorded with a NEXUS model FT-IR instrument (Thermo Nicolet, USA). KBr discs of the complexes were used to record the infrared spectra in transmission mode over the MID-IR range 4000-400 cm^{-1} at a standard resolution of 4 cm^{-1}. Product identification was also facilitated by means of HPLC coupled to Electrospray Mass Spectrometry (HPLC-ESMS).

3.2.2 Synthesis of ligands

All the ligands used in the formation of $Os(L^n\text{-}S,O)_3$ complexes are described in the scheme illustrated below:

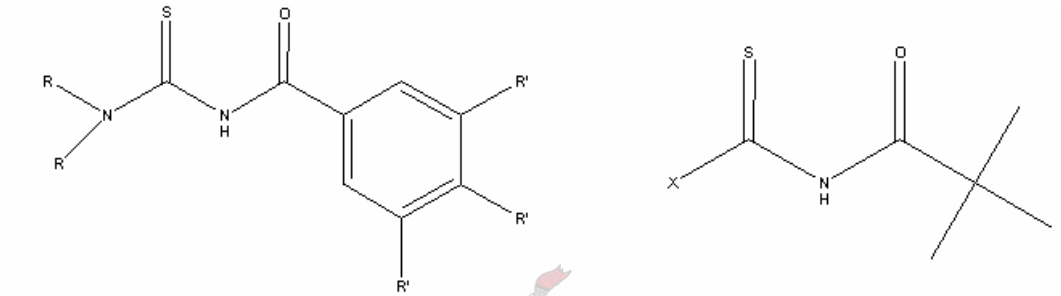

HL^1 : R=CH_2CH_3 , R'=H
HL^2 : R=CH_2CH_2OH , R'=H
HL^3 : R=CH_2CH_3 , R'=3,4,5-trimethoxy

HL^5 : X= $N(CH_2CH_3)_2$
HL^6 : X= pyrrolidine
HL^7 : X= morpholine

Ligand HL^1 was synthesised by the author, whereas the other ligands (HL^2 - HL^7) were synthesised by J. Miller [12]. All ligands were checked for purity as described below.

***N,N*-diethyl-*N'*-benzoylthiourea (HL^1):**

To a 250 cm^3 two-neck round bottom flask containing 75 cm^3 HPLC-grade acetone was added anhydrous potassium thiocyanate (3.0 g, 30.9 mmol). The colourless solution was stirred gently under nitrogen until all solids were dissolved. Benzoyl chloride (4.2 g, 29.9 mmol) was added to the thiocyanate solution in drop wise fashion over a period of 40 min at room temperature. The resulting white solution was refluxed (67 - 68 ºC) with stirring for 45 min. The crude benzoyl isothiocyanate solution was left to cool to room temperature, where after diethylamine (2.2 g, 30.1 mmol) dissolved in 75 cm^3 anhydrous acetone was added dropwise over 40 min while stirring at room temperature. The solution was once again heated to reflux for 45 min with stirring. Upon completion of heating the mixture was cooled to room temperature, where after it was slowly poured into an open beaker containing 100 cm^3 distilled water. Approximately 200 cm^3 of acetone was evaporated off, resulting in a crude white precipitate which was collected by suction filtration

and washed with distilled water. Recrystallisation from acetone/water solution (80:20 v/v) afforded white needle-like crystals. A yield of 85.4 % (6.0 g, 25.4 mmol) was obtained; m.p. 98-100 ºC; *Anal*. Found: C, 60.91; H, 6.92; N, 11.60 %. Calculated for $C_{12}H_{16}N_2SO$: C, 60.99; H, 6.82 ; N, 11.85 %.

***N,N*-di(2-hydroxyethyl)-*N'*-benzoylthiourea (HL^2):**

Ligand synthesised by Koch, *et al*. [13]. 70.0 % yield; m.p. 120-122 ºC; *Anal*. Found: C, 53.8; H, 5.8; N, 10.1 %. Calculated for $C_{12}H_{16}N_2SO_3$: C, 53.7; H, 6.0; N, 10.4 %.

***N,N*-diethyl-*N'*-(3,4,5-trimethoxybenzoyl)thiourea (HL^3):**

Ligand synthesised by Miller [12]. 89.5 % yield; m.p. 158-160 ºC; *Anal*. Found: C, 55.1; H, 6.95; N, 8.67; S, 6.92 % Calculated for $C_{15}H_{22}N_2SO_4$: C, 55.2; H, 6.81; N, 8.58; S, 9.82 %.

***N,N*-diethyl-*N'*-pivaloylthiourea (HL^5):**

Ligand synthesised by Miller [12]. 98.0 % yield; m.p. 90-91 ºC; *Anal*. Found: C, 55.6; H, 9.09; N, 13.2; S, 15.1 % Calculated for $C_{10}H_{20}N_2SO$: C, 55.5; H, 9.33; N, 12.9; S, 14.8 %.

***N* -pyrrolidyl-*N'*-pivaloylthiourea (HL^6):**

Ligand synthesised by Miller [12]. 90.1 % yield; m.p. 136 ºC; *Anal*. Found: C, 56.0; H, 8.77; N, 13.3; S, 14.8 % Calculated for $C_{10}H_{18}N_2SO$: C, 56.0; H, 8.48; N, 13.1; S, 15.0 %.

***N*-morpholino-*N'*-pivaloylthiourea (HL^7):**

Ligand synthesised by Miller [12]. 97.2 % yield; m.p. 134-135 ºC; *Anal*. Found: C, 52.0; H, 8.25; N, 12.25; S, 13.8 % Calculated for $C_{10}H_{18}N_2SO_2$: C, 52.1; H, 7.89; N, 12.2; S, 13.9 %.

3.2.3 Synthesis of Os(III) complexes

All osmium(III) complexes of *N,N*-dialkyl-*N'*-acyl(aroyl)thioureas were prepared in solvent mixtures of acetonitrile and water. Deprotonation of the ligands was ensured by the addition of a mild base such as sodium acetate, usually in slight excess with regard to the particular ligand. An acetonitrile solution of the metal, either Os(III) or Os(IV), was added in such an amount as to afford a 3:1 ligand to metal ratio. Heating periods under reflux were followed by varying work-up procedures depending on the ligand used for complex formation. Progress of complex formation

was monitored by means of thin layer chromatography, while impure products were purified by column chromatography using aluminium oxide as stationary phase.

All reactions were performed under inert N_2 atmosphere, although the resulting work-up and purification procedures were carried out in the atmosphere. The quadrivalent osmium salt $Na_2[OsCl_6]$ was dried *in vacuo* over P_2O_5 for at least 3 h before being used, while the tervalent salt was used in its hydrated form of $OsCl_3 \cdot 3H_2O$. An outline for the synthesis of $[Os(L^1\text{-}S,O)_3]$ is described in ***Scheme 3.1*** below:

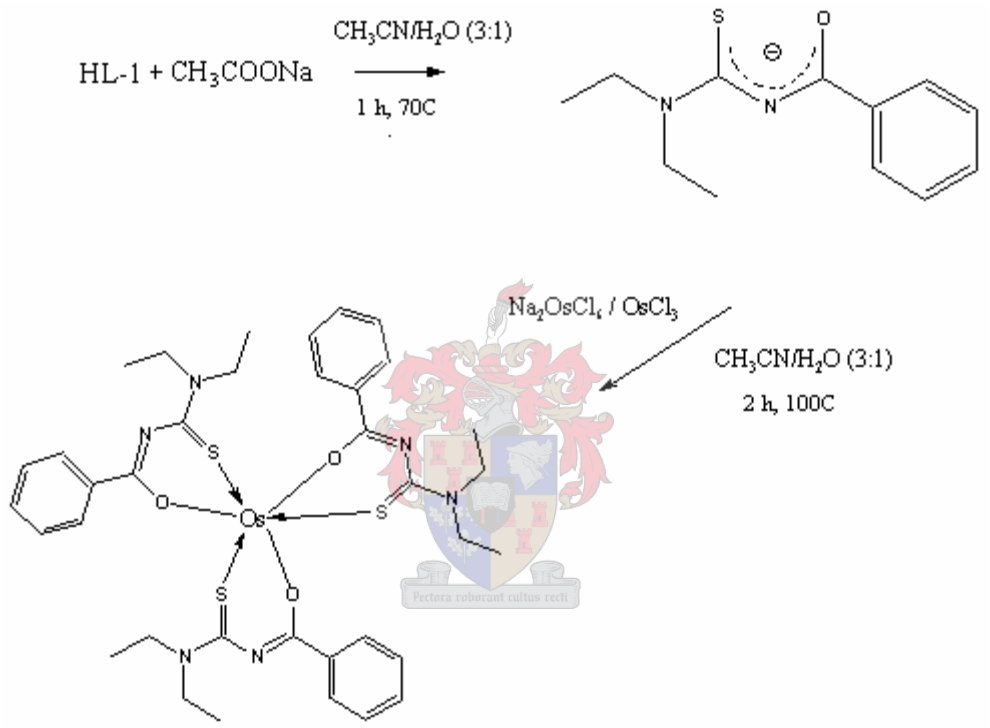

Scheme 3.1. **Scheme for the synthesis of $[Os(L^1\text{-}S,O)_3]$**

Tris(*N,N*-diethyl-*N'*-benzoylthioureato)osmium(III), *fac*-$[Os(L^1\text{-}S,O)_3]$:

To a 100 cm^3 round-bottom flask containing 20 cm^3 of an acetonitrile-water mixture (3:1 v/v) was added solid HL^1 (131.2 mg, 0.555 mmol), followed by a slight excess of hydrated sodium acetate (84.6 mg, 0.622 mmol). The clear and colourless solution was heated with stirring at 60 ºC for a duration of 45 min. Anhydrous $Na_2[OsCl_6]$ (82.6 mg, 0.184 mmol) dissolved in 8 cm^3 of acetonitrile was added in drop wise fashion to the deprotonated ligand solution over 15 min while heating at 103-105 ºC. The dark brown solution was allowed to reflux for one hour, where after it was cooled down to room temperature and stirred for another hour. The resultant dark brown

precipitate was isolated by centrifugation, followed by washing with distilled water and drying *in vacuo* over P_2O_5 for several hours. To the filtrate remaining after centrifugation was added 15 cm^3 distilled water, followed by extraction of remaining product into dichloromethane. The volume of the dark brown dichloromethane solution was evaporated under vacuum to dryness, followed by re-dissolving in a minimum amount of acetonitrile. Drop wise addition of a large excess diethyl ether afforded dark brown precipitate in solution, which was collected by centrifugation as before. Recrystallisation from dichloromethane of both product fractions afforded purple-brown crystals.
A yield of 55.6 % was recovered; m.p. *decomposes*; *Anal*. Found: C, 47.92; H, 4.69; N, 9.19 %. Calculated for $C_{36}H_{45}N_6S_3O_3Os$: C, 48.25; H, 5.06; N, 9.38 %; ν_{max} (cm^{-1}): 1487 (CO), 1412 (CN) and 1353 (CS); $(m + 1)/z$: 897.19 (calc. for $C_{36}H_{45}N_6S_3O_3Os$: 897.22).

Tris[*N,N*-(2-hydroxyethyl)-*N'*-benzoylthioureato]osmium(III), *fac*-[Os(L^2-*S,O*)$_3$] :
To a 100 cm^3 round-bottomed flask containing 20 cm^3 of an acetonitrile-water mixture (3:1 v/v) was added solid HL^2 (99.4 mg, 0.370 mmol), followed by a slight excess of hydrated sodium acetate (56.5 mg, 0.415 mmol). The solution was heated with stirring at 60 ºC for a duration of one hour, with all ligand dissolved. $OsCl_3{\cdot}3H_2O$ (42.6 mg, 0.121 mmol) dissolved in 8 cm^3 of acetonitrile was added in drop wise fashion to the deprotonated ligand solution over 10 min while heating at 103-105 ºC. The nearly black solution was refluxed for 4 h, where after it was allowed to stir overnight at room temperature. Solvent was removed under reduced pressure, followed by re-dissolving in a minimal amount of acetonitrile. Addition of excess diethyl ether afforded dark brown precipitate, which was collected by centrifugation and followed by washing with distilled water and drying *in vacuo* over P_2O_5. The product was isolated via column chromatography using aluminium oxide as stationary phase and eluting with CH_2Cl_2.
A yield of 58.65 % was recovered; m.p. *decomposes*; *Anal*. Found: C, 43.23; H, 4.71; N, 8.64 %. Calculated for $C_{36}H_{45}N_6S_3O_3Os$: C, 43.58; H, 4.57; N, 8.47 %; ν_{max} (cm^{-1}): 1485 (CO), 1408 (CN) and 1352 (CS); $(m + 1)/z$: 993.09 (calc. for $C_{36}H_{45}N_6S_3O_3Os$: 993.21)

Tris[*N,N*-diethyl-*N'*-(3,4,5-trimethoxybenzoyl)thioureato]osmium(III), *fac*-[Os(L^3-*S,O*)$_3$] :
To a 100 cm^3 round-bottomed flask containing 20 cm^3 of an acetonitrile-water mixture (3:1 v/v) was added solid HL^3 (144.3 mg, 0.441 mmol), followed by a slight excess of hydrated sodium acetate (67.8 mg, 0.498 mmol). The colourless solution was heated with stirring at 60 ºC for a duration of 45 min. Anhydrous $Na_2[OsCl_6]$ (65.5 mg, 0.146 mmol) dissolved in 5 cm^3 of

acetonitrile was added drop wise to the ligand solution over 10 min while heating at 105-107 ºC. The dark brown solution was allowed to reflux for 2 h, whereafter it was stirred for 12 h at room temperature. All of the solvent was removed under reduced pressure, resulting in dark brown solids with gel-like consistency. The aqueous fraction was removed by means of prolonged drying *in vacuo* over P_2O_5. Dark brown solid product was washed with copious amounts of distilled water, followed by drying *in vacuo* over P_2O_5 for several hours. The solids were redissolved in CH_3CN and transferred to a column packed with aluminium oxide as stationary phase. The desired product was isolated after elution with CH_3CN/CH_2Cl_2.

A yield of 55.41 % was recovered; m.p. *decomposes*; *Anal*. Found: C, 45.96; H, 5.64; N, 7.32 %. Calculated for $C_{45}H_{63}N_6S_3O_{12}Os$: C, 46.34; H, 5.44; N, 7.20 % ν_{max} (cm^{-1}): 1489 (CO), 1409 (CN) and 1353 (CS); $(m + 1)/z$: 1167.63 (calc. for $C_{45}H_{63}N_6S_3O_{12}Os$: 1167.44).

Tris(*N,N*-diethyl-*N'*-pivaloylthioureato)osmium(III), *fac*-[Os(L^5-*S,O*)$_3$] :

To a 100 cm^3 round-bottom flask containing 20 cm^3 of an acetonitrile-water mixture (3:1 v/v) was added solid HL^5 (109.9 mg, 0.508 mmol), followed by a slight excess of hydrated sodium acetate (77.5 mg, 0.570 mmol). The solution was gently heated at 60 ºC with stirring for a duration of 45 min. $OsCl_3 \cdot 3H_2O$ (59.2 mg, 0.169 mmol) dissolved in 8 cm^3 acetonitrile was added drop wise over 15 min to the ligand solution while heating at 103-105 ºC. The intensely dark brown solution was heated for a total of 5 h, where after it was left to stir overnight at room temperature. The solvent was removed under reduced pressure, resulting in dark brown solids. To the latter was added 20 cm^3 distilled water, and the product was extracted into dichloromethane organic phase. After removal of CH_2Cl_2 under vacuum, the crude product was dried *in vacuo* over P_2O_5 for several hours. The brown product was re-dissolved in methanol, left to evaporate, and dried *in vacuo* over P_2O_5 at room temperature for several days. The product was isolated via column chromatography using aluminium oxide as stationary phase and eluting with CH_2Cl_2.

A yield of 53.7 % was recovered; m.p. *decomposes*; *Anal*. Found: C, 43.39; H, 7.02; N, 9.89 %. Calculated for $C_{30}H_{57}N_6S_3O_3Os$: C, 43.09; H, 6.87; N, 10.05 % ν_{max} (cm^{-1}): 1481 (CO), 1419 (CN) and 1354 (CS). $(m + 1)/z$: 837.60 (calc. for $C_{30}H_{57}N_6S_3O_3Os$: 837.24).

Tris(*N*-pyrrolidyl-*N'*-pivaloylthioureato)osmium(III), *fac*-[Os(L^6-*S,O*)$_3$] :

To a 100 cm^3 round-bottomed flask containing 20 cm^3 of an acetonitrile-water mixture (3:1 v/v) was added solid HL^6 (102.8 mg, 0.480 mmol), followed by a slight excess of $CH_3COONa \cdot 3H_2O$

(73.1 mg, 0.537 mmol). The solution was gently heated at 60 ºC with stirring for a duration of 1 h. $OsCl_3 \cdot 3H_2O$ (55.2 mg, 0.157 mmol) dissolved in 8 cm^3 acetonitrile was added drop wise over 10 min to the ligand solution while heating at 100-102 ºC. The mixture was refluxed for a total time of 9 h, where after it was allowed to cool to room temperature. The volume of the dark brown acetonitrile-water solution was evaporated under vacuum to dryness, followed by re-dissolving in a minimum amount of methanol and slow evaporation. Drying under vacuum afforded dark coloured solids, which were washed liberally with distilled water, followed by prolonged heating *in vacuo* over P_2O_5. The desired product was purified by means of column chromatography, using aluminium oxide as stationary phase and eluting with CH_2Cl_2. The product was collected as orange-brown solids.

A yield of 36.04 % was recovered; m.p. *decomposes*; *Anal*. Found: C, 43.18; H, 6.38; N, 9.91 %. Calculated for $C_{30}H_{51}N_6S_3O_3Os$: C, 43.40; H, 6.19; N, 10.12 %; ν_{max} (cm^{-1}): 1482 (CO), 1422 (CN) and 1356 (CS); (m + 1)/z : 831.72 (calc. for $C_{30}H_{51}N_6S_3O_3Os$: 831.18).

Tris(*N*-morpholino-*N'*-pivaloylthioureato)osmium(III), *fac*-[Os(L^7-*S,O*)$_3$] :

To a 100 cm^3 round-bottomed flask containing 20 cm^3 of an acetonitrile-water mixture (3:1 v/v) was added solid HL^7 (101.8 mg, 0.442 mmol), followed by a slight excess of $CH_3COONa \cdot 3H_2O$ (66.9 mg, 0.492 mmol). The solution was gently heated at 60 ºC with stirring for 1 h, followed by slow drop wise addition of $OsCl_3 \cdot 3H_2O$ (50.7 mg, 0.145 mmol) dissolved in 8 cm^3 while heating at 100-102 ºC. The dark brown mixture was heated for a total of 5 h, where, after cooling to room temperature, the solvent was removed under vacuum. Extraction of the crude product into CH_2Cl_2 organic phase followed the addition of 20 cm^3 distilled water. The dark brown organic solvent was once again removed under pressure, where after remaining solids were re-dissolved in a minimum amount of methanol, which was left to evaporate slowly. Drying *in vacuo* over P_2O_5 afforded pale brown crude product. The product was isolated via column chromatography using aluminium oxide as stationary phase and eluting with CH_2Cl_2.

A yield of 58.59 % was recovered; m.p. *decomposes*; *Anal*. Found: C, 41.24; H, 5.97; N, 9.83 %. Calculated for $C_{30}H_{51}N_6S_3O_6Os$: C, 41.03; H, 5.85; N, 9.57 %; ν_{max} (cm^{-1}): 1479 (CO), 1424 (CN) and 1354 (CS); (m + 1)/z : 879.77 (calc. for $C_{30}H_{51}N_6S_3O_6Os$: 879.20).

3.2.4 Crystal Structure Determination

Crystals of dimension and structure suitable for X-ray diffraction analysis were grown through the vapour diffusion method. Hexane vapours were slowly diffused into a concentrated dichloromethane solution of tris(*N,N*-diethyl-*N'*-benzoylthioureato)osmium(III)**,** at a temperature of approximately 5 °C. After two weeks dark amber-brown crystals began to form at the solvent interface. Residual solvent was evaporated off, and a suitable crystal plate was chosen for X-ray diffraction analysis.

A suitable crystal was mounted on a thin glass fibre and coated in silicone-based oil to prevent decomposition. Data were collected on a Nonius Kappa CCD diffractometer using graphite monochromated Mo Kα radiation (λ = 0.7107 Å) with a detector to crystal distance of 45 mm. 237 oscillation frames were recorded, each of width 1º in ϕ, followed by 106 frames of 1° width in ω (with κ ≠ 0). Crystals were indexed from the first ten frames using the DENZO package [14] and positional data were refined along with diffractometer constants to give the final cell parameters. Integration and scaling (DENZO, Scalepack [14]) resulted in unique data sets corrected for Lorentz-polarisation effects and for the effects of crystal decay and absorption by a combination of averaging of equivalent reflections and an overall volume and scaling correction. Crystallographic data are displayed in ***Table 3.4***. The structure was solved using SHELXS-97 [15] and developed *via* alternating least squares cycles and Fourier difference synthesis (SHELXL-97 [15]) with the aid of the interface program X-SEED [16]. All non-hydrogen atoms of the Osmium complex were modelled anisotropically. Hydrogen atoms were assigned an isotropic thermal parameter 1.2 times that of the parent atom (1.5 times for terminal atoms) and allowed to ride on their parent atoms. The Osmium atom is placed on a 3-fold axis in space group P $\bar{3}$ at Wyckoff position *d* (1/2 , 2/3, *z*). The packing of this complex results in the formation of a hydrophobic channel running parallel to the *c*-axis and centred at $x = y = 0$. The presence of solvent in this channel could be inferred by the electron density located there, but the action of a 3-fold rotation axis and centre of inversion result in a great deal of disorder which could not be resolved. One hexane molecule was included in the model, and refined successfully, though with high isotropic thermal parameters. All manipulations and measurements of final crystal structure dimensions were carried out using ORTEP software, while the POV-RAY graphical software package was utilised for graphical enhancement and display purposes.

3.3 Results and Discussion

3.3.1 Absorption Spectrophotometry

Absorption spectra of pure and well defined Os(III) complexes were recorded in dichloromethane solutions at room temperature. Each of the complexes exhibited a single absorption band in the visible region, accompanied by an intense absorption in the high energy UV region. The low-energy absorption band corresponds to an Os ($d\pi^*$) ← L^n-*S,O* ($p\pi$) transition, explaining the vivid brown-red colours of the complex solutions. The high-energy absorption band in the UV-region arises from a ligand centered L^n-*S,O* ($p\pi^*$) ← L^n-*S,O* ($p\pi$) transition. The absorption spectrum of tris(*N,N*-diethyl-*N*′-benzoylthioureato)osmium(III) is shown as an example:

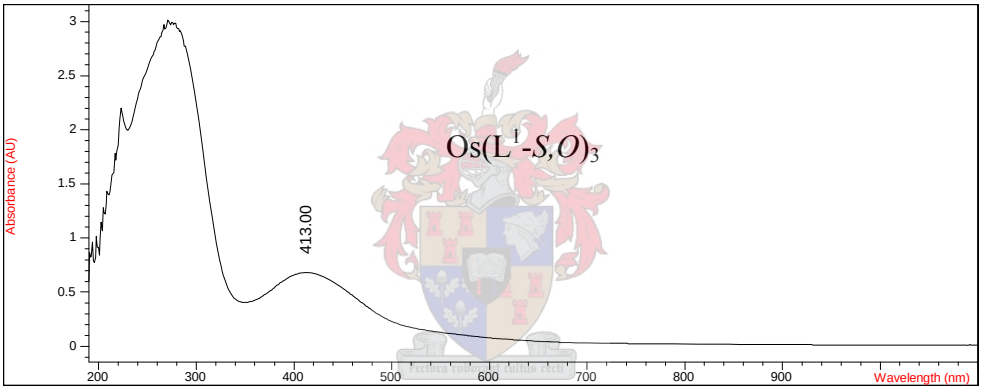

Fig. 3.1. **Absorption spectrum of Tris(*N,N*-diethyl-*N*′-benzoylthioureato)osmium(III). Recorded in CH_2Cl_2 at room temperature.**

A summary of the absorption bands for a selection of Os(III) complexes is contained in ***Table 3.1***

Complex	Absorption bands (nm)	
	Os ($d\pi^*$) ← L^n-*S,O* ($p\pi$)	L^n-*S,O* ($p\pi^*$)← L^n-*S,O* ($p\pi$)
$Os(L^1\text{-}S,O)_3$	413	271
$Os(L^5\text{-}S,O)_3$	377	259
$Os(L^6\text{-}S,O)_3$	372	259
$Os(L^7\text{-}S,O)_3$	365	281

Table 3.1. **LMCT transitions of $[Os(L^n\text{-}S,O)_3]$ complexes, recorded in CH_2Cl_2 at room temperature.**
$[Os(L^1\text{-}S,O)_3]$ = tris(*N,N*-diethyl-*N*'-benzoylthioureato)osmium(III)
$[Os(L^5\text{-}S,O)_3]$ = tris(*N,N*-diethyl-*N*'-pivaloylthioureato)osmium(III)
$[Os(L^6\text{-}S,O)_3]$ = tris(*N*-pyrrolidyl-*N*'-pivaloylthioureato)osmium(III)
$[Os(L^7\text{-}S,O)_3]$ = tris(*N*-morpholino-*N*'-pivaloylthioureato)osmium(III)

Upon comparison of the visible and UV region absorptions bands relating to $[Os(L^1\text{-}S,O)_3]$ and $[Os(L^5\text{-}S,O)_3]$, it becomes evident that quite a significant energy difference exists. It seems that substituting the benzoyl group of $[Os(L^1\text{-}S,O)_3]$ with the pivaloyl alkyl moiety (affording $[Os(L^5\text{-}S,O)_3]$), has the effect of blue-shifting the said absorptions maxima. These energy shifts can be adequately explained by considering the fundamental electronic configurations and photochemical interactions related to the formed complexes.

Ligand to metal charge transfers (LMCT) occur from electronically filled p-orbitals of the ligand to the unoccupied t_{2g} orbitals ($d\pi^*$) of the metal, *viz.* ligand p-orbitals of symmetry that do not participate in σ-overlapping (t_{1g}, t_{2g}, t_{1u} and t_{2u}), which contain electron density, will give rise to charge transfers to metal centred dπ-orbitals of t_{2g} symmetry.

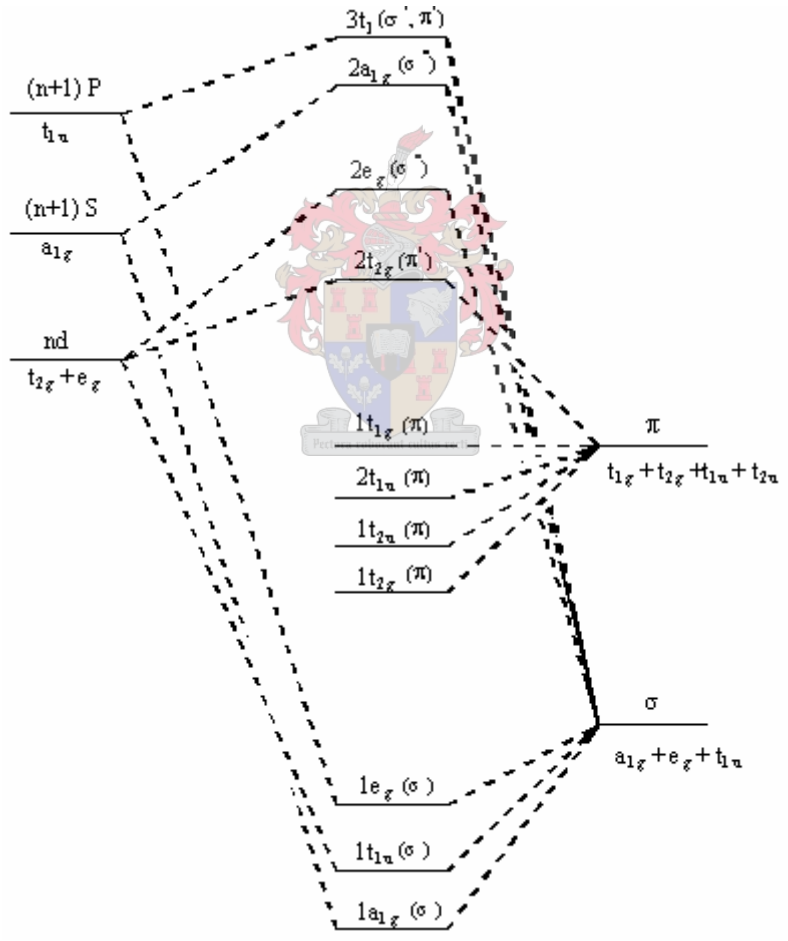

Fig 3.2. **Simplified molecular orbital diagram for octahedral osmium complexes exhibiting LMCT transitions.**

Firstly, consider the σ-interactions between metal and ligand orbitals. Ligand orbitals of a_{1g}, e_g and t_{1u} symmetry will overlap with s-, p- and d-orbitals of the metal (of corresponding symmetries a_{1g}, t_{1u} and e_g) to form complex bonding and anti-bonding orbitals (σ and σ^* in nature). Metal dπ-

orbitals of t_{2g} symmetry will not participate in σ-bonding, as will the ligand pπ-orbitals of t_{1g}, t_{2g} and t_{2u} symmetries (majority of the electron density associated with t_{1u}-orbitals will participate in σ-interactions, although a residual amount will be left for π-interactions). Consequently, metal and ligand orbitals of t_{2g} symmetry will participate in π-bonding, with a subsequent lowering in energy of the t_{2g} orbitals of the formed complex. Now, electron-filled ligand pπ-orbitals of t_{1g}, t_{1u} and t_{2u} symmetries may give rise to LMCTs. These transfers will be from the afore-mentioned ligand pπ-orbitals to either $d\pi^*$ (t_{2g}) or $d\sigma^*$ (e_g) metal-centred energy levels.

Assume for the moment that the ligands are coordinated to the metal without deprotonation of the amidic hydrogen. The ligand pπ-orbitals of t_{1g}, t_{1u} and t_{2u} symmetries are situated energetically slightly lower compared to the metal $d\pi^*$ (t_{2g}) and $d\sigma^*$ (e_g) orbitals, arising from the difference in electronegativity between the metal ion and the ligating donor atoms, the latter possessing greater eletronegativity.

Now, upon deprotonation of the amidic hydrogen of the ligand, an increased amount of electron density will be distributed over both ligating donor atoms, sulphur and oxygen, effectively lowering the inherent optical electronegativity of each ligating donor atom. Consequently, the electron filled pπ-orbitals of t_{1g}, t_{1u} and t_{2u} symmetries will now lie closer energetically to the metal t_{2g} ($d\pi^*$) and e_g ($d\sigma^*$) orbitals. Therefore, LMCTs will now be observed at increased wavelengths, since a reduced amount of energy needs to be absorbed to effect a charge transfer.
This can be inferred from the comparison of $[OsCl_6]^{3-}$, $[OsCl_6]^{2-}$, $[Os(L^1\text{-}S,O)_3]$ and $[Os(L^5\text{-}S,O)_3]$ absorption spectra. The hexachloroosmate ions exhibit two LMCTs, while the other two complexes seem to exhibit only one LMCT.

Complex	**Charge Transfer (nm)**	
	$d\pi^*$ (t_{2g}) ← pπ (t_{1u})	**$d\pi^*$ (t_{2g}) ← pπ (t_{2u})**
$[OsCl_6]^{3-}$	282	262
$[OsCl_6]^{2-}$	371	340
$[Os(L^1\text{-}S,O)_3]$	413	---
$[Os(L^5\text{-}S,O)_3]$	377	---

Table 3.2. **Comparison of LMCTs for hexahalide- and $Os(L^n\text{-}S,O)_3$ complexes; recorded in CH_2Cl_2 at room temperature**

Compare the 1st LMCTs of $[OsCl_6]^{3-}$ and $[Os(L^5\text{-}S,O)_3]$. Substitution of the six chlorine atoms with three bidentate HL^5 ligands has the net result of changing the ligating atoms from chlorine to sulphur and oxygen. The difference in optical electronegativity (χ_o) between chlorine and oxygen is only slight. Therefore, the difference in energy between the ligand pπ-orbitals and the metal dπ*-orbitals would not have been altered too greatly (changing Cl^- with HL^5). But, the difference in χ_o between chlorine and sulphur is more pronounced, being exacerbated by the increased electron density situated on the ligating sulphur atom (arising from delocalisation in chelate ring), resulting in the ligand pπ-orbitals being situated closer energetically to the metal dπ*-orbitals. Therefore, the single LMCT will be observed at a longer wavelength, explaining the red-shift of the absorption maximum. Furthermore, charge transfer bands should theoretically be possible for the thiourea complexes. These may be as follows: $d\pi^*$ (t_{2g}) ← pπ (t_{1g}), $d\pi^*$ (t_{2g}) ← pπ (t_{2u}) and $d\pi^*$ (t_{2g}) ← pπ (t_{2g}), although the latter is unlikely, since ligand orbitals of t_{2g} symmetry will be involved with π-interactions. For low field ligands charge transfers to metal $d\sigma^*$ (e_g) levels are also possible, although they are inherently weak in intensity. It is assumed that the unobserved high energy LMCTs are obscured by intense ligand-centered charge transfers occurring in the UV region.

3.3.2 X-ray Crystallography

Fig. 3.4 illustrates the crystal structure obtained for $[Os(L^1\text{-}S,O)_3]$. Crystallographic data and structure refinement parameters for $[Os(L^1\text{-}S,O)_3]$, obtained from X-ray diffraction analysis are contained in ***Table 3.4***.

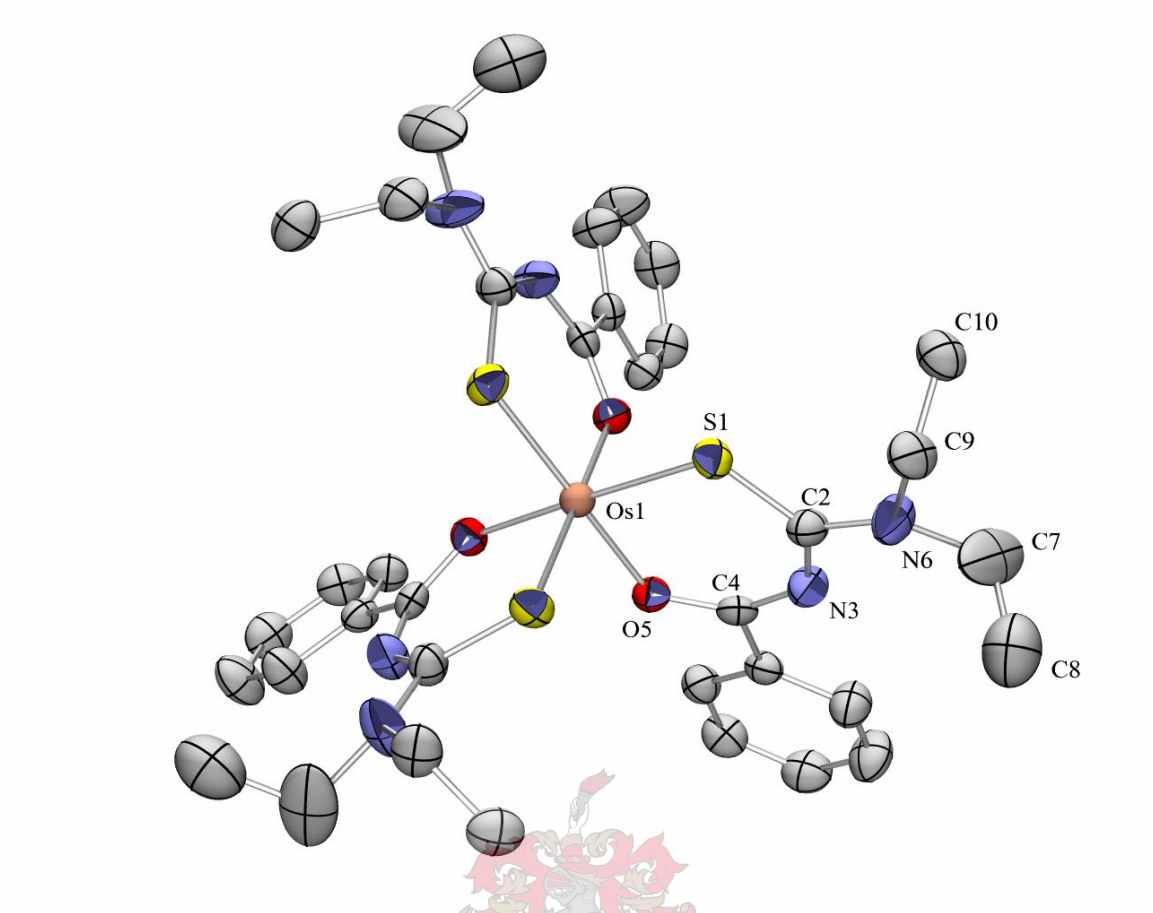

Fig. 3.4. **Crystal structure of [Os(L^1-S,O)$_3$]. Trigonal crystal system with *D3* symmetry (R = 3.78%)**

Crystal data and structure refinement

Empirical formula	$C_{54}H_{87}N_6O_3OsS_3$
Formula weight	1154.68
Temperature	203(2) K
Wavelength	0.71073 Å
Crystal system, space group	Trigonal, P-3 (No. 147)
Unit cell dimensions	a = 16.544 (2) Å α = 90 º
	b = 16.544 (2) Å β = 90 º
	c = 8.4556 (17) Å γ = 120 º
Volume	2004.2 (6) Å^3
Z, Calculated density	2, 1.913 Mg/m^3
Absorption coefficient	3.402 mm^{-1}
F(000)	1202
Crystal size	0.25 × 0.20 × 0.05 mm

Theta range for data collection	3.45 to 27.86 º
Limiting indices	$-21 \leq h \leq 21$, $-21 \leq k \leq 20$, $-8 \leq l \leq 10$
Reflections collected / unique	20318 / 3174 [R(int) = 0.0432]
Completeness to theta = 27.86	99.2 %
Max. and min. transmission	0.8483 and 0.4835
Refinement method	Full-matrix least-squares on F^2
Data / restraints / parameters	3174 / 5 / 168
Goodness-of-fit on F^2	1.090
Final R indices [$I > 2\sigma(I)$]	$R_1 = 0.0378$, $wR_2 = 0.1028$
R indices (all data)	$R_1 = 0.0489$, $wR_2 = 0.1080$
Extinction coefficient	0.0026 (7)
Largest diff. peak and hole	2.138 and -0.775 e.A^{-3}

Table 3.4. **Crystallographic data and parameters of [Os(L^1-*S,O*)$_3$]**

Fig. 3.5 exhibits the partial crystal structure of [Os(L^1-*S,O*)$_3$], with the inclusion of a disordered hexane molecule.

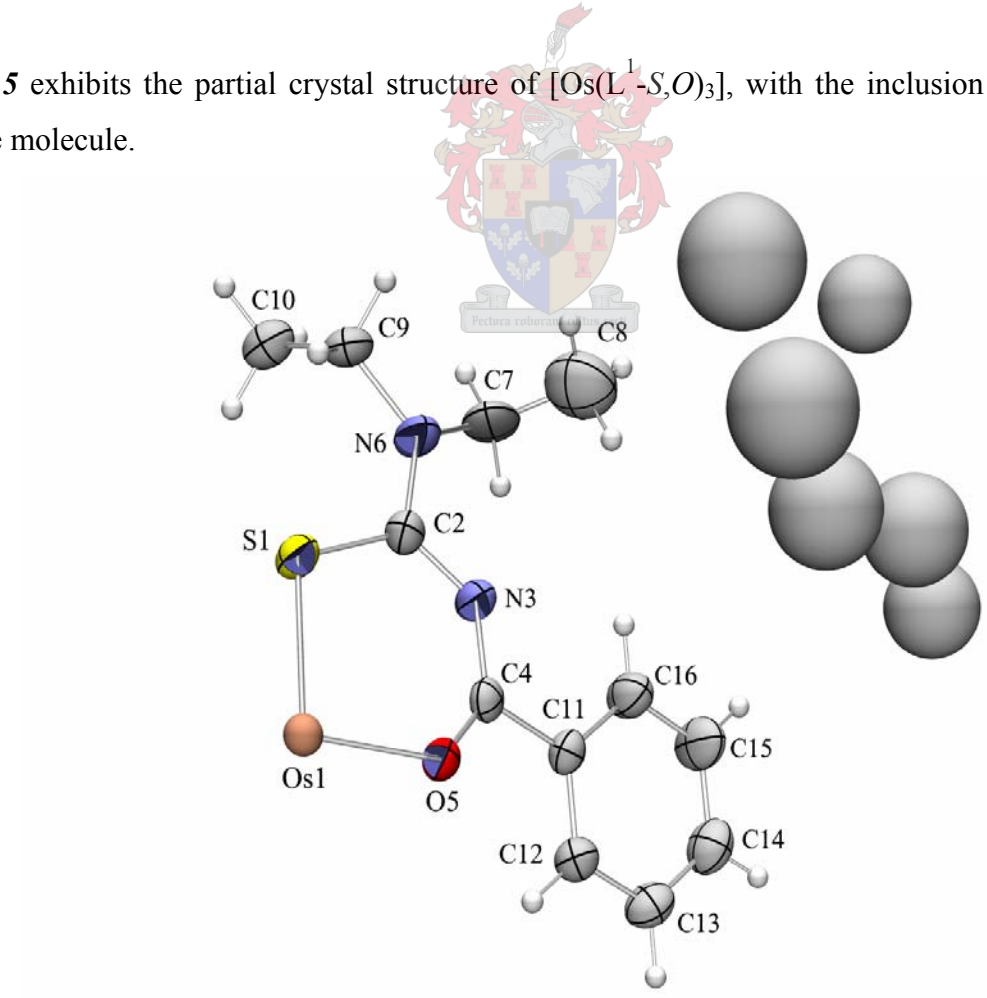

Fig. 3.5. **Partial crystal structure of [Os(L^1-S,O)$_3$] with the inclusion of a disordered hexane molecule.**

Structural dimensions are contained in the ***Table 3.5*** below. Bond lengths, angles and related dimensions are all reported with reference to the numbering scheme contained in ***Fig. 3.5***.

Bond	Distance (Å)	Bond	Distance (Å)
Os - S_1	2.309	N_6 - C_9	1.487
Os - O_5	2.063	N_6 - C_7	1.656
C_2 - S_1	1.728	C_9 - C_{10}	1.507
C_4 - O_5	1.258	C_7 - C_8	1.450
N_3 - C_2	1.356	C_{11} - C_{16}	1.385
N_3 - C_4	1.319	C_{11} - C_{12}	1.390
C_2 - N_6	1.324	C_{16} - C_{15}	1.392
C_4 - C_{11}	1.497	C_{12} - C_{13}	1.394
		C_{15} - C_{14}	1.381
		C_{13} - C_{14}	1.367

Table 3.5. **Selected bond lengths and bond angles of [Os(L^1-*S,O*)$_3$]**

Each unit cell consists of two tris(*N,N*-diethyl-*N'*-benzoylthioureato)osmium(III) complex structures, with hexane solvent channels located at the vertices of each unit cell, running parallel with the c-axis. Presence of the solvent channels was inferred by the occurrence of a large amount of electron density, although the action of the 3-fold rotation axis and centre of inversion resulted in a great deal of disorder which was difficult to resolve entirely. From ***Fig. 3.5*** it seems that the innate electron density associated with the diethyl and phenyl moieties are directed towards the said solvent channels.

Fig. 3.6 demonstrates the presence of the solvent channels, running parallel with the c-axis, and located at the four vertices of the unit cell. Clearly the hexane structures are not very well resolved, stemming from their inherent high degree of disorder as described in the preceding paragraph.

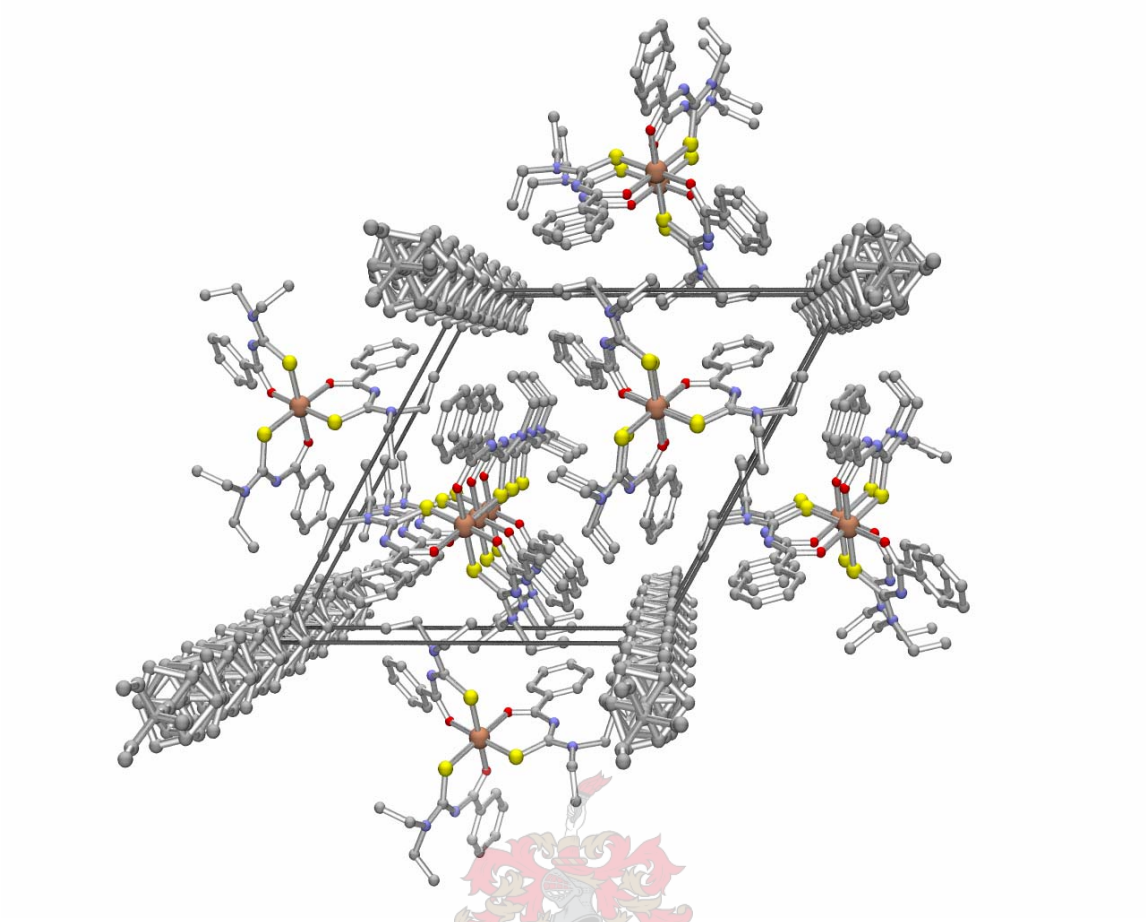

Fig. 3.6. **Successive unit cell packing of $[Os(L^1\text{-}S,O)_3]$, exhibiting residual solvent (hexane) present as channels running parallel to the *c*-axes**

Fig. 3.7 illustrates the packing order of multiple unit cells, with clear orientation of the dialkyl moieties on top of each other.

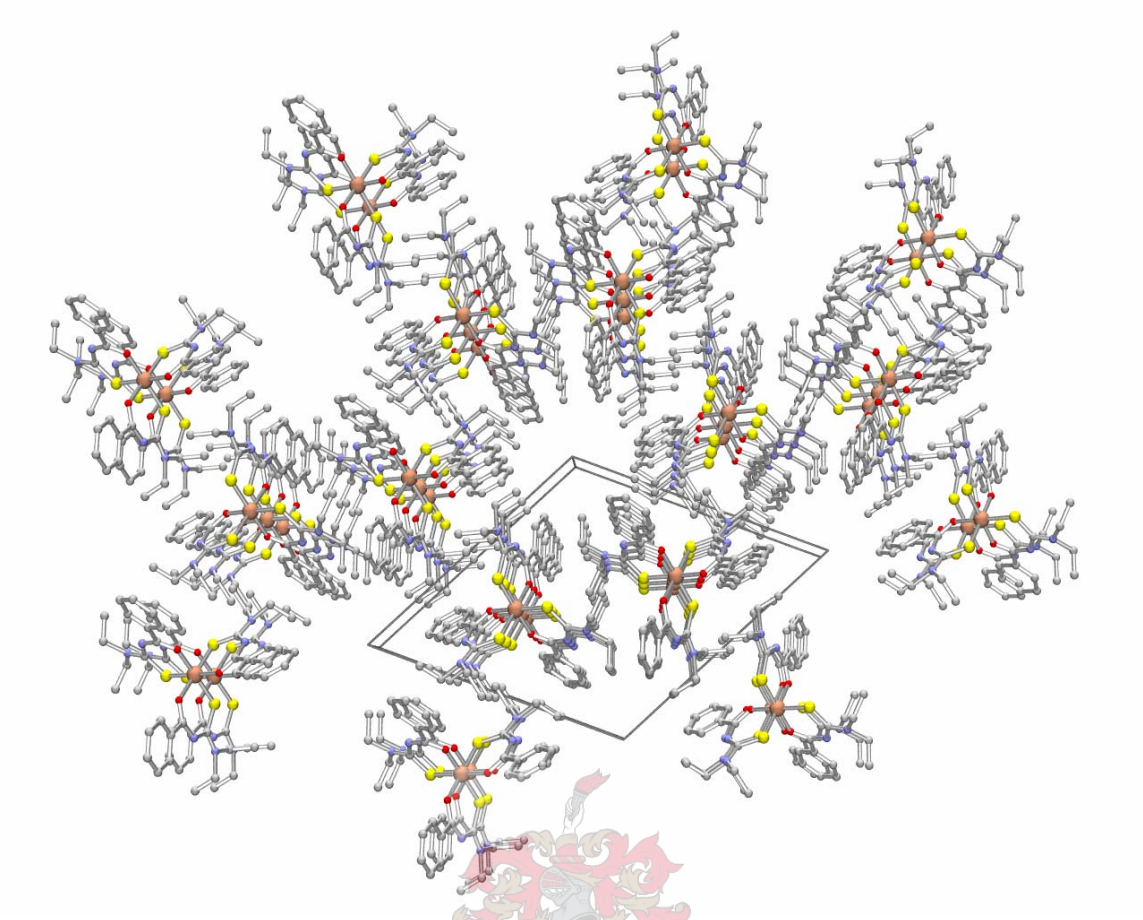

Fig. 3.7. **Successive unit cell packing of $[Os(L^1\text{-}S,O)_3]$**

Orientation of the phenyl rings within successive unit cells are quite clearly illustrated in ***Fig. 3.8*** , where one of the aromatic rings in each *tris*-chelated complex assume a vertical orientation running parallel with the *c*-axis, and at nearly right angle with the chelate ring structures.

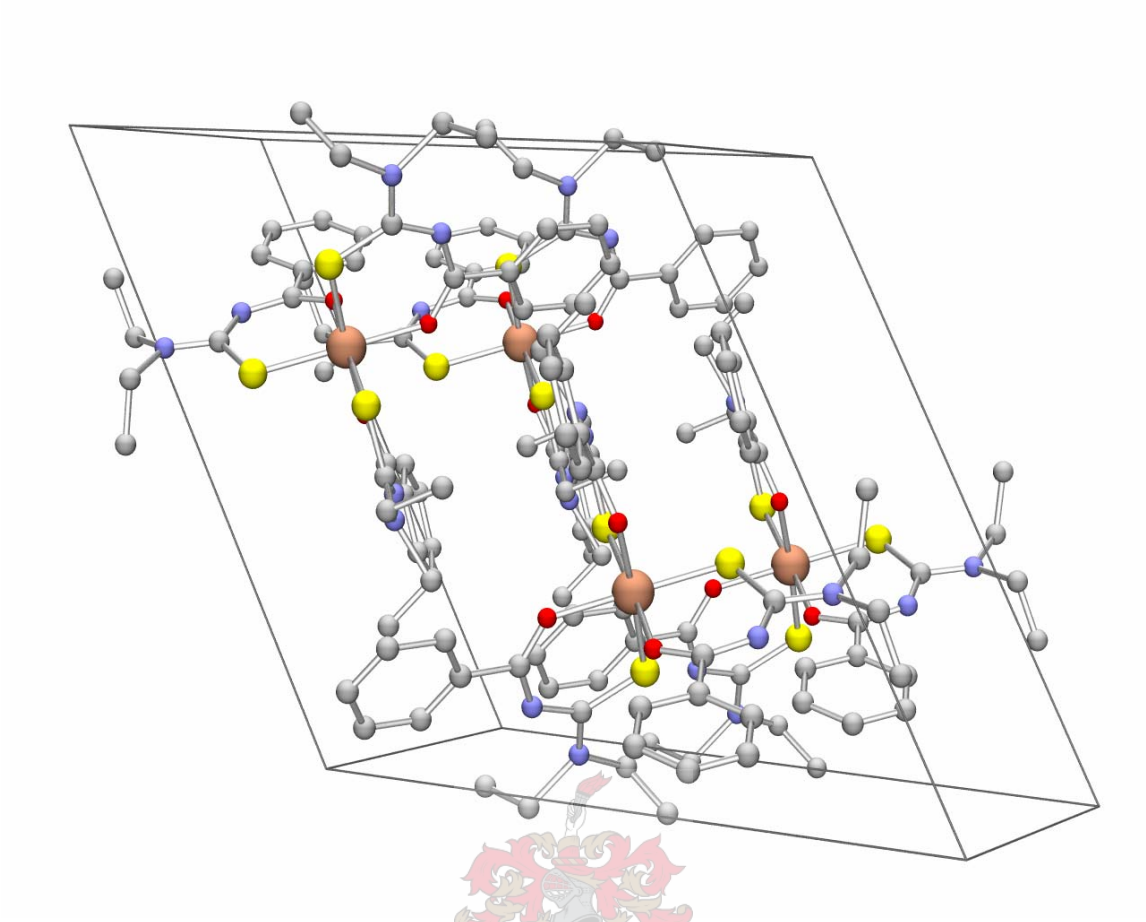

Fig. 3.8. **Singular unit cell of [Os(L^1-S,O)$_3$]. Of note is the out-of-plane alignment of one of the phenyl rings**

The complex resolved as a six-coordinate structure consisting of three deprotonated *N*,*N*-diethyl-*N'*-benzoylthiourea ligands, coordinated in a bidentate fashion through the sulphur and oxygen donor atoms. The tris-chelate configuration resulted in a distorted octahedral geometry, with subsequent lowering in the symmetry from O_h to D_3 symmetry. Octahedral geometry may be considered as a special case of the D_{3d} antiprism, which occurs when two perfectly staggered equilateral triangles of with side *s* are separated by an exact distance of $(2/3)^{1/2}s$. Distortions brought upon by coordination of specific bidentate ligands lead to twisting of the two triangles, defined by an angle φ [17].

Theoretically, for undistorted octahedra the angle φ is set at 60º. In the case of [Os(L^1-*S*,*O*)$_3$] this angle is calculated as 58.58º, which corresponds well with the reported value of 58.1º for the complex [Ru(L^1-*S*,*O*)$_3$] [9]. Further proof of distorted octahedral configuration becomes clear with analysis of the angles (*cf.* ***Fig. 3.5***) between the axes of coordination. S_1 – Os – S_1 angles between adjacent ligands are all 90.04º, while the corresponding O_5 – Os – O_5 angles are 83.94º (whereas optimal octahedral angles should equal 90º). O_5 – Os – S_1 angles along the bonding axes are all 175.74º, a deviation of 4.26º from the optimal 180º of octahedral geometry.

The distorted octahedral geometry of [Os(L^1-*S*,*O*)$_3$] compares well with the analogous complexes of rhodium [10] and ruthenium [9].

Length(Å)/Angle(°)	[Os(L^1-*S*,*O*)$_3$]	[Ru(L^1-*S*,*O*)$_3$]	[Rh(L^1-*S*,*O*)$_3$]
M – S_1	2.31	2.29	2.28
M – O_5	2.06	2.05	2.03
S_1 – C_2	1.73	1.69	1.72
O_5 – C_4	1.26	1.24	1.26
N_3 - C_2	1.36	1.34	1.36
N_3 - C_4	1.32	1.32	1.32
C_2 – N_6	1.32	1.33	1.33
C_4 – C_{11}	1.50	1.49	1.52
S_1 – M – O_5	92.51	91.90	94.20
M – S_1 – C_2	108.8	108.6	107.7
M – O_5 – C_4	129.8	130.3	128.6
S_1 – C_2 – N_3	128.4	130.3	129.1
O_5 – C_4 – N_3	130.8	131.2	131.4
C_2 – N_3 – C_4	128.3	126.5	127.4

Table 3.6. **Comparative bond lengths and bond angles of [Os(L^1-*S*,*O*)$_3$], [Ru(L^1-*S*,*O*)$_3$] and [Rh(L^1-*S*,*O*)$_3$]**

The C_2 – S_1 bond in this complex is comparable to the analogous bond found in the Au(I) complex formed with *N*,*N*-diethyl-*N*′-benzoylthiourea (1.70 Å), where the atoms C_2 – S_1 – Au are aligned in a linear fashion [18]. This distance implies partial double bond character, its length of 1.728 Å being significantly longer than the average C = S bond length of 1.60 Å, but also shorter than the average C – S length of 1.82 Å (average bond lengths found in Huheey *et al* [19]).

From the *CRC Handbook of Chemistry and Physics* [20], the average C = S bond length of thiourea compounds is stated as 1.681 Å, which relates to the ligand in its unbounded state. The C_2 – S_1 bond length of [Os(L^1-*S*,*O*)$_3$] therefore indicates a reduction in double bond character, which is consistent with the delocalisation of charge associated with the six-membered chelate ring.

The C_4 – O_5 bond length of 1.258 Å is considerably shorter than that of the typical average C – O bond length (1.430 Å) [19], and therefore seems to be more double bond in nature. In fact, it

doesn't deviate greatly from the average C = O bond length (1.20 Å) found in [19], therefore indicating substantial double bond character. Moreover, C = O bond lengths of unbounded urea ligands, 1.230 Å [20], compare favourably with the $C_4 – O_5$ bond length.

Comparison of the $C_4 – O_5$ and $C_2 – S_1$ bond lengths seem to elucidate the manner through which the deprotonated ligand coordinates to the metal ion. According to HSAB (hard-soft acid-base) theory, trivalent osmium is considered to be a soft metal ion, preferentially coordinating with ligands containing "soft" donor atoms such as phosphorous or sulphur, as opposed to "hard" donor atoms such as nitrogen or oxygen. The carbonyl moiety of the dialkyl-benzoylthiourea ligand might be regarded as a "hard" Lewis base, whereas the thiocarbonyl moiety would exhibit "soft" Lewis base character. Therefore, on the basis of HSAB theory one would expect the ligand to coordinate preferentially through the thiocarbonyl group. The earlier $C_4 – O_5$ and $C_2 – S_1$ bond length discussion could in fact substantiate the following postulation. Upon deprotonation of the amidic hydrogen, the larger percentage of delocalisation extends in the direction of the $C_2 – S_1$ bond, although delocalisation also occurs towards carbonyl moiety.

Bonds $N_3 – C_2$ (1.356 Å) and $N_3 – C_4$ (1.319 Å) clearly exhibit partial double bond character (therefore inferring delocalisation present in the chelate ring), since they are much shorter than the average N – C single bond lengths of 1.47 Å [19]. Moreover, the corresponding bond lengths of the Au(I) complex [18], where no delocalisation occurs, are slightly longer in length.

Complex	Bond Lengths (Å)	
	$N_3 – C_2$	$N_3 – C_4$
[Os(L^1-*S,O*)$_3$]	1.36	1.32
[AuCl(L^1-*S,O*)]	1.42	1.38

Table 3.7. **Comparison of nitrogen-carbon bond lengths**

The $C_2 – N_6$ bond length measures 1.324 Å, which implies partial double bond character, and is much shorter than typical average C – N single bond (1.47 Å) [19], thus implying that charge delocalisation extends towards the amino side of the chelate ring rather than to the phenyl side, since the $C_4 – C_{11}$ bond measures 1.497 Å, which corresponds more closely to a typical average C – C bond length of 1.54 Å [19].

The atoms $N_6 - C_2 - N_3 - C_4$ form a plane that is nearly planar (176.6º). The six-membered chelate ring ($Os - S_1 - C_2 - N_3 - C_4 - O_5$) forms a plane that deviates only 0.2º from perfect planarity. These near planar orientations, coupled with the shorter than expected bond lengths along the six-membered chelate ring all point towards the presence of delocalisation.

Carbon-carbon bond lengths situated in the phenyl ring all compare with the typical average C – C sp^2 bond length of 1.380 Å [20].

	Reference		
Bond	**[Os(L^1-*S,O*)$_3$]**	***CRC Handbook***	**Note**
$C_2 - S_1$	1.728	1.681	$(X_2N)_2 - \mathbf{C} = \mathbf{S}$ (thioureas)
$C_4 - O_5$	1.258	1.230	$[(C_x)_n - N]_2 - \mathbf{C} = \mathbf{O}$ (ureas)
$C_4 - N_3$	1.319	1.363	$[(C_x)_n - \mathbf{N}]_2 - \mathbf{C} = O$ (ureas)
$C_2 - N_3$	1.356	1.346	$(X_2\mathbf{N})_2 - \mathbf{C} = S$ (thioureas)
$C_7 - C_8$	1.450	1.530	$X - \mathbf{C}H_2 - \mathbf{C}H_3$
$C_9 - C_{10}$	1.507		
$C_{phenyl} - C_4$	1.497	1.500	$\mathbf{C_{phenyl}} - \mathbf{C}(= O) - NH_2$
C = C	1.385	1.380	$H - \mathbf{C} = \mathbf{C} - H$

Table 3.8. **Dimension comparisons of [Os(L^1-*S,O*)$_3$] against corresponding literature values.**

Metal to sulphur bond length of the [Os(L^1-*S,O*)$_3$] complex compares favourably with those of the analogous ruthenium [9] and rhodium [10] complexes. *N,N*-dimethyldithiocarbamato ligands form bidentate four-membered *S,S*-chelates with osmium(IV/III), resulting in average Os – S bond lengths of 2.38Å [21].

3.4 Summary

A series of osmium complexes containing ligands of the type *N,N*-dialkyl-*N'*-(acyl)aroylthiourea have been synthesised and characterised. An excess amount of ligand contributed towards reduction of the tetravalent Os(IV) to trivalent Os(III), where after the ligands were complexated with Os(III) to afford tris-chelated octahedral complexes.

The first known complex of type tris(*N,N*-diethyl-*N'*-benzoylthioureato)osmium(III), [(Os(L^1-*S,O*)$_3$)] has been synthesised and characterised crystallographically. Comparison with ruthenium [9] and rhodium [10] analogues revealed comparative dimensions in terms of bond lengths and angles.

Results from this chapter indicate that osmium in its trivalent form seems to be the preferable oxidation state for future liquid-liquid extraction studies. This can be corroborated by the study of Schuster, *et al.* [22], in which Os(III) was claimed to be extracted with ligands of type *N,N*-diethyl-*N'*-benzoylthiourea. However, no attempts were made by these authors to characterise the extracted species.

References

[1] K.R. Koch, *Coord Chem Rev*, 216-217 (2001) 473.

[2] P. Vest, M. Schuster and H. Konig, *Fresenius Z Anal Chem*, 335 (1989) 759.

[3] M. Schuster and M. Schwarzer, *Anal Chim Acta*, 328 (1996) 1.

[4] Mautjana, A. N. MSc Dissertation (2000), University of Cape Town.

[5] G. Fitzl, L. Beyer, J. Sieler, R. Richter, J. Kaiser and E. Hoyer, *Z Anorg Allg Chem*, 433 (1977) 237.

[6] K.R. Koch, C. Sacht and S. Bourne, *S Afr J Chem*, 48 (1995) 71.

[7] R.A. Bailey, K.L. Rothaupt and R.K. Kullnig, *Inorg Chim Acta*, 147 (1988) 233.

[8] R. Richter, L. Beyer and J. Kaiser, *Z Anorg Allg Chem*, 461 (1980) 67.

[9] R. Richter, J. Sieler, E. Hoyer, L. Beyer, O. Lindqvist and L. Andersen, *Z Anorg Allg Chem*, 580 (1990) 167.

[10] W. Bensch and M. Schuster, *Z Anorg Allg Chem*, 615 (1992) 93.

[11] M. Schuster, H. Konig and B. Kugler, *Fres J Anal Chem*, 338 (1990) 717.

[12] Miller, J. D. Ph.D. Thesis (2000), University of Cape Town.

[13] K.R. Koch, C. Sacht and S. Bourne, *Inorg Chim Acta*, 232 (1995) 109.

[14] Z. Otwinowski and W. Minor, *Methods Enzymol*, 276 (1996) 307.

[15] Sheldrick, G. M., SHELX-97 (1997), University of Göttingen.

[16] Barbour, L. J., X-SEED (1999), University of Missouri-Columbia.

[17] E.I. Stiefel and G.F. Brown, *Inorg Chem*, 11 (1972) 434.

[18] W. Bensch and M. Schuster, *Z Anorg Allg Chem*, 611 (1992) 99.

[19] J.E. Huheey, E.A. Keiter and R.L. Keiter, *Inorganic Chemistry. Principles of Structure and Reactivity*, HarperCollins College Publishers, New York (1993).

[20] D.R. Lides, *CRC Handbook of Chemistry and Physics*, CRC Press, Washington DC (2002).

[21] K.W. Given and L.H. Pignolet, *Inorg Chem*, 16 (1977) 2982.

[22] M. Schuster and H. Konig, *Fres Z Anal Chem*, 331 (1988) 383.

Chapter 4

A preliminary study of the substitution reactions of ruthenium-polypyridine complexes with *N*,*N*-dialkyl-*N*′-acyl(aroyl)thioureas

4.1 Introduction

Ever since the first report of emission from the complex $Ru(bpy)_2^{3+}$ [1], there has been a considerable interest in ruthenium polypyridine complexes, mainly because of their chemical stability, excited state reactivities, redox properties, excited state lifetimes and luminescence emissions.

Polypyridine ruthenium(II) derivatives are incorporated intensively in intramolecular electron transfer processes due to their interesting spectroscopic and electrochemical properties. An example would be the strong absorptions in the visible spectrum arising from metal-to-ligand charge-transfer processes. These transitions produce long-lived excited triplet states (especially for tris(bipyridine)ruthenium(II) complexes), which make these particular compounds extremely efficient phosphorescence materials [2].

Yet they also contribute to the study of fundamental chemical processes, in particular photochemically induced charge-transfer [3], ligand substitution in various solvent media [4], and stereochemical isomerization processes [5].

Moreover, the electronic absorption and electrochemical properties of the bis(bipyridyl)ruthenium chromophore make it a sensitive spectator ion in with which to investigate metal-ligand interactions [6-8].

Since the photochemistry and redox behaviour of polypyridyl ruthenium complexes are overwhelmingly ligand dependent [9], the afore mentioned properties can be altered via specific ligand design. Therefore, significant research focus has been on tailoring ligands to afford goal-specific photochemical properties once incorporated into the Ru(II) core.

There exists a substantial and diverse amount of cis-disubstituted bis(bipyridine)ruthenium(II) complexes with a variety of ligands including phosphines [10], arsines [11], halides [12], stibines,

thioethers [13], thiolates [14], oximes [15], nitrogen-based heterocycles [16] and organometallic donors.

Diverse motivations have led to the syntheses of the above mentioned complexes.. They range from incorporating these complexes into solar energy conversion schemes [17], to being used as electrochemical reduction catalysts in converting acetylene to ethane and ethylene [18].

Complexes of the type $RuCl_2(PPh_3)_2(N)_2$ (where N = py, bpy or phen) exhibit promising application as catalysts to the field of homogeneous hydrogenation of unsaturated organics [19]. This process necessitates the dissociation of a coordinated ligand (in this case most likely phosphine) to generate an electronically unsaturated species which may react with the substrate.

Polypyridyl ruthenium complexes have also been utilised as excellent oxidation catalysts, e.g. in the oxidation of water to oxygen and hydrogen [20], and in the conversion of chloride to chlorine [21] All the complexes mentioned above are constantly contributing to ongoing development in different branches of chemistry, such as photochemistry, photoelectrochemistry, electrochemistry, chemiluminescence and electron/energy transfer.

To our knowledge there have been no systematic investigations into the possibility of incorporating ligands of type *N,N*-dialkyl-*N'*-acyl(aroyl)thiourea into the bis(bipyridine)ruthenium(II) complex motif. In this chapter we attempt to conduct preliminary investigations into the substitution reactions of ruthenium-polypyridine complexes with *N,N*-dialkyl-*N'*-acyl(aroyl)thioureas, with a view towards future application of the resultant products in analytical and process chemistry fields.

4.2 Experimental Section

4.2.1 Analytical Methods

Solutions of the individual complexes were contained in 2 mm quartz cuvettes and their UV-Vis absorption spectra were measured with an HP Agilent Diode Array Spectrophotometer. Infrared spectra were recorded with a NEXUS model FT-IR instrument (Thermo Nicolet, USA). KBr discs of the complexes were used to record the infrared spectra in transmission mode over the MID-IR range 4000-400 cm^{-1} at a standard resolution of 4 cm^{-1}. Product identification was also facilitated by means of HPLC coupled to Electrospray Mass Spectrometry (HPLC-ESMS).

4.2.2 Synthesis of starting materials

The starting material $Ru(bpy)_2Cl_2 \cdot 2H_2O$ was synthesised according to a literature method, with additional scale-down modifications [10]. *N,N*-diethyl-*N'*-benzoylthiourea (HL^1), *N,N*-diethyl-*N'*-pivaloylthiourea (HL^5) and *N* -pyrrolidyl-*N'*-pivaloylthiourea (HL^6) were prepared according to the method under section *3.2.2* of chapter 3. All synthetic procedures were carried out under inert N_2 atmosphere, while subsequent work-up was performed with exposure to the atmosphere.

***cis*-Bis(2,2'-bipyridine)dichlororuthenium(II) dihydrate, $Ru(bpy)_2Cl_2 \cdot 2H_2O$:**

Approximately 100.0 mg of $RuCl_3 \cdot xH_2O$ was weighed off and dried *in vacuo* over P_2O_5 for a period of 2 h. To 15 cm^3 of degassed *N,N*-dimethylformamide (DMF) contained in a 100 cm^3 flask was added lithium chloride (237.3 mg, 5.598 mmol) with gentle heating. Upon complete dissolvation, anhydrous $RuCl_3$ (107.7 mg, 0.412 mmol) was slowly and carefully added to the clear solution, followed by addition of 2,2′-bipyridine (130.0 mg, 0.832 mmol). The dark green solution was refluxed at 165-167 ºC with stirring for a period of 8 h, where after it was allowed to cool to room temperature. The dark purple reaction mixture was then added drop wise to 100 cm^3 of anhydrous acetone while stirring vigorously, and was left to stir at room temperature for a further 30 min. Overnight cooling at *ca.* 0 ºC afforded dark purple crystals in solution, which were collected through centrifugation, followed by washing with distilled water (3 × 10 cm^3 aliquots) and diethyl ether (3 × 10 cm^3 aliquots). Drying *in vacuo* over P_2O_5 for several hours resulted in clean isolated product, with a yield of 53.4 % (114.4 mg, 0.220 mmol) being recovered. m.p. *decomposes*; *Anal*. Found: C, 44.14; H, 3.75; N, 9.51 %. Calculated for $C_{20}H_{20}N_4Cl_2O_2Ru$: C, 46.16; H, 3.87; N, 10.77 %.

***N,N*-diethyl-*N'*-benzoylthiourea (DEBT or HL^1):**

A yield of 85.4 % (6.0 g, 25.4 mmol) was obtained (*cf.* Section *3.2.2,* Chapter 3); m.p. 98-100 ºC; *Anal*. Found: C, 60.91; H, 6.92; N, 11.60 %. Calculated for $C_{12}H_{16}N_2SO$: C, 60.99; H, 6.82 ; N, 11.85 %.

***N,N*-diethyl-*N'*-pivaloylthiourea (DEPT or HL^5):**

Ligand synthesised by Miller [22]. 98.0 % yield; m.p. 90-91 ºC; *Anal*. Found: C, 55.6; H, 9.09; N, 13.2; S, 15.1 % Calculated for $C_{10}H_{20}N_2SO$: C, 55.5; H, 9.33; N, 12.9; S, 14.8 %.

***N* -pyrrolidyl-*N'*-pivaloylthiourea (PPT or HL^6):**

Ligand synthesised by Miller [22]. 90.1% yield; m.p. 136 ºC; *Anal*. Found: C, 56.0; H, 8.77; N, 13.3; S, 14.8 % Calculated for $C_{10}H_{18}N_2SO$: C, 56.0; H, 8.48; N, 13.1; S, 15.0 %.

4.2.3 Synthesis of substituted bis(bipyridine) complexes

The complexes were all synthesised according to a general procedure, allowing for slight modifications depending on the ligand incorporated in the substitution reaction. An outline for the synthesis of $[Ru(bpy)_2(L^1\text{-}S,O)]PF_6$ is given in the scheme below:

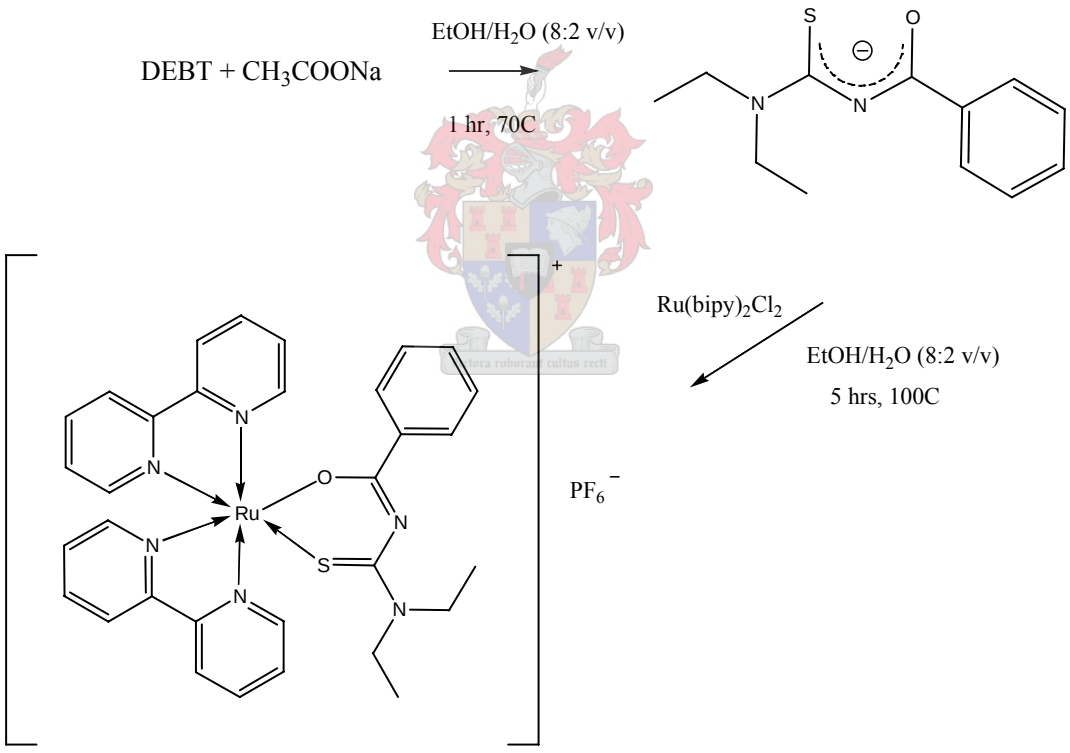

Fig. 4.1. **Scheme for the synthesis of $[Ru(bpy)_2(L^1\text{-}S,O)]PF_6$**

cis-Bis(2,2′-bipyridine)(_N,N_-diethyl-_N′_-benzoylthioureato)ruthenium(II) hexafluorophosphate, [Ru(bpy)$_2$(L^1-_S,O_)]PF_6:

To a 100 cm^3 round-bottomed flask containing 20 cm^3 of an ethanol-water mixture (4:1 v/v) was added HL^1 (50.4 mg, 0.213 mmol), followed by a slight excess of sodium acetate trihydrate (34.0 mg, 0.250 mmol). The colourless ligand solution was heated gently with stirring at 60 ºC for 45 min. $Ru(bpy)_2Cl_2 \cdot 2H_2O$ (64.1 mg, 0.123 mmol) dissolved in 20 cm^3 of ethanol-water mixture (4:1 v/v) was added drop wise to the deprotonated ligand solution over 20 min while heating at 101-103 ºC. The dark mulberry-red solution was refluxed for a period of 5 h, where after it was allowed to stir overnight at room temperature. The solvent was removed under reduced pressure, whereafter 20 cm^3 of distilled water was added. To the aqueous dark red solution was added an excess of NH_4PF_6 (92.0 mg, 0.564 mmol) while stirring at room temperature. Flocculent mulberry-red precipitate fell out of solution, and was collected by centrifugation, followed by washing with distilled water and drying *in vacuo* over P_2O_5 for several hours. A yield of 76 % (74.3 mg, 0.0936 mol) was recovered. m.p. *decomposes*; *Anal*. Found: C, 48.47; H, 3.96; N, 10.47 %. Calculated for $C_{32}H_{31}N_6F_6OPSRu$: C, 48.42; H, 3.94; N, 10.59 %. ν_{max} (cm^{-1}): 1483 (CO), 1418 (CN) and 1356 (CS); (m + 1)/z : 649.23 (calc. for $C_{32}H_{31}N_6OSRu$: 649.77).

cis-Bis(2,2′-bipyridine)(_N,N_-diethyl-_N′_-pivaloylthioureato)ruthenium(II) hexafluorophosphate, [Ru(bpy)$_2$(L^5-_S,O_)]PF_6:

To a 100 cm^3 round-bottomed flask containing 20 cm^3 of an ethanol-water mixture (4:1 v/v) was added HL^5 (46.7 mg, 0.216 mmol), followed by a slight excess of $CH_3COONa \cdot 3H_2O$ (33.9 mg, 0.249 mmol). The colourless ligand solution was heated gently with stirring at 60 ºC for 1 h. $Ru(bpy)_2Cl_2 \cdot 2H_2O$ (66.0 mg, 0.127 mmol) dissolved in 10 cm^3 of ethanol-water mixture (4:1 v/v) was added drop wise to the deprotonated ligand solution over 12 min while heating at 102-103 ºC. The dark purple-red solution was heated with stirring for 5 h, where after it was cooled to room temperature and stirred overnight. The volume of the reaction mixture was evaporated under reduced pressure, followed by addition of 20 cm^3 distilled water. An excess of solid NH_4PF_6 (45.0 mg, 0.276 mmol) was added to the aqueous mixture, followed by stirring at room temperature for 15 min. Flocculent dark-red precipitate fell out of solution, and was collected by centrifugation, followed by washing with distilled water and drying *in vacuo* over P_2O_5 for several hours. A yield of 96 % (94.4 mg, 0.122 mmol) was recovered. m.p. *decomposes*; *Anal*. Found: C, 46.12; H, 4.97; N, 11.04 %. Calculated for $C_{30}H_{35}N_6F_6OPSRu$: C, 46.57; H, 4.56; N, 10.86 %; ν_{max} (cm^{-1}): 1481 (CO), 1420 (CN) and 1355 (CS); (m + 1)/z : 629.20 (calc. for $C_{30}H_{35}N_6OSRu$: 629.79).

cis-Bis(2,2′-bipyridine)(_N_-pyrrolidyl-_N′_-pivaloylthioureato)ruthenium(II) hexafluorophosphate, [Ru(bpy)$_2$(L^6-_S,O_)]PF_6:

To a 100 cm^3 round-bottomed flask containing 10 cm^3 of an ethanol-water mixture (4:1 v/v) was added HL^6 (11.7 mg, 0.0546 mmol), followed by a slight excess of $CH_3COONa{\cdot}3H_2O$ (8.8 mg, 0.0647 mmol). The colourless ligand solution was heated gently with stirring at 60 ºC for 45 min. $Ru(bpy)_2Cl_2{\cdot}2H_2O$ (14.8 mg, 0.0284 mmol) dissolved in 10 cm^3 of ethanol-water mixture (4:1 v/v) was added drop wise to the deprotonated ligand solution over 12 min while heating at 100-102 ºC. The plum-red solution was heated with stirring for 5 h, where after it cooled to room temperature and was allowed to stir overnight. The volume of the reaction mixture was removed under reduced pressure, followed by the addition of 10 cm^3 distilled water. An excess of solid NH_4PF_6 (10.0 mg, 0.0613 mmol) was added to the light red aqueous mixture, followed by stirring at room temperature for 15 min. Flocculent deep-red precipitate fell out of solution, and was collected by centrifugation, followed by washing with distilled water and drying *in vacuo* over P_2O_5 for several hours. A yield of 83 % (35.0 mg, 0.0454 mmol) was recovered. m.p. *decomposes*; *Anal*. Found: C, 46.24; H, 4.68; N, 10.75 %. Calculated for $C_{30}H_{33}N_6F_6OPSRu$: C, 46.69; H, 4.31; N, 10.89 %; ν_{max} (cm^{-1}): 1480 (CO), 1422 (CN) and 1358 (CS); (m + 1)/z : 627.08 (calc. for $C_{30}H_{33}N_6OSRu$: 627.77).

4.3 Results and Discussion

4.3.1 Absorption Spectrophotometry

Firstly, we must consider the photochemical phenomena associated with the metal to ligand charge transfers that are associated with all the compounds in this section. Visible light absorption in these complexes are characterised by intense absorption bands arising from $\pi^* \leftarrow d\pi$ metal to ligand charge transfer (MLCT) transitions, *viz.* transfer of electron density from metal t_{2g} ($d\pi$) orbitals (which are largely non-bonding) to bipyridyl π^* orbitals (half-populated and anti-bonding). Simplified molecular orbital and state diagrams are provided in order to elucidate possible transitions.

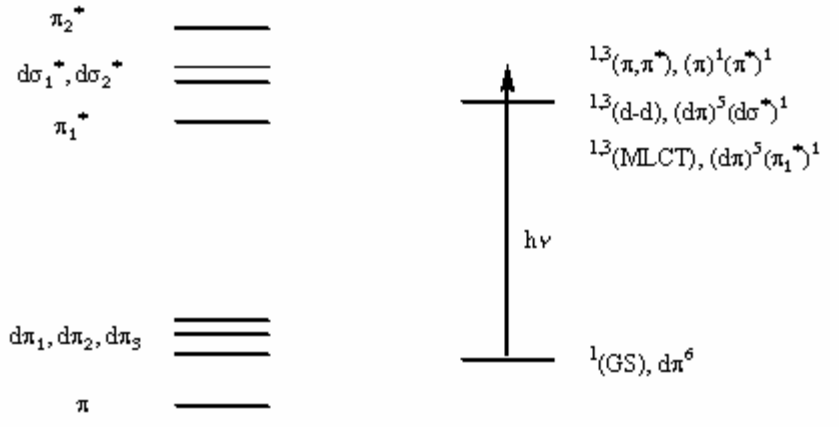

Fig. 4.2. **Simplified orbital and state diagrams relating to photo-induced transitions of polypyridine complexes. The singlet ground state may be excited to singlet and triplet states through MLCT, d-d metal transitions, or ligand-centered π-π* transitions.**

For complexes such as $Ru(bpy)_2XY$ and $Ru(bpy)_2(L\text{-}L)$ (where L-L may be any bidentate ligand, and X, Y are monodentate ligands), the coordinate system is defined with the non-bipyridyl ligand(s) coordinated along the +*x* and +*y* axes. Therefore the filled degenerate metal orbitals (d_{xz}, d_{yz} and d_{xy}) of t_{2g} symmetry will be the highest occupied molecular orbitals (HOMOs), while the bipyridyl π^* orbitals are positioned as the lowest unoccupied molecular orbitals (LUMOs). The latter are split into an antisymmetric (ψ) and a symmetric (χ) orbital with respect to the C_2 axis of the bipyridine molecule [23]. The charge transfer configuration can therefore be described as $\pi^*(\psi)$, $\pi^*(\chi) \leftarrow d\pi\ (t_{2g})$. In the past there had been some discussion on whether both symmetry transitions could be excited in the visible region, since from semi-empirical MO calculations [24] it had been shown that the $\pi^*(\chi) \leftarrow d\pi\ (t_{2g})$ transition was located at higher energy in the UV region.

Ceulemans, *et al.* [7] presented experimental and theoretical evidence for $[Ru(bpy)_3]^{2+}$ supporting $\pi^*(\psi) \leftarrow d\pi\ (t_{2g})$ transitions in the visible region, while $\pi^*(\chi) \leftarrow d\pi\ (t_{2g})$ transitions in the UV region was masked by ligand-centered transitions. However, in a series of *cis*-$Ru(bpy)_2X_2$ complexes, the optical electronegativities of the metal t_{2g} levels may be significantly decreased by the non-chromophoric X ligands (that are either σ- or π-donating), resulting in a red-shift of the entire MLCT absorption spectrum [6]. Therefore both transitions, $\pi^*(\psi) \leftarrow d\pi\ (t_{2g})$ and $\pi^*(\chi) \leftarrow d\pi\ (t_{2g})$ are identifiable in the visible region; moreover, it was also concluded that the two transitions were separated by a constant interval of *ca.* 146 nm, regardless of the nature of the ligand X.

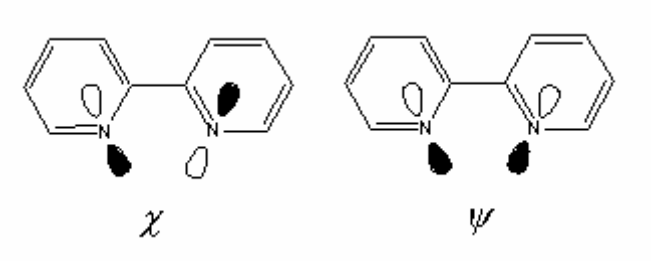

Fig. 4.3. **Symmetric and antisymmetric orientations of the unfilled π^* orbitals of bipyridine**

For all the complexes, two rather intense absorption bands occur in the UV region, and both are assigned to be intra-ligand transitions, labelled as $\pi^* \leftarrow \pi$ (1) and $\pi^* \leftarrow \pi$ (2). The position of the transition $\pi^* \leftarrow \pi$ (2) remains quite constant throughout the complex series. Assignment of this band has been inferred from studies on the absorption spectrum of the protonated uncoordinated bipyridine molecule, which exhibits an intense absorption at 281 nm. Comparatively, this absorption shifts to 300 nm for the mono-protonated species, and has been assigned as an intra-ligand transition [25]. The absorption band for bypiridine at 281 nm therefore shifts to lower energy upon coordination to the metal ion, which is consistent with observations made from related π-conjugated systems. This decrease may emanate from the induced positive charge on the energy levels of bipyridine. Bryant, *et al.* noted that the position of the transition $\pi^* \leftarrow \pi$ (2) shifted to higher energy in a similar order to the increase in average ligand field strength of coordinated ligands [6]. This phenomenon is apparently due to changes in the metal-ligand π-interactions. Metal t_{2g} (dπ) orbitals will be at low energy when ligands of high field strength are coordinated to the $Ru(bpy)_2$ moiety, resulting from metal-ligand π-bonding. This lowering in energy leads to an increase in energy of the bipyridine $\pi^* \leftarrow \pi$ transition due to greater t_{2g} - π interactions (metal-ligand π-bonding).

Starting material – $Ru(bpy)_2Cl_2 \cdot 2H_2O$:

The product was dissolved in HPLC-grade acetonitrile and the UV-Vis absorption spectrum acquired at room temperature. Two absorption bands occur in the visible region, with two other intense bands occurring in the high energy UV range.

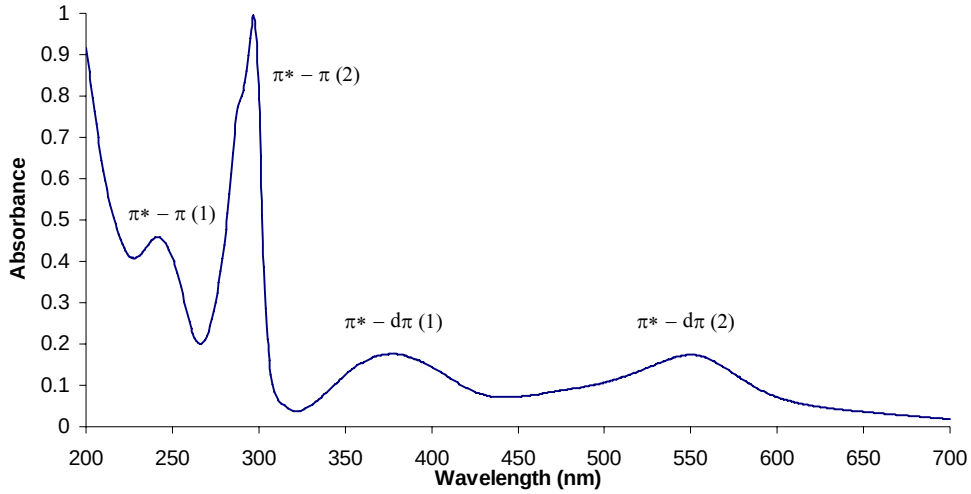

Fig. 4.4. **Absorption spectrum of $Ru(bpy)_2Cl_2 \cdot 2H_2O$ recorded in acetonitrile at room temperature**

The intense high energy bands are assigned to intra-ligand transitions involving the two bipyridine ligands. Henceforth these transitions will be labelled as $\pi^* \leftarrow \pi$ (1) and $\pi^* \leftarrow \pi$ (2).

Absorption bands in the visible region arise from metal-to-ligand charge transfers (MLCT), *viz.* transitions from electron rich dπ orbitals of the metal core to empty π^*-orbitals of bipyridine. Let them be labelled $\pi^* \leftarrow d\pi$ (1) and $\pi^* \leftarrow d\pi$ (2). A summary of the afore mentioned absorption bands occurring in different solvent media are listed below:

Solvent	UV region (nm)		Visible region (nm)	
	$\pi^* \leftarrow \pi$ (1)	$\pi^* \leftarrow \pi$ (2)	$\pi^* \leftarrow d\pi$ (1)	$\pi^* \leftarrow d\pi$ (2)
CH_3CN	242	297	378	550
CH_2Cl_2	244	299	380	556
DMF	Not visible	299	382	560
$[Ru(bpy)_2(CH_3CN)_2]^{2+}$	242	298	426	---

Table 4.1. **Absorption maxima of $Ru(bpy)_2Cl_2 \cdot 2H_2O$ in a series of solvents. The substitution product was obtained through exposure of an acetonitrile solution of $Ru(bpy)_2Cl_2$ to sunlight for several hours.**

The substitution product was discovered in a serendipitous manner, with the colour of the original acetonitrile solution changing from purple-violet to a deep-red. It is most likely that the two chlorine ligands were substituted with two CH_3CN molecules, the process being aided by exposure to visible light, therefore promoting a photosubstitution reaction. This hypothesis is confirmed by the work of Pinnick, *et al.* [26], who performed photosubstitution reactions of $Ru(bpy)_2XY$ with ligands spanning the range of the spectrochemical series.

The high energy MLCT, $\pi^* \leftarrow d\pi$ (1), which is usually situated at ca. 380 nm for $Ru(bpy)_2Cl_2$ is red-shifted to 426 nm, while the low energy $\pi^* \leftarrow d\pi$ (2) MLCT is not present in the absorption spectrum. The MLCTs of $Ru(bpy)_2Cl_2$ may be explained as follows: the electron withdrawing capabilities of bipyridine and chlorine might be considered to be roughly equal, therefore the metal orbitals situated along the bipyridine bonding axes (d_{xz}, d_{yz}) and orientated towards the chlorine ligands (d_{xy}) will be nearly degenerate. Substitution of the chlorines with acetonitrile molecules results in the bipyridine ligands possessing greater electron withdrawal capabilities, consequently leading to stabilisation of the metal (d_{xz}, d_{yz}) orbitals, and lifting of the degeneracy. Moreover, π-interactions from the chlorine ligands with the metal ion (that stabilise t_{2g} levels) are now removed, being replaced with a higher degree of σ-interaction emanating from the acetonitrile ligands, raising the energy of the metal (d_{xy}) orbital and positioning it as the HOMO. The energy difference between the ligand LUMOs and the metal HOMO is now reduced, resulting in the low energy absorption band at 426 nm (most likely to be a $\pi^*(\psi) \leftarrow d\pi$ (t_{2g}) transition).

Wavelength positions for the MLCTs vary to a slight degree as solvent media are varied. This phenomenon is adequately described in the review of Meyer [3], who conjectured that the energies of equilibrated MLCT excited states may be solvent dependent, since significant changes in radial distribution are involved in MLCT transitions (the radial distributions relate to the $(d\pi)^6$ ground and $(d\pi)^5(\pi^*)^1$ excited states).

Substitution Product - $[Ru(bpy)_2(L^1\text{-}S,O)]PF_6$:

The said product was taken up immediately in an acetonitrile solution, affording a deep purple-red colour. The absorption spectrum possesses the same profile as the starting material, *viz.* two absorption bands occurring in the visible region, with two further intense bands in the high energy UV range.

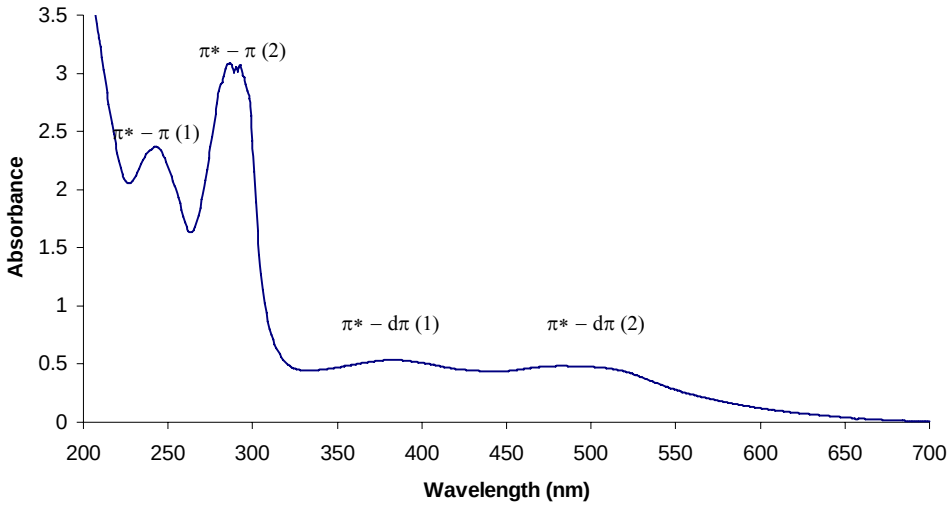

Fig. 4.5. **Absorption spectrum of $[Ru(bpy)_2(L^1\text{-}S,O)]PF_6$ recorded in acetonitrile at room temperature**

Solvent	UV region (nm)		Visible region (nm)	
	$\pi^* \leftarrow \pi$ (1)	$\pi^* \leftarrow \pi$ (2)	$\pi^* \leftarrow d\pi$ (1)	$\pi^* \leftarrow d\pi$ (2)
CH_3CN	243	287	382	487

Table 4.2. **Absorption maxima of $[Ru(bpy)_2(L^1\text{-}S,O)]PF_6$ in acetonitrile**

As for the case of the starting material $Ru(bpy)_2Cl_2$, the visible region exhibits two MLCT transitions, $\pi^*(\psi) \leftarrow d\pi$ (t_{2g}) and $\pi^*(\chi) \leftarrow d\pi$ (t_{2g}). Although the high-energy MLCT, $\pi^* \leftarrow d\pi$ (1), has been red-shifted slightly in comparison with the corresponding MLCT of $Ru(bpy)_2Cl_2$, it is the low-energy MLCT, $\pi^* \leftarrow d\pi$ (2), which is of most interest. It has underwent quite a significant blue-shift of *ca.* 63 nm.

From the experimental data, it would lead us to believe that in comparison to the chlorine ligands, the bidentate deprotonated *N,N*-diethyl-*N'*-benzoylthiourea (DEBT) exhibits a greater amount of π-acidity. It is known that the chlorine ligand interacts almost exclusively through σ-bonds with the metal, resulting in a small amount of backbonding from metal to ligand. These σ-interactions raise the energy levels of the populated metal dπ levels, therefore reducing the energy difference between the former and the π^* orbitals of bipyridine, thus explaining the MLCT.

However, once the chlorines are substituted with the deprotonated DEBT, the MLCT is now located at a higher energy. Therefore, one deduces that the metal dπ orbitals must be at lower energy, therefore more stabilised, causing the energy difference between the latter and the π^* orbitals to be substantial. The same line of reasoning may be used for explaining the blue-shift of the $\pi^* \leftarrow \pi$ (2) intra-ligand transition.

Substitution Product - $[Ru(bpy)_2(L^5\text{-}S,O)]PF_6$:

The said product was taken up immediately in an acetonitrile solution, affording a deep purple-red colour. The absorption spectrum possesses the same profile as the preceding substitution product, *viz.* two absorption bands occurring in the visible region, with two further intense bands in the high energy UV range.

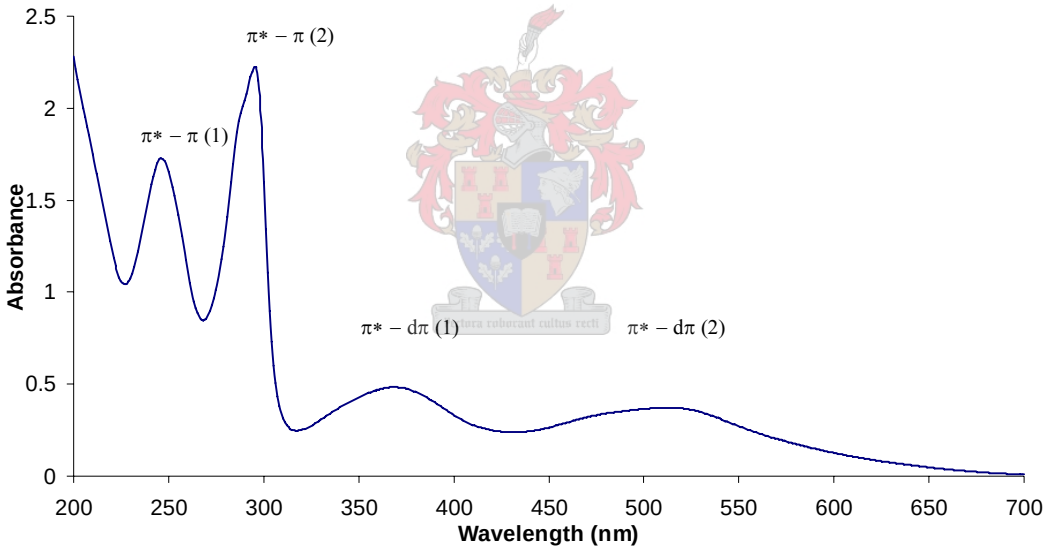

Fig. 4.6. **Absorption spectrum of $[Ru(bpy)_2(L^5\text{-}S,O)]PF_6$ recorded in acetonitrile at room temperature**

Solvent	UV region (nm)		Visible region (nm)	
	$\pi^* \leftarrow \pi$ (1)	$\pi^* \leftarrow \pi$ (2)	$\pi^* \leftarrow d\pi$ (1)	$\pi^* \leftarrow d\pi$ (2)
CH_3CN	246	295	369	513

Table 4.3. **Absorption maxima of $[Ru(bpy)_2(L^5\text{-}S,O)]PF_6$ in acetonitrile**

The spectral profile is the same as for the previous product, though the most notable changes are the positions of the MLCT's and the bipyridine-centered intra-ligand transitions.

Concentrating on the low-energy MLCT for the moment, one notices that it is red-shifted by *ca.* 26 nm when compared to the corresponding MLCT of $[Ru(bpy)_2(L^5\text{-}S,O)]PF_6$. This is mainly due to the influence of the non-chromophoric thiourea ligand, in terms of electron distribution and inductive effects caused by this particular ligand. The difference between the two ligands being the pendant groups attached to the carbonyl unit. For DEBT it is a benzoyl moeity, while DEPT exhibits a tert-butyl substituent. One deducts then that it is exactly these two different pendant groups that cause the interesting energy shifts.

Since the experimental data suggests that there is indeed a considerable amount of backbonding occurring between the metal core and DEBT, one would expect that with the presence of delocalised electron density situated on the benzoyl moiety, this is indeed a favourable situation. Moreover, the delocalised negative charge localised on the S – C – N – C – O moiety (after deprotonation) must surely also contribute.

In comparison, the DEPT rather possesses a tert-butyl pendant group, which will afford a considerable inductive effect, therefore enhancing the σ-interaction with the metal core. Consequently, the dπ-orbitals will increase in energy, and be situated closer energetically to the LUMO π^*- orbitals of bipyridine, therefore explaining the red-shift of the low-energy MLCT.

Substitution Product - $[Ru(bpy)_2(L^6\text{-}S,O)]PF_6$:

The said product was taken up immediately in an acetonitrile solution, affording a deep purple-red colour. The absorption spectrum possesses almost exactly the same profile as the preceding substitution product, *viz.* two absorption bands occurring in the visible region, with two further intense bands in the high energy UV range.

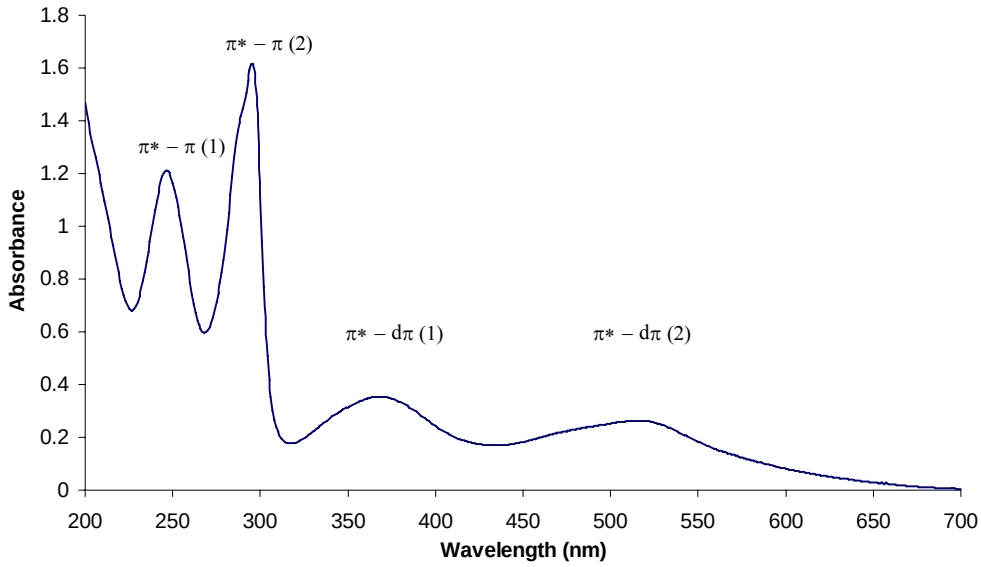

Fig. 4.7. **Absorption spectrum of $[Ru(bpy)_2(L^6\text{-}S,O)]PF_6$ recorded in acetonitrile at room temperature**

Solvent	UV region (nm)		Visible region (nm)	
	$\pi^* \leftarrow \pi$ (1)	$\pi^* \leftarrow \pi$ (2)	$\pi^* \leftarrow d\pi$ (1)	$\pi^* \leftarrow d\pi$ (2)
CH_3CN	246	295	368	515

Table 4.4. **Absorption maxima of $[Ru(bpy)_2(L^6\text{-}S,O)]PF_6$ in acetonitrile**

The spectral profile is almost exactly the same as for $[Ru(bpy)_2(L^5\text{-}S,O)]PF_6$, with only a very slight difference in the absorption position of the $\pi^* \leftarrow d\pi$ (2) transition. From this it could possibly be inferred that the amino group attached to the thiocarbonyl group has little or no effect on the absorption mechanisms observed.

4.4 Summary

A series of *cis*-bis(2,2′-bipyridine)(*N,N*-dialkyl-*N*′-acyl(aroyl)thioureato)ruthenium(II) complexes have been successfully synthesised and characterised. The electronic absorption behaviour of the formed complexes has been investigated in detail via UV-Vis spectrophotometry.

This preliminary study has opened the way for further study into tailoring the *N,N*-dialkyl-*N*′-acyl(aroyl)thiourea ligand for specific photochemical purposes, and incorporation into a variety of different analytical and process chemistry fields.

References

[1] T.P. Paris and W.W. Brandt, *J Am Chem Soc*, 81 (1959) 5001.

[2] D.M. Roundhill, *Photochemistry and Photophysics of Metal Complexes*, Plenum Press, New York and London (1994).

[3] T.J. Meyer, *Pure & Appl Chem*, 58 (1986) 1193.

[4] R.F. Jones and D.J. Cole-Hamilton, *Inorg Chim Acta*, 53 (1981) L3.

[5] D.W. Thompson, J.R. Schoonover, D.K. Graff, C.N. Fleming and T.J. Meyer, *J Photochem Photobiol A: Chem*, 137 (2000) 131.

[6] G.M. Bryant and J.E. Fergusson, *Aust J Chem*, 24 (1971) 275.

[7] A. Ceulemans and L.G. Vanquickenborne, *J Am Chem Soc*, 103 (1981) 2238.

[8] B. Durham, J.V. Caspar, J.K. Nagle and T.J. Meyer, *J Am Chem Soc*, 104 (1982) 4803.

[9] A. Juris and V. Balzani, *Coord Chem Rev*, 84 (1988) 85.

[10] B.P. Sullivan, D.J. Salmon and T.J. Meyer, *Inorg Chem*, 17 (1978) 3334.

[11] A.J. Bard, E. Garcia and J. Kwak, *Inorg Chem*, 27 (1988) 4377.

[12] D.S. Eggleston, *Inorg Chem*, 24 (1985) 4573.

[13] M.J. Root, *Inorg Chem*, 24 (1985) 2731.

[14] M.A. Greaney, *Inorg Chem*, 28 (1989) 912.

[15] R. Llanguri, J.J. Morris, W.C. Stanley, E.T. Bell-Loncella, M. Turner, W.J. Boyko and C.A. Bessel, *Inorg Chim Acta*, 315 (2001) 53.

[16] X. Xiao, J. Sakamoto, M. Tanabe, S. Yamazaki, S. Yamabe and T. Matsumura-Inoue, *Journal of Electroanalytical Chemistry*, 527 (2002) 33.

[17] G. Sprintschnik, H.W. Sprintschnik, P.P. Kirsch and D.G. Whitten, *J Am Chem Soc* , 98 (1976) 2337.

[18] K. Tanaka, M. Morimoto and T. Tanaka, *Inorg Chim Acta*, 56 (1989) L61.

[19] A.A. Batista, M.O. Santiago, C.L. Donnici, I.S. Moreira, P.C. Healy, S.J. Berners-Price and S.L. Queiros, *Polyhedron*, 20 (2001) 2123.

[20] W.J. Dressick, T.J. Meyer, B. Durham and D.P. Rillema, *Inorg Chem*, 21 (1982) 3451.

[21] C.D. Ellis, J.A. Gilbert, W.R. Murphy and T.J. Meyer, *J Am Chem Soc*, 105 (1983) 4842.

[22] Miller, J. D. Ph.D. Thesis. (2000). University of Cape Town.

[23] L.E. Orgel, *J Chem Soc*, (1961) 3683.

[24] B. Mayoh and P. Day, *Theor Chim Acta*, 49 (1978) 259.

[25] K. Nakamoto, *J Phys Chem*, 64 (1960) 1420.

[26] D.V. Pinnick and B. Durham, *Inorg Chem*, 23 (1984) 1440.

Conclusions

During the initial stages of this study the behaviour of Os(IV), as $[OsCl_6]^{2-}$, in acidic media was investigated. It was found that the hexachloro-osmate ion remained stable in acidic solutions of concentration as low as 0.1 M. For concentration strengths lower than 0.1 M it was noted that black precipitates were forming. Heating of these solutions at 80 ˚C or higher resulted in the gradual aquation of the hexachloro-osmate ion, to form $[Os(H_2O)Cl_5]^-$.

Attempted liquid-liquid extraction of $[OsCl_6]^{2-}$ with *N,N*-dibutyl-*N′*-benzoylthiourea at room temperature for a period of 24 h resulted in no meaningful transfer of osmium into the organic phase. Increased reaction temperatures and elevated ligand to osmium ratios (up to 24 times molar excess of ligand) afforded no positive extraction results even after extended periods of agitation.

Incorporation of a phase transfer catalyst, in the form of tetrabutylammonium tetrafluoroborate (TBATFB), into the liquid-liquid extraction studies resulted in a quantitative transfer of the $[OsCl_6]^{2-}$ ion into the organic phase after only 15 min agitation at room temperature. Experiments with two different ligands, *N,N*-dibutyl-*N′*-benzoylthiourea and *N,N*-diethyl-*N′*-benzoylthiourea, resulted in organic phase absorption spectra that were comparable to each other, therefore suggesting that the osmium-TBATFB ion pair present in the organic phase did not react with either of the ligands. This was confirmed by evaluating the effect of TBATFB concentration on osmium present in the aqueous phase. In the absence of *N,N*-dialkyl-*N′*-benzoylthiourea ligands the absorption spectra were comparable to the situation where they were incorporated into the extraction experiment. A directly proportional relationship between increasing TBATFB concentration and increasing osmium concentration (in the organic phase) was established. The following reaction scheme is suggested, which illustrates the fashion in which transport of the $[OsCl_6]^{2-}$ ion occurs :

$$[OsCl_6]^{2-} + [(C_4H_9)_4N]BF_4 \rightarrow [(C_4H_9)_4N]_2OsCl_6$$

Under specific experimental conditions, it is possible to reduce the tetravalent $OsCl_6^{2-}$ species, by means of $SnCl_2$, to a bivalent bimetallic species. The following reaction scheme is proposed:

$$[OsCl_n]^{2-n} + m[SnCl_3]^- \rightarrow [OsCl_{n-m}(SnCl_3)_m]^{2-(n+m)} \rightarrow [Os(SnCl_3)_5Cl]^{4-}$$

In the presence of a sufficient amount of $SnCl_2$ to afford quantitative reduction of Os(IV) to Os(II), and with the aid of a phase transfer catalyst, it seems that although the reduced species present as $[Os(SnCl_3)_5Cl]^{4-}$ was transported into the organic phase by the phase transfer catalyst, no observable reactions with *N,N*-dialkyl-*N′*-benzoylthioureas were observed.

In order to elucidate the perceived "inertness" of the tetravalent $[OsCl_6]^{2-}$ species, a series of complexes of osmium with the *N,N*-dialkyl-*N′*-acyl(aroyl)thioureas was prepared and characterised. Also reported is the crystal structure of the first example of an Os(III) complex, tris(*N,N*-diethyl-*N′*-benzoylthioureato)osmium(III). It was discovered that the *N,N*-dialkyl-*N′*-acyl(aroyl)thiourea ligand, present in its deprotonated form and in excess w.r.t. osmium, facilitated in the reduction of Os(IV) to Os(III), thereby assisting complex formation.

In the final part of the study, substitution reactions of ruthenium polypyridine complexes with *N,N*-dialkyl-*N′*-acyl(aroyl)thioureas were investigated. A series of *cis*-bis(2,2′-bipyridine)(*N,N*-dialkyl-*N′*-acyl(aroyl)thioureato)ruthenium(II) complexes were synthesised and characterised. The resultant products of the substitution reactions afforded interesting photochemical properties. Absorption spectra of the complexes revealed several metal to ligand charge transfers. Further investigations may produce interesting application of these products into the fields of photochemistry, photoelectrochemistry, electrochemistry, chemiluminescence and electron/energy transfer.